ABSTRACT

Spectral Properties of Quantum Graphs with Symmetry

Erica K. Swindle, Ph.D.

Advisor: Jonathan M. Harrison, Ph.D.

Quantum graphs were first introduced as a simple model for studying quantum mechanics in geometrically complex systems. For example, Pauling [97] used quantum graphs to study organic molecules by viewing the atomic nuclei as nodes and the chemical bonds as one-dimensional connecting wires on which the electrons traveled. In 1997, Kottos and Smilansky [76] proposed the use of quantum graphs as a model for studying quantum chaos. Quantum chaos is the study of quantum systems with underlying classical dynamics that exhibit chaos. It is conjectured that the energy levels, or spectra, of quantum systems with classically chaotic dynamics exhibit spacing statistics that are predicted by the Gaussian ensembles of random matrix theory [27]. This contrasts with quantum systems with corresponding integrable classical dynamics which have been shown to be modeled by a Poisson process [22]. However, in certain cases of chaotic dynamics, the spectral statistics fall in a category of intermediate statistics, which combine features associated with the Poisson and random matrix models. In the field of quantum graphs, this is the case with the quantum star graph [14, 12], one of the simpler models studied. Quantum circulant graphs, the Cayley graphs of cyclic groups, are a natural extension of star graphs because of their rotational symmetry. Chapter three of this dissertation finds secular equations for quantum circulant graphs which are used to study their spectra. In chapter four,

the nearest neighbor spacing statistics and two-point correlation function of circulant graphs are numerically analyzed. When the edge lengths of a circulant graph are incommensurate, it displays random matrix statistics; however, when edge length symmetry is introduced, intermediate statistics appear. Predictions for intermediate statistics are also derived analytically and compared to the numerics in this chapter. The quantum graph spectral zeta function for circulant graphs is found in chapter five and used to compute the spectral determinant and vacuum energy. The final chapter examines the spectra of quantum Cayley graphs of general finite groups.

Spectral Properties of Quantum Graphs with Symmetry

by

Erica K. Swindle, B.S., M.S.

A Dissertation

Approved by the Department of Mathematics

_____

Lance L. Littlejohn, Ph.D., Chairperson

Submitted to the Graduate Faculty of
Baylor University in Partial Fulfillment of the
Requirements for the Degree
of
Doctor of Philosophy

Approved by the Dissertation Committee

_____

Jonathan M. Harrison, Ph.D., Chairperson

_____

Klaus Kirsten, Ph.D.

_____

Mark R. Sepanski, Ph.D.

_____

Brian Z. Simanek, Ph.D.

_____

B.F.L. Ward, Ph.D.

Accepted by the Graduate School
August 2019

_____

J. Larry Lyon, Ph.D., Dean

Page bearing signatures is kept on file in the Graduate School.

TABLE OF CONTENTS

LIST OF FIGURES

ACKNOWLEDGMENTS

It would be an understatement to say that this dissertation would not have happened without the help and support of numerous individuals. First and foremost, I want to thank my advisor, Dr. Jon Harrison, for the countless hours spent explaining (and re-explaining) difficult concepts, reading (and re-reading) numerous drafts, and giving helpful feedback (sometimes more than once). I deeply appreciate the amount of time you have invested in me and your persistent patience with my occasional stubbornness.

For encouragement and helpful feedback, I would like to thank the rest of my dissertation committee: Dr. Klaus Kirsten, Dr. Mark Sepanski, Dr. Brian Simanek, and Dr. B.F.L. Ward. In particular, I wish to thank Dr. Sepanski for going above and beyond as a graduate program director. I also would like to thank all the other professors in the mathematics department at Baylor who I have had the privilege of taking a course from. Thank you for continuing to inspire my love of mathematics and for demonstrating genuine interest and concern for me as person. I am also grateful for the tireless work put in by the chair and staff of the mathematics department during my time here: Dr. Lance Littlejohn, Judy Dees, Rita Massey, and Margaret Salinas. Your efforts are often under-appreciated but you make everything we do possible.

I would like to express my gratitude to Dr. Gregory Berkolaiko for helpful advice and encouragement when I was stuck on my research. I would also like to thank Dr. Tracy Weyand for her insight and enthusiastic support during her time as a postdoc here. I am also especially grateful to my colleague, Tori Hudgins, for being my traveling buddy, work accountability partner, and good friend.

I also wish to thank my cohort of graduate students for support over the years. In particular, I want to express my great appreciation for the female graduate students in the math department and the community that we have built. Thank you for your endless encouragement. In particular, I want to thank Dr. Katie Elliott, who is the only individual in the intersection of those two sets. You have supported me personally and professionally for so many years and I'm so grateful for your friendship.

To Karen Rollins, Dr. Lauri Rogers, Dr. Melanie Illich, Sarah Ritter, and Dr. Emma Wood, I am forever grateful for everything you have done for me. To my church family at Trinity, thank you for welcoming me into your community on such short notice and feeding me during the final weeks of my dissertation writing. To the many friends who have come in and out of my life and have supported and encouraged me, you have my deepest gratitude.

Thank you to Gareth for seeing me to the finish line. Thank you to Jonathan and Nora for being fantastic and understanding siblings. Thank you to my parents for loving and supporting me my entire life.

Finally, thank you to my Lord and Savior. 2 Timothy 4:7.

To the girl who wants to know everything there is to know about math

CHAPTER ONE

Literature Review

A quantum graph refers to a metric graph equipped with a differential operator. Although the term *quantum graph* doesn't begin to appear until the late 1990s and early 2000s, when they were first introduced as a model for quantum chaos and quantum wires, the study of mathematical objects falling under the umbrella of quantum graphs dates to the 1930s. Quantum graphs are significant because they can serve as models for a myriad of naturally occurring systems in physics, mathematics, and chemistry. The study of quantum graphs merits our attention because it offers a simple, yet nontrivial, model for studying quantum phenomena which are challenging to analyze in higher dimensions. The goal of this chapter is to evaluate the history, significance, and applications of quantum graphs, specifically through the lens of quantum chaos.

1.1 History of Quantum Graphs

1.1.1 Origins of Graph Theory

In 1736, Leonhard Euler laid the foundations for the field that would come to be known as graph theory with his resolution of the Seven Bridges of Königsberg problem [38]. In Königsberg, there were four distinct landmasses connected by seven different bridges. As the citizens of Königsberg would stroll around the city, they devised a game of trying to find a path around the city that crossed each bridge exactly once. Although no such path could be found, no one was able to prove that it was impossible either. This puzzle intrigued Euler, and he devised a mathematical way of showing the impossibility of a solution.

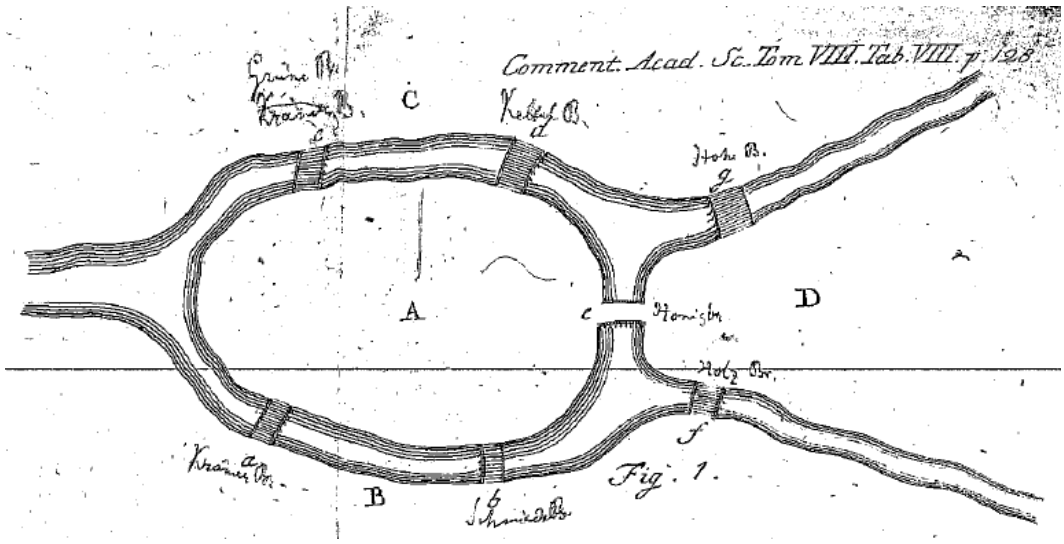

Figure 1.1. Euler's diagram for the Seven Bridges of Königsberg. Courtesy of the MAA Euler Archive; see also [38].

Let us represent, as Euler did in figure 1.1, each of the landmasses in the city of Königsberg by a capital letter, A, B, C, D. A bridge crossing between two landmasses, say from A to B, would then be represented by the sequence AB or BA, depending on the direction of crossing. Since the path chosen within each landmass is irrelevant to the problem, a journey through the city could be given as a sequence of letters representing the landmasses traveled on.

Figure 1.2 shows a mathematical representation of the Königsberg bridge problem using a graph. By converting the landmasses into vertices of a graph and the bridges into edges connecting the different vertices, Euler implemented a new kind of geometry. Up to this point, most geometry involved some notion of distance, such as length or area. This new "geometry of position" [38] was primarily concerned with relative positions of the objects involved and opened the door for the new fields of graph theory and topology.

Euler's solution to this problem utilized paths on graphs. Notice that a path which traverses each of the seven bridges no more than once requires a sequence of at most eight letters. Now consider an individual landmass, for example A. The letter A

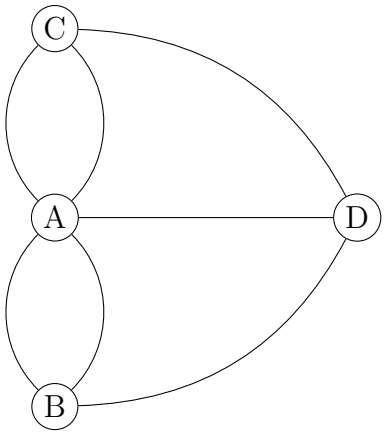

Figure 1.2. A graph depiction of the Seven Bridges of Königsberg.

must be present at least three times in the sequence in order to cross all five bridges connected to this landmass, since two occurrences can cover at most four crossings. Similarly, the letters B, C, and D must be present at least twice in the sequence in order to cross each of their three bridges. Adding this up, we see that a sequence using every bridge must contain at least nine letters, which contradicts our original assertion that the necessary sequence requires at most eight letters.

There are many other interesting topics related to the study of graphs, but the idea of paths on graphs as sequences of vertices will continue to be relevant for our study. We will also often be interested in looking at the orbits on a graph, which are paths that begin and end at the same vertex. This idea of traversing a graph will turn out to be important in our application of quantum graphs to the study of quantum chaos.

1.1.2 Introduction of Quantum Graphs

One of the main principles of quantum mechanics is the concept of wave-particle duality. This is the discovery that particles also exhibit wave-like properties. In a quantum system, this can be modeled via the wavefunction, a mathematical description of the state of a quantum system. Integrating the square modulus of the

wavefunction over a region of space gives the probability that the particle described by the wavefunction is found in that region.

One of the first models a student in a course on quantum mechanics will consider is that of a particle confined to a one-dimensional box. Inside of the box, the potential is zero, so the movement of the particle is unrestricted. The potential outside the box goes to infinity, guaranteeing that the particle has zero probability of being outside the box. Determining the wavefunction in this context amounts to solving the time-independent Schrödinger equation, a second-order differential equation, as a boundary value problem on an interval of some given length.

This model can be viewed from a graph-theoretic perspective by considering the endpoints of the interval as graph vertices and the interval as the edge connecting these two vertices. In this model, viewing the edge as an interval requires introducing a notion of distance to the graph. Such a graph, one where the edges are considered to have lengths, is known as a *metric graph*. By linking together various one-dimensional boxes at the ends of the intervals, we obtain a quantum mechanical system modeled by a differential equation on the edges of a metric graph. The boundary of each interval is now a vertex connecting different intervals, so we choose boundary conditions at the vertices which govern the interactions between the different one-dimensional boxes. Typically, this is done in a way that defines a self-adjoint operator in order for the operator to represent an observable. This is a quantum graph: a metric graph equipped with a differential operator (such as the Schrödinger operator) and appropriate (typically self-adjoint) boundary conditions at the vertices.

In 1936, Pauling [97] sought to study the spectrum of free electrons in aromatic organic molecules using a quantum graph model. The simplest of these molecules is benzene, which consists of a hexagonal ring of six carbon atoms each of which is bonded to a hydrogen atom. Many other aromatic molecules are derivatives of

benzene and share aspects of this hexagonal ring structure. For example, figure 1.3 depicts the molecule anthracene and its induced currents between carbon atoms.

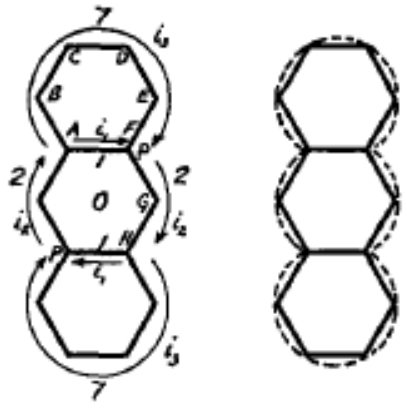

Figure 1.3. The molecule anthracene and the induced currents between atoms. Reprinted from [97] with the permission of AIP Publishing.

The use of quantum graphs as a model for aromatic hydrocarbons was given a more detailed treatment in [103], where it was applied to organic molecules with conjugated systems; that is systems containing alternating single and double chemical bonds. The idea behind the free-electron model is that certain electrons are able to move throughout the entire molecule, as opposed to being restricted to a single atom or bond. Thus, by representing the various atoms in the molecule by graph vertices and the chemical bonds between them by connecting edges, a quantum graph model emerges. Figure 1.4 depicts Ruedenberg and Scherr's conception of a one-dimensional mathematical model for a branching point in an organic hydrocarbon.

Although it was later determined that this model overlooks several key assumptions in its reduction to a one-dimensional problem, the use of quantum graphs to study the spectra of carbon structures is reemerging in the past few decades. Graphene, a regular hexagonal lattice of carbon atoms, has attracted a lot of attention in recent years. Graphene has many structural properties which make it useful in engineering and manufacturing, such as its relative strength, flexibility, and efficient

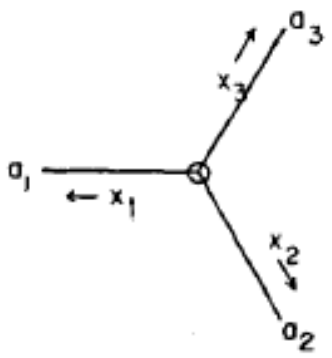

Figure 1.4. A one-dimensional space modeling a branching point in the bond skeleton of an organic molecule. Reprinted from [103] with the permission of AIP Publishing.

conductivity. In 2010, the Nobel Prize in Physics was awarded "for groundbreaking experiments regarding the two-dimensional material graphene" [1]. At present, there is a high demand for research on this promising new carbon allotrope. For more on the applications of quantum graphs to the study of graphene and other carbon nano-structures, see [86].

Another relevant structure of current interest which can be modeled by quantum graphs is the photonic crystal [80, 85, 81]. A photonic crystal is a periodic dielectric medium which affects the propagation of electromagnetic waves in a similar way to how a semi-conductor affects the motion of electrons. The phenomenon of Anderson localization refers to the absence of diffusion of waves in a medium with random impurities or random perturbations. This can be modeled by a Schrödinger operator with a random potential on a quantum graph [105, 40, 65]. Additionally, quantum graphs can serve as models in mesoscopic and nanoscopic systems, such as quantum wires and carbon nanotubes, which have relevance for advances in nanotechnology [107, 113].

1.1.3 Connections Between Discrete and Quantum Graphs

Discrete or combinatorial graphs can often have many of their properties encoded in matrices. One obvious example is the adjacency matrix, which gives information about how vertices are connected in a graph. Another example is the discrete Laplacian, which is a diagonal matrix of vertex degrees minus the aforementioned adjacency matrix. Studying the spectral properties of these matrices is a field known as spectral graph theory, and there are many useful connections between the spectra of quantum graphs and their corresponding discrete graph spectra. For a quantum graph equipped with the Laplace operator and standard vertex conditions, if the edges of the graph have the same length L, then λ is in the spectrum if and only if $1 - \cos(L\sqrt{\lambda})$ is in the corresponding spectrum of the discrete Laplace operator [30, 95].

Another similarity between the two fields is the study of zeta functions, various analogues of the Riemann zeta function. The Ihara zeta function on discrete graphs was introduced in the 1960s [67] and can be used to relate closed paths on the graph to the spectrum of its adjacency matrix. The Ihara zeta function is defined as a product over closed non-backtracking paths on the graph, and it can be expressed as the inverse of the characteristic polynomial of an oriented adjacency matrix. For quantum graphs, spectral properties of the graph are often related to sums over periodic orbits via trace formulae. A spectral zeta function for a quantum graph can also be obtained in this way, but in chapter five, we will examine how a contour integral technique introduced by Kirsten and McKane in [71, 72] can be used to obtain a spectral zeta function for a quantum graph.

1.2 Quantum Chaos

At the turn of the 20th century, the foundations of quantum mechanics were being laid through the work of such physicists as Planck, Einstein, Bohr, de Broglie,

Born, Dirac, Heisenberg, Pauli, and Schrödinger. Around the same time, chaotic behavior in classical mechanics was beginning to emerge, albeit slowly, for example in the study of the three-body problem by Poincaré.

1.2.1 Chaotic Dynamics

The study of chaos theory involves dynamical systems that are considered to exhibit deterministic chaotic behavior. Although there is no single agreed upon mathematical definition of chaos, many share the characteristic of sensitivity to initial conditions. That is, a slight change in initial conditions results in a drastically different outcome. One of the first major observations of this phenomenon was in the three-body problem by Henri Poincaré. The three-body problem involves determining the motion of three point masses based on their interactions from their mutual gravitational field. One often cited example models the motion of the Sun, Moon, and Earth, though in practice any three particles can be used. As opposed to the two-body problem, the three-body problem cannot be solved analytically for an arbitrary set of initial conditions. Poincaré observed that certain cases of the three-body problem resulted in trajectories with seemingly random behavior. One example he studied was a particular case of the restricted three-body problem, in which two of the three bodies are held in orbit around their mutual center of mass and the mass of the third body is much smaller than the other two [98, 99, 100, 101]. Minor changes in the mass of the relatively infinitesimal third body would lead to distinct changes in its trajectory, giving rise to the appearance of *chaotic* behavior.

Another property typically shared by chaotic dynamical systems is ergodicity. Loosely speaking, a dynamical system is ergodic if the average of some function along a trajectory is equal to the average over all points in the space. A useful example of ergodicity is provided by considering dynamical billiards. A dynamical billiard is a particle modeled by a point confined to some two-dimensional region of the plane.

The particle moves in a straight line until hitting the region's boundary, at which point it bounces off without losing speed. The reflection off the boundary is specular; that is, the angle of incidence equals the angle of reflection. Figure 1.5(a) depicts the trajectory of a particle in a billiard with a circular boundary and figure 1.5(b) displays a trajectory in a Bunimovich stadium.

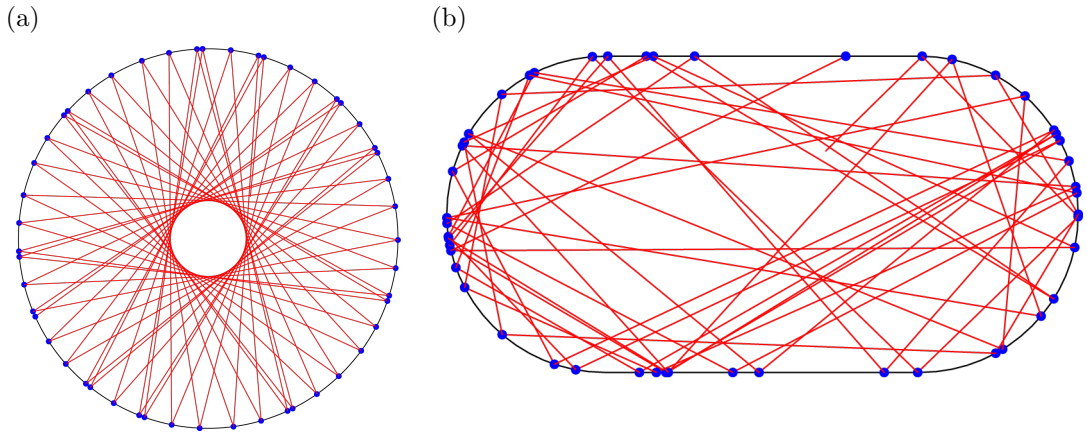

Figure 1.5. Dynamical billiards: (a) a trajectory of a particle in a circular billiard; (b) a trajectory of a particle in the Bunimovich stadium.

A dynamical billiard is ergodic if the average of a function defined on the region along an individual trajectory over time is equal to the average over the region of space. Intuitively, one can think about a system in which the trajectory of a single particle will eventually cover the entire space evenly. The trajectory in the Bunimovich stadium in figure 1.5(b) is an example of an ergodic dynamical system because over time, the particle is equally likely to be anywhere inside the stadium. On the other hand, the system depicted in figure 1.5(a) is not ergodic because the probability of the particle being near the center of the circle is zero, regardless of how long the trajectory continues. The trajectory of a particle in a circular billiard is an example of integrable dynamics.

Ergodicity is actually the weakest condition in a hierarchy of similar properties studied in ergodic theory. These include strong and weak mixing, Kolmogorov systems

(or K-systems), and Bernoulli systems. It is generally accepted that every chaotic system will fall somewhere in this hierarchy, but not every ergodic system is said to be chaotic.

1.2.2 The BGS Conjecture and Random Matrices

Quantum chaos seeks to understand the link between quantum mechanics and dynamical systems exhibiting classically chaotic behavior. For example, the billiards shown in figure 1.5 are classical systems with dynamics determined by specular reflections, as described in the previous section. One can define a corresponding quantum billiard by considering the Laplace equation on the same region with Dirichlet conditions at the boundary where the wavefunction vanishes. A question of interest to those studying quantum chaos is how the chaotic dynamics of the billiard are reflected in the properties of the eigenvalues and eigenfunctions of the corresponding quantum system.

In 1984, Bohigas, Giannoni, and Schmit observed that the spectral statistics of quantum systems corresponding to classically chaotic systems appeared to share certain universal properties. They conjectured that

> Spectra of time reversal-invariant systems whose classical analogs are K-systems show the same fluctuation properties as predicted by GOE (alternative stronger conjectures that cannot be excluded would apply to less chaotic systems, provided that they are ergodic). [27]

Here the GOE refers to the Gaussian orthogonal ensemble of random matrices, and K-systems are the Komolgorov systems included in the hierarchy of ergodic theory. This conjecture sparked a great deal of interest in the more general relationship between the spectra of classically chaotic quantum systems and the eigenvalue statistics of ensembles of random matrices. Although the original conjecture was specific to K-systems and the GOE, the general correspondence between classical chaos and random matrix statistics is referred to as the BGS conjecture.

The Gaussian orthogonal ensemble is the collection of real symmetric $N \times N$ matrices with independent entries along and above the diagonal distributed according to a normal Gaussian distribution. The probability distribution on this space of matrices is invariant under orthogonal transformations, which, along with independent matrix elements, is sufficient to derive a Gaussian distribution [58]. In the 1950s, Wigner introduced this ensemble as a model for the Hamiltonians of large nuclei. To be an effective model, the matrices must be Hermitian, and the invariance under orthogonal conjugation is required for the matrix to describe a Hamiltonian with time-reversal symmetry.

A Hamiltonian without time-reversal symmetry would be modeled by the space of Hermitian matrices with a probability distribution that is invariant under unitary transformations, which gives rise to the Gaussian unitary ensemble, or GUE. This is a collection of complex Hermitian matrices with independent Gaussian distributed elements along and above the diagonal. The third commonly studied Gaussian ensemble is the GSE, or Gaussian symplectic ensemble, which is the ensemble of matrices whose elements are Gaussian distributed quaternions. The GSE corresponds to systems with anti-unitary time-reversal symmetry.

Besides looking at properties of the spectrum, another area of study in quantum chaos considers the properties of the eigenfunctions [117, 36, 118]. A system with quantum ergodicity has wavefunctions which are equidistributed. More specifically, for a sequence of wavefunctions, there exists a dense subsequence such that the limit of the integral of some function against the square modulus of the wavefunctions over any region is equal to the integral of the function over the region, assuming normalization [108, 93]. The need for a subsequence is a result of the presence of *scars*, which are wavefunctions that are localized around a classical periodic orbit. A system is said to possess quantum unique ergodicity if all sequences of its wavefunctions are equidistributed [88, 104].

1.2.3 Quantum Graphs as a Model of Quantum Chaos

Kottos and Smilanksy were the first to propose quantum graphs as a useful model to study quantum chaos. In their seminal 1997 paper [76], they showed that the eigenvalues of the Schrödinger operator on a fully connected square graph matched the nearest-neighbor spacing distributions for the eigenvalues of the GOE and GUE as predicted by Bohigas, Giannoni and Schmit. The key innovation here is that quantum graphs possess enough complexity to exhibit the characteristics of a chaotic system, but because of their one-dimensional nature, they are also simple enough to allow for greater mathematical analysis.

To understand the underlying chaotic dynamics of a quantum graph, we may view a path on a graph as a classical trajectory. Along each edge, the one-dimensional motion is determined. However, each vertex may present multiple possible directions for the trajectory to continue, the choice of which is expressed using probability. For example, if a particular vertex is connected to d distinct edges, then a path entering that vertex may have d choices, each with probability $1/d$, for which direction it will continue. The probability does need not be equal for each choice of direction, and indeed, this will not be the case for the graphs we consider. However, these transition probabilities are independent of previous choices, which creates a Markov chain with states described by vectors indexed by the directed edges of the graph. Ergodicity on the graph implies that the probability of a trajectory ending on a particular edge of the graph is equally likely after a large number of steps. This brings to mind the idea of ergodicity as presented for dynamical billiards, where a particular trajectory will eventually cover the interior of the billiard.

Since the introduction of quantum graphs as a model for quantum chaos, their study has been applied to a wide range of topics in the field. Kottos and Smilansky [76, 77] discovered an exact trace formula for the spectrum of quantum graphs (an earlier trace formula was discovered by Roth [102] in a different context) which was

used to derive the form factor, the Fourier tranform of the two-point correlation function for the spectrum, in terms of periodic orbits on the graph. This was used to analyze the spectral statistics of several classes of graphs, including star graphs [14, 12], binary graphs [110], line graphs [94], and regular graphs [106]. In many of these cases, random matrix statistics were observed, but star graphs were a notable exception, displaying a form of intermediate statistics. Additional results for the spectral statistics on graphs have also been obtained [8, 19, 20, 10, 29, 28, 63, 26].

Quantum graphs have also been used to approach scattering problems [78, 79, 112], study quantum ergodicity and eigenfunction statistics [16, 17, 15, 51, 47, 70], and apply supersymmetric integral techniques [45, 46, 48, 49]. A thorough review of the applications of quantum graphs in quantum chaos can be found in [50].

1.3 Symmetry

1.3.1 Circulant Graphs

Since the analogy for classical chaos on a graph relies on the transition probabilities at the vertices of a graph, one might imagine that a certain amount of well-connectedness is required for the graph to be sufficiently chaotic to display random matrix statistics. Indeed, Berkolaiko and Keating showed in 1999 that the spectral statistics for quantum star graphs, one of the simplest types of graphs, did not match the predictions of random matrix theory [14], and they later showed, along with Winn, that star graphs have no quantum ergodicity [17], despite being ergodic in the classical sense. Tanner [110] proposed a conjecture in 2001 that related the agreement with random matrix statistics to the spectral gap of the transition matrix. The spectral gap is the difference between the largest and second largest eigenvalues, and the spectral gap of the adjacency matrix for a graph is often used as a measure of how well-connected a given graph is.

Another measure of the well-connectedness of a graph is the graph diameter, which is the maximum distance between two vertices on the graph. Marklof and Strömbergsson were interested in looking at the diameter of random graphs. Although this is a combinatorial graph property rather than a quantum one, it can also be said that graphs with poor connectedness, in their case cycles, behave differently than a typical graph. In many graph models, the diameter grows logarithmically with respect to an increase in the number of vertices. However, on a cycle, this quantity grows linearly. In their paper [89], Marklof and Strömbergsson considered a generalization of cycles, known as circulant graphs. These can be seen as an interconnected collection of cycles that behave much better with regards to growth in diameter.

In a similar fashion, a circulant graph can be seen as an extension of a star graph. In any graph, each vertex is locally a star graph, but in a circulant graph, every vertex is locally *the same* star graph. Additionally, circulant graphs have rotational symmetry, which is another property shared with star graphs. This allows techniques used on star graphs to be extended to circulant graphs, which we will make full use of in chapters three, four, and five of this thesis.

1.3.2 Applications of Symmetry in Quantum Graphs

Throughout much of the second half of the 20th century, many mathematicians and physicists were interested in answering the question posed by Marc Kac, "Can one hear the shape of a drum?" [69]. This is fundamentally a question of isospectrality; that is, do there exist differently shaped drums with identical spectra? In 1992, Gordon, Webb, and Wolpert [53, 54] used a method developed by Sunada [109] to construct a counterexample to Kac's original supposition, but there is still plenty of interest in the field of isospectrality.

In the early 2000s, as research in quantum graphs was beginning to flourish, a similar question was posed as to whether or not one could hear the shape of a

graph [57]. Gutkin and Smilansky showed that it was possible to hear the shape of a quantum graph under certain conditions. These conditions require a graph with incommensurate edge lengths and no loops (an edge connecting a vertex to itself) or double edges. However, when those conditions are not satisfied, many examples of isospectral graphs have been found.

Band, Parzanchevski, and Ben-Shach [7, 96] developed a method based on Sunada's that is used to construct isospectral quantum graphs. These quotient graphs are constructed using representations of finite symmetry groups on the quantum graph. The method allows one to construct isospectral graphs from graphs with symmetry groups.

Although not a question of isospectrality, Joyner, Müller, and Sieber [68] used the method of quotient graphs to construct a quantum graph which displayed GSE random matrix statistics. Previously, these statistics had only been found in systems whose wavefunctions had half-integer spin, where the time-reversal operator is anti-unitary. By constructing a quotient graph with geometric symmetry under the quaternion group, GSE statistics were obtained for a system without spin. Finding and studying the spectra of quotient graphs with symmetry based on more general finite groups is the aim of chapter six.

CHAPTER TWO

Background Information

The study of quantum graphs intersects with a wide swath of different mathematical fields. The basic concepts and terminology of graph theory, functional analysis, algebraic representation theory, and probability and statistics all make appearances, which still neglects to cover the various physical applications that can also be found. This dissertation will attempt to be as self-contained as possible, but a deep dive into all the topics represented would require volumes. So, before introducing the necessary definitions and theorems, the author would like to recommend some additional texts for the interested reader.

The definitive textbook on quantum graphs is [18] and many of the significant results in the field are referenced there. Some other useful introductory papers include [82, 83, 84, 50] and more recently [11, 6]. There are numerous texts on graph theory, but [35] provides a thorough introduction, as well as including more modern developments. For insights into the relevant subfields of algebraic graph theory and spectral graph theory, the author recommends [52] and [31], respectively.

2.1 Notions from Graph Theory

A *combinatorial graph (or graph)* Γ consists of a set of vertices $\mathcal{V} = \{v_i\}$ and a set of undirected edges $\mathcal{E} = \{e_j\}$ connecting pairs of vertices. Let $V = |\mathcal{V}|$, the number of vertices in Γ, and $E = |\mathcal{E}|$, the number of edges. Two vertices u and v are said to be *adjacent*, written $u \sim v$, if there exists an edge $e \in \mathcal{E}$ connecting them, which we will often denote by the unordered pair $\{u, v\}$. If $e \in \mathcal{E}$ is an edge connecting the vertex $v \in \mathcal{V}$ to some other vertex in $\mathcal{V}$, e is said to be *incident* to v. Denote the set of all edges incident to the vertex $v \in \mathcal{V}$ by $\mathcal{E}_v$. The *degree* of a vertex

d_v is defined as the number of edges incident to the vertex v. The *adjacency matrix* of a graph is a $V \times V$ matrix J, where

$$J_{ij} = \begin{cases} 1 & \text{if } i \sim j \\ 0 & \text{otherwise.} \end{cases} \tag{2.1}$$

A *path* on a graph can be given as a connected sequence of edges, $e_1 e_2 \dots e_m$, or vertices, $v_0 v_1 \dots v_m$, such that e_i connects v_{i-1} and v_i for all $i = 1, \dots m-1$. A *closed path* is a path in which $v_0 = v_m$; that is, the path ends on the vertex where it began. The *topological length* of a path is the number of edges in that path, m in the above example. The *topological distance* between two vertices in a graph is defined as the minimum number of edges in a path between them.

2.1.1 Directed Graphs

By assigning a direction to each edge in a graph, the graph becomes a *directed graph*, or digraph. Directed edges are often referred to as *bonds*, particularly in the physics literature, though this notation also appears elsewhere. Each bond b has an *origin vertex*, $o(b)$, and a *terminal vertex*, $t(b)$. The *reversal* of b is the bond with opposite direction, denoted $\bar{b}$. So, $o(b) = t(\bar{b})$ and $t(b) = o(\bar{b})$. Using this notation, a path on a directed graph is defined as a sequence of bonds $b_1 b_2 \dots b_m$ such that $t(b_i) = o(b_{i+1})$ for all $i = 1, \dots, m-1$, and a closed path is one in which $t(b_m) = o(b_1)$. One standard way of converting an undirected graph into a directed graph is to replace each edge with two directed bonds, b and $\bar{b}$. Unless otherwise specified, directed graphs in this dissertation are assumed to be defined in this way.

2.1.2 Metric Graphs

A combinatorial graph Γ becomes a *metric graph* $\mathcal{G}$ by assigning each edge of Γ a positive length $L_e \in (0, \infty)$. One straightforward way of obtaining a metric graph

is to embed the graph Γ in $\mathbb{R}^n$ and define the lengths of the edges as the distance between vertices in the natural way. However, we do not require that a metric graph is able to be embedded for a particular choice of edge lengths.

On a metric graph $\mathcal{G}$, an edge of length L_e can be viewed as corresponding to a closed interval $[0, L_e]$, oriented so that 0 is associated to one vertex and L_e is associated to the other. There are two possible ways of achieving this, but the chosen orientation will not affect the operators we study. We may then consider coordinates $x_e \in [0, L_e]$ on each edge in the natural way. The distance between the coordinate x_e and the vertex associated to 0 is x_e and the distance between the coordinate and the vertex associated to L_e is $L_e - x_e$. Then the *metric distance (or distance)* between any two points $x, y \in \mathcal{G}$ is defined as the minimum metric distance between them, measured along the edges of the graph.

On a directed graph where each edge has been replaced by the bonds b and $\overline{b}$, we let $L_b = L_{\overline{b}}$ in the associated metric graph. We choose to orient the interval associated to each bond b in such a way that the coordinate $x_b = 0$ at $o(b)$ and $x_b = L_b$ at $t(b)$, and similarly on the reversal $\overline{b}$, the coordinate $x_{\overline{b}} = 0$ at $o(\overline{b})$ and $x_{\overline{b}} = L_b$ at $t(\overline{b})$. This orientation is shown in figure 2.1, and consequently, x_b and $x_{\overline{b}}$ are related by $x_{\overline{b}} = L_b - x_b$, as shown.

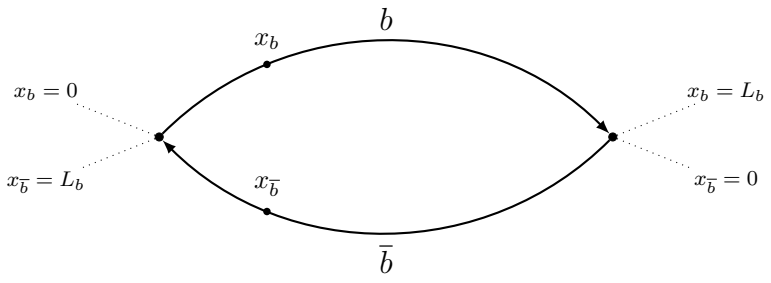

Figure 2.1. A pair of directed bonds, b and $\overline{b}$. Each bond is associated to the interval $[0, L_b]$ with opposite orientations.

If we assign a metric to a combinatorial graph in the way described in the previous section, this allows us to define functions $f_e(x_e)$ on each edge $e \in \mathcal{E}$ as functions on its associated interval. Then, functions on $\mathcal{G}$ are defined as an E-tuple of the functions f_e. In this way, a function $f(x)$ on $\mathcal{G}$ is defined at every intermediate point along each edge of the graph. From this, we can construct function spaces, such as the space of continuous functions $C(\mathcal{G})$ or the square-integrable functions, $L^2(\mathcal{G}) := \bigoplus_{e\in\mathcal{E}} L^2[0, L_e]$.

A quantum graph $(\mathcal{G}, \mathcal{H})$ is defined as a metric graph $\mathcal{G}$ equipped with a differential operator $\mathcal{H}$ acting on the functions of the graph. We will often suppress $\mathcal{H}$ in notation and refer to $\mathcal{G}$ as a quantum graph. The most commonly studied operator is the Laplace operator, or negative second derivative, acting on functions defined on each edge,

$$\mathcal{H} : \ f(x_e) \mapsto -\frac{\mathrm{d}^2 f}{\mathrm{d}x_e^2} \ . \tag{2.2}$$

Another commonly studied operator is the Schrödinger operator [74]. The magnetic Schrödinger operator acts on a directed bond b as

$$f(x_b) \mapsto -\left(\frac{\mathrm{d}}{\mathrm{d}x_b} - \mathrm{i}A_b\right)^2 f(x_b) + V(x_b)f(x_b) \ , \tag{2.3}$$

where V is an electric potential and A_b is a magnetic vector potential. Unlike the Laplace operator and general Schrödinger operator, the magnetic Schrödinger operator is dependent on the choice of direction of the bonds since $A_b = -A_{\bar{b}}$.

The chosen direction for the bonds is also relevant for the Dirac operator. All self-adjoint realizations of the Dirac operator on a metric graph were defined in [29]. The time-independent Dirac operator on an interval is

$$f(x_b) \mapsto -\mathrm{i}\hbar c\alpha \frac{\mathrm{d}f}{\mathrm{d}x_b} + mc^2\beta f(x_b) \ , \tag{2.4}$$

where α and β are matrices satisfying $\alpha^2 = \beta^2 = 1$ and $\alpha\beta + \beta\alpha = 0$, which is the Dirac algebra in one dimension.

For the remainder of this dissertation, our operator of study will be the Laplacian (2.2). In order to fully define this operator, we must assign it a domain. In our case, the set of functions on $\mathcal{G}$ must belong in the direct sum of the second Sobolev space on each edge, which we denote $\widetilde{H^2}(\mathcal{G}) = \bigoplus_{e\in\mathcal{E}} H^2[0, L_e]$. Matching conditions at the vertices, referred to as *vertex conditions*, are then chosen to complete the definition of the operator domain to make it self-adjoint. We will discuss these in detail in the next section.

2.2.1 Vertex Conditions

It is often desirable in the study of quantum graphs that vertex conditions be chosen in a way which makes the operator self-adjoint, as this lends itself naturally to applications. A standard choice for vertex conditions in this case are the *Neumann-like (or Neumann-Kirchoff) conditions*,

$$f(x) \text{ is continuous on } \mathcal{G}, \text{ and} \tag{2.5}$$

$$\forall v \in \mathcal{V}, \quad \sum_{e\in\mathcal{E}_v} \frac{\mathrm{d}}{\mathrm{d}x_e} f_e(v) = 0 \ . \tag{2.6}$$

All derivatives are assumed to be taken in the outgoing direction from v, so $\frac{\mathrm{d}}{\mathrm{d}x_e} f_e(v)$ is either $f_e'(0)$ or $-f_e'(L_e)$, depending on the chosen orientation of the edge.

Another important set of vertex conditions are the *Dirichlet conditions*. These require that

$$f_e(v) = 0 \text{ for all } v \in \mathcal{V},\ e \in \mathcal{E}_v \ . \tag{2.7}$$

The result is a decoupling of the edges of the graph, since these conditions remove any relationship between them. Despite this, Dirichlet conditions will turn out to

be relevant in the study of symmetric quantum graphs, so we will return to them in future chapters.

For the Laplace operator acting on a quantum graph, there is a complete characterization of vertex conditions which define a self-adjoint operator. These conditions are defined locally, meaning the conditions at each vertex only involve values of the function and its derivatives at the ends of the intervals incident to the vertex. In general, non-local conditions can always be made local by identifying the necessary vertices into a single vertex with local conditions. There are three equivalent characterizations of the self-adjoint vertex conditions for a quantum graph [18, 73, 43, 59]. In each of the following, we assume the statement holds for every vertex v with degree d_v of the quantum graph.

The first characterization expresses the vertex conditions at v using two $d_v \times d_v$ matrices, $\mathbb{A}_v$ and $\mathbb{B}_v$. Matching conditions at v are defined by the matrix equation

$$\mathbb{A}_v \boldsymbol{F}(v) + \mathbb{B}_v \boldsymbol{F'}(v) = 0 \ , \tag{2.8}$$

where $\boldsymbol{F}(v)$ is a vector of function values at v on each incident edge and $\boldsymbol{F'}(v)$ is a vector of the values of the corresponding derivatives at v, taken in the outgoing direction. For the vertex conditions (2.8) to define a self-adjoint Laplacian, the matrix $\mathbb{A}_v\mathbb{B}_v^*$ must be self-adjoint and the $d_v \times 2d_v$ augmented matrix $(\mathbb{A}_v|\mathbb{B}_v)$ must have maximal rank. Neumann-like vertex conditions (2.5)–(2.6) given in this way can take the form,

$$\mathbb{A}_v = \begin{pmatrix} 1 & -1 & & & \\ & 1 & -1 & & \\ & & \ddots & \ddots & \\ & & & 1 & -1 \\ 0 & & \cdots & & 0 \end{pmatrix} \qquad \mathbb{B}_v = \begin{pmatrix} 0 & & & \\ & \ddots & & \\ & & & 0 \\ 1 & \cdots & & 1 \end{pmatrix} \ , \tag{2.9}$$

where the remaining elements in $\mathbb{A}_v$ and $\mathbb{B}_v$ are zero. We can recover the Neumann-like conditions by substituting the matrices in (2.9) into (2.8). The first $d_v - 1$ equations

requires continuity at v, while the last equation requires the sum of derivatives at v to be zero.

The self-adjoint vertex conditions at v can also be defined uniquely by a $d_v \times d_v$ unitary matrix $\mathbb{U}_v$. In this case, the function must satisfy

$$\mathrm{i}(\mathbb{U}_v - \mathbb{I})\boldsymbol{F}(v) + (\mathbb{U}_v + \mathbb{I})\boldsymbol{F'}(v) = 0 \ , \tag{2.10}$$

where $\boldsymbol{F}(v)$ and $\boldsymbol{F'}(v)$ are defined in the same manner as (2.8). One can check the equivalence of these conditions by noting that the matrix $\mathbb{U}_v = -(\mathbb{A}_v - \mathrm{i}\mathbb{B}_v)^{-1}(\mathbb{A}_v + \mathrm{i}\mathbb{B}_v)$ is unitary for matrices $\mathbb{A}_v$ and $\mathbb{B}_v$ defining self-adjoint vertex conditions, and substituting this into (2.10) yields (2.8) after simplification.

Finally, we can define self-adjoint vertex conditions in terms of three orthogonal projection operators $P_{D,v}$, $P_{N,v}$, and $P_{R,v}$, where $P_{R,v} := \mathbb{I}_{d_v} - P_{D,v} - P_{N,v}$, and an invertible self-adjoint operator Λ_v. The projection operators act on the space $\mathbb{C}^{d_v}$ and Λ_v acts on the subspace $P_{R,v}\mathbb{C}^{d_v}$. Here, we require that

$$\begin{aligned} P_{D,v}\boldsymbol{F}(v) &= 0 \ , \\ P_{N,v}\boldsymbol{F'}(v) &= 0 \ , \\ P_{R,v}\boldsymbol{F'}(v) &= \Lambda_v P_{R,v}\boldsymbol{F}(v) \ . \end{aligned} \tag{2.11}$$

We refer to $P_{D,v}$ and $P_{N,v}$ as the Dirichlet and Neumann parts of the vertex conditions, respectively. $P_{R,v}$ is called the Robin part, and one can easily check that it does not appear under the Neumann-like (2.5)–(2.6) or Dirichlet conditions (2.7) described above.

One of the main objects of study in the field of quantum graphs is the spectrum of the operator associated to the quantum graph. As shorthand, we will often refer to this as the spectrum of the quantum graph. For the Laplace operator, this means we consider the set of all $\lambda = k^2$ which satisfy

$$-\frac{\mathrm{d}^2 f}{\mathrm{d}x^2} = k^2 f(x) \ . \tag{2.12}$$

The vertex conditions for a particular quantum graph will determine the eigenfunctions and corresponding eigenvalues of the quantum graph. In general, we will be using Neumann-like conditions (2.5)-(2.6), and the set of eigenvalues under these conditions will be referred to as the *Neumann spectrum*. Similarly, if we consider (2.12) with Dirichlet conditions at the vertices (2.7), we will refer to the set of eigenvalues as the *Dirichlet spectrum*.

2.2.2 Scattering Matrices

Consider a quantum graph consisting of the Laplacian and a metric graph with a single vertex v incident to a set of edges of infinite length. If all the edges of the graph are oriented so that 0 corresponds to the vertex v, then we may view the exponential function $\mathrm{e}^{-\mathrm{i}kx_e}$ on some edge e associated to $[0,\infty)$ as an incoming plane-wave which will scatter when it hits v into outgoing plane-waves $\mathrm{e}^{\mathrm{i}kx}$ along all the edges incident to v. A solution to the Laplace equation (2.12) on the interval $[0,\infty)$ can be written as a superposition of these exponential functions, so

$$\begin{cases} f_e(x_e) = \mathrm{e}^{-\mathrm{i}kx} + \sigma^{(v)}_{e,e}\mathrm{e}^{\mathrm{i}kx} & \text{on the edge } e \ , \\ f_{e'}(x_{e'}) = \sigma^{(v)}_{e',e}\mathrm{e}^{\mathrm{i}kx} & \text{on the edge } e' \neq e \ . \end{cases} \tag{2.13}$$

The $\sigma^{(v)}_{e,e}$ and $\sigma^{(v)}_{e',e}$ are scattering coefficients which determine how the incoming plane-wave scatters at the vertex v. In particular, $\sigma^{(v)}_{e,e}$ is the reflection coefficient which determines the backscattering on the edge e and $\sigma^{(v)}_{e',e}$ is the scattering amplitude from the edge e onto the edge e'. These scattering coefficients can be collected into a $d_v \times d_v$ matrix $\sigma^{(v)}(k)$ that encodes scattering at the vertex v. This matrix, known as the *vertex scattering matrix*, can be determined directly from any of the vertex

conditions (2.8), (2.10), or (2.11). This is summarized in the following lemma, given as a theorem in [18].

Lemma 2.1. *For vertex conditions on a quantum graph giving rise to a self-adjoint differential operator, the matrix $\sigma^{(v)}(k)$ is unitary, and*

I) If the vertex conditions are given in the form (2.8)*, then*

$$\sigma^{(v)}(k) = -(\mathbb{A}_v + \mathrm{i}k\mathbb{B}_v)^{-1}(\mathbb{A}_v - \mathrm{i}k\mathbb{B}_v) \ . \tag{2.14}$$

II) If the vertex conditions are given in the form (2.10)*, then*

$$\sigma^{(v)}(k) = -(\mathbb{U}_v - \mathbb{I} + k(\mathbb{U}_v + \mathbb{I}))^{-1}(\mathbb{U}_v - \mathbb{I} - k(\mathbb{U}_v + \mathbb{I})) \ . \tag{2.15}$$

III) If the vertex conditions are given in the form (2.11)*, then*

$$\sigma^{(v)}(k) = -P_{D,v} + P_{N,v} - (\Lambda_v - \mathrm{i}k)^{-1}(\Lambda_v + \mathrm{i}k)P_{R,v} \ . \tag{2.16}$$

Notice that an immediate consequence of the third part of this lemma is that $\sigma^{(v)}$ is k-independent whenever the Robin part $P_{R,v} = 0$. There are other equivalent characterizations of k-independence that can be found in [18]. For the remainder of this dissertation, our vertex conditions will contain no Robin part, and therefore the scattering matrix will be independent of k. In particular, the scattering matrix $\sigma^{(v)}$ at a vertex v with Neumann-like vertex conditions (2.9) is

$$\sigma^{(v)} = -(\mathbb{A}_v + \mathrm{i}k\mathbb{B}_v)^{-1}(\mathbb{A}_v - \mathrm{i}k\mathbb{B}_v) = \frac{2}{d_v}\mathbb{E} - \mathbb{I} \ , \tag{2.17}$$

where d_v is the degree of v and $\mathbb{E}$ is a $d_v \times d_v$ matrix of all ones.

Now let the edge e be viewed as two directed bonds b and $\overline{b}$, as described in section 2.1.1. We number the bonds $b = 1, \ldots, E$ and let $\overline{b} = b + E$. Then the *bond*

scattering matrix is the $2E \times 2E$ matrix $S(k)$ whose elements are determined by the vertex scattering matrices,

$$[S(k)]_{b'b} = \delta_{t(b),v}\delta_{o(b'),v}\sigma^{(v)}_{b',b} \ . \tag{2.18}$$

Example 2.2 (The Quantum Star Graph). A standard introductory example in the field is the quantum star graph, shown in figure 2.2, equipped with the Laplace operator and Neumann-like vertex conditions (2.5)–(2.6). The simple structure of the quantum star graph allows for easy direct computation, and we will return to this example often throughout this chapter.

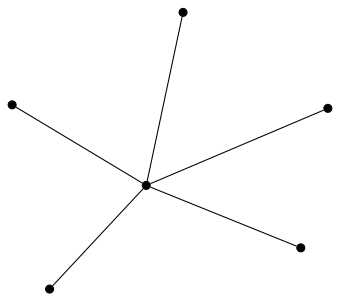

Figure 2.2. A star graph with five edges.

The bond scattering matrix for a quantum star graph can be easily derived. Neumann-like vertex conditions at the central vertex of a star graph are given by the matrices (2.9), so the vertex scattering matrix at the central vertex is $\sigma^{(v)} = \frac{2}{E}\mathbb{E} - \mathbb{I}$, as in (2.17). The scattering matrix at the outlying vertices is the 1×1 identity matrix $\sigma^{(v)} = 1$. Therefore, the bond scattering matrix for a quantum star graph is the block matrix

$$S = \begin{pmatrix} 0 & \frac{2}{E}\mathbb{E} - \mathbb{I} \\ \mathbb{I} & 0 \end{pmatrix} \ , \tag{2.19}$$

which is k-independent since the vertex conditions are Neumann-like.

2.3 Secular Equations

One way of studying the spectrum of a quantum graph is through a secular equation. A *secular equation* is an equation whose roots correspond to the eigenvalues of the quantum graph. One way of finding a secular equation is by using the scattering matrix approach, which can give a secular equation for any set of self-adjoint vertex conditions.

2.3.1 Bond Scattering Matrix Approach

Consider the solution to (2.12) along an edge e which has been replaced by two directed bonds, b and $\overline{b}$. This solution can be written as a superposition of plane-waves, one living on each of the two directed bonds,

$$f_b(x_b) = a_b \mathrm{e}^{\mathrm{i}kx_b} + a_{\overline{b}} \mathrm{e}^{\mathrm{i}kx_{\overline{b}}} \ . \tag{2.20}$$

The plane-wave $\mathrm{e}^{\mathrm{i}kx_b}$ is outgoing with respect to the vertex $o(b)$, and $\mathrm{e}^{\mathrm{i}kx_{\overline{b}}}$ is outgoing with respect to the vertex $o(\overline{b})$. However, these bonds are associated to the same edge e, so their coordinates are related by $x_{\overline{b}} = L_b - x_b$. Thus, $f_b(x_b)$ may be written

$$\begin{aligned} f_b(x_b) &= a_b \mathrm{e}^{\mathrm{i}kx_b} + a_{\overline{b}} \mathrm{e}^{\mathrm{i}kL_b - x_b} \\ &= a_b \mathrm{e}^{\mathrm{i}kx_b} + \mathrm{e}^{\mathrm{i}kL_b} a_{\overline{b}} \mathrm{e}^{-\mathrm{i}kx_b} \ . \end{aligned} \tag{2.21}$$

For some vertex v, let $\boldsymbol{\alpha}$ be a vector of the coefficients for the outgoing plane-waves relative to v. This means that, for every edge $e \in \mathcal{E}_v$ which has been replaced with the directed bonds b and $\overline{b}$, either $v = o(b)$, in which case a_b is the outgoing coefficient, or $v = o(\overline{b})$, in which case $a_{\overline{b}}$ is the outgoing coefficient. Similarly, let $\boldsymbol{\beta}$ be a vector of the coefficients for the incoming plane-waves relative to v. That is, if $v = t(b)$, then $\mathrm{e}^{\mathrm{i}kL_b} a_b$ is the incoming coefficient, and if $v = t(\overline{b})$, then the incoming coefficient is $\mathrm{e}^{\mathrm{i}kL_b} a_{\overline{b}}$. Then these vectors are related via the vertex scattering matrix

by

$$\boldsymbol{\alpha} = \sigma^{(v)}(k)\boldsymbol{\beta} \ . \tag{2.22}$$

Noting that the outgoing amplitudes at one vertex correspond to the incoming amplitudes at another vertex, we may collect these in a single vector $\boldsymbol{\gamma}$ of all $2E$ coefficients,

$$\boldsymbol{\gamma} = (a_1, \ldots, a_E, a_{\overline{1}}, \ldots, a_{\overline{E}})^T \ . \tag{2.23}$$

Then for $\boldsymbol{\gamma}$ to define an eigenfunction on the graph, it must satisfy

$$\boldsymbol{\gamma} = S(k)\mathrm{e}^{\mathrm{i}k\mathbf{L}}\boldsymbol{\gamma} \ , \tag{2.24}$$

where $S(k)$ is the bond scattering matrix (2.18) and $\mathbf{L}$ is a diagonal matrix of the edge lengths,

$$\mathbf{L} = \begin{pmatrix} L_1 & & & & & \\ & \ddots & & & & \\ & & L_E & & & \\ & & & L_1 & & \\ & & & & \ddots & \\ & & & & & L_E \end{pmatrix} \ . \tag{2.25}$$

Non-trivial solutions to (2.24) are found by solving

$$\det(\mathbb{I} - S(k)\mathrm{e}^{\mathrm{i}k\mathbf{L}}) = 0 \ , \tag{2.26}$$

which is a secular equation for the quantum graph. If the bond scattering matrix S is k-independent, the secular equation ensures that one can find the eigenvalues of the quantum graph with correct multiplicity. The following theorem was given as several theorems with associated proofs in [18].

Theorem 2.3. *Consider the eigenvalue problem for the operator $\mathcal{H}$ acting as $-\frac{\mathrm{d}^2}{\mathrm{d}x_e^2}$ on each edge e of a metric graph $\mathcal{G}$ with finitely many edges. The operator domain consists of functions belonging to $\widetilde{H^2}(\mathcal{G})$ which satisfy self-adjoint vertex conditions*

given in one of the forms (2.8), (2.10), *or* (2.11). *If the vertex conditions have no Robin part, then* $k^2 \in \mathbb{C} \setminus \{0\}$ *is an eigenvalue with multiplicity* m *if and only if* k *is a root of* (2.26) *with the same multiplicity.*

The agreement of the multiplicities relies on the fact that linearly independent vectors $\boldsymbol{\gamma}$ in (2.24) uniquely define linearly independent eigenfunctions of (2.12) on $\mathcal{G}$. Because the matrix $S(k)\mathrm{e}^{\mathrm{i}k\mathbf{L}}$ is unitary, $\mathbb{I} - S(k)\mathrm{e}^{\mathrm{i}k\mathbf{L}}$ is diagonalizable, so the dimension of its nullspace is equal to the algebraic multiplicity of 0 as its eigenvalue. This in turn corresponds to the multiplicity of a root of the secular equation (2.26).

Example 2.4 (The Quantum Star Graph Revisited). Consider the quantum star graph with E edges as described in example 2.2. The bond scattering matrix is

$$S = \begin{pmatrix} 0 & \frac{2}{E}\mathbb{E} - \mathbb{I} \\ \mathbb{I} & 0 \end{pmatrix} , \tag{2.27}$$

as in (2.19), and consequently the secular equation may be written as

$$\det \begin{pmatrix} \mathbb{I} & (\mathbb{I} - \frac{2}{E}\mathbb{E})\mathrm{e}^{\mathrm{i}k\mathbf{L}} \\ -\mathrm{e}^{\mathrm{i}k\mathbf{L}} & \mathbb{I} \end{pmatrix} = 0 . \tag{2.28}$$

Simplification via row operations, determinant identities, and multiplication by the non-zero factor $\det \mathrm{e}^{\mathrm{i}k\mathbf{L}}$ ultimately yields

$$\left(\sum_{j=1}^{E} \tan(kL_j) \right) \prod_{j=1}^{E} \cos(kL_j) = 0 , \tag{2.29}$$

which is a secular equation for the quantum star graph equipped with the Laplace operator and Neumann-like vertex conditions.

2.3.2 Direct Application of Vertex Conditions

Although the bond scattering matrix derivation of a secular equation applies very broadly to any quantum graph with given self-adjoint vertex conditions, in prac-

tice this version of the secular equation can be difficult to analyze for large or complicated graphs. However, by placing restrictions on the vertex conditions or considering particular classes of discrete graphs, different techniques can be used to find alternative forms of the secular equation, which are simpler and more amenable to analysis. This has been done for quantum star graphs, where a direct application of the vertex conditions yields a simpler form of the secular equation. We will utilize this technique extensively in future chapters, but here we provide the star graph example to illustrate the basics of the method.

Consider the eigenvalue equation on each edge of the star graph,

$$-\frac{\mathrm{d}^2 f_e}{\mathrm{d}x_e^2} = k^2 f_e(x_e) \ , \tag{2.30}$$

whose solutions can be written as

$$f_e(x_e) = A_e \sin kx_e + B_e \cos kx_e \ . \tag{2.31}$$

If we choose an edge orientation so that L_e is associated to the central vertex along each edge e, the vertex conditions (2.5)–(2.6) can be written,

$$f_e(L_e) = \phi \text{ for some constant } \phi \text{ and } \forall e \in \mathcal{E} \ , \tag{2.32}$$

$$f_e'(0) = 0 \text{ at each peripheral vertex} \ , \tag{2.33}$$

$$\sum_{j=1}^{E} f_j'(L_j) = 0 \ . \tag{2.34}$$

Applying condition (2.33) to (2.31) requires $A_e = 0$. Assuming that $\cos kL_e \neq 0$, we can evaluate the f_e at the central vertex and use continuity (2.32) to solve for $B_e = \phi \sec kL_e$, so

$$f_e(x_e) = \phi \sec kL_e \cos kx_e \ , \tag{2.35}$$

where ϕ is some constant representing the value of the function on the quantum graph at the central vertex.

To get a secular equation, we can sum the derivatives along each of the edges evaluated at the central vertex, as in condition (2.34), to obtain

$$\sum_{j=1}^{E} \tan kL_j = 0 \ . \tag{2.36}$$

It is assumed that $k \neq 0$, as this is a trivial eigenvalue, and $\phi \neq 0$, which would be equivalent to Dirichlet conditions at the central vertex.

Notice that (2.36) agrees with (2.29), except that the latter includes the term $\prod_{j=1}^{E} \cos(kL_j)$. Recall that the derivation of (2.36) required the assumption that $\cos kL_e \neq 0$ for any L_e, which corresponds to the case where $\phi = 0$. Treating this case separately, the Neumann-like condition (2.34) at the central vertex implies k^2 is an eigenvalue of multiplicity $m-1$ whenever k is a pole of m of the tan functions. The secular equation (2.29) makes this case explicit, but (2.36) obtains the majority of the spectrum. In fact, when the edge lengths are incommensurate, all the eigenvalues can be found from (2.36).

2.4 Weyl's Law

A *spectral counting function* is a function which counts the total number of eigenvalues less than some parameter λ. In 1911 [115], Herman Weyl described the asymptotic behavior of the spectral counting function for the Laplace-Beltrami operator with Dirichlet boundary conditions on some bounded domain in $\mathbb{R}^n$ as the parameter λ approaches infinity. It is now common in spectral theory to refer to similar results for any differential operator as a Weyl law.

For the spectrum of a quantum graph, it is often useful to count the roots of the secular equation, $k = \sqrt{\lambda}$, instead of the eigenvalues of the graph since the set

of values k on an interval grows linearly with the size of the interval. The function $N(a,b)$ which counts the roots in (a,b) will be referred to as an algebraic counting function. Spectral counting functions for quantum graphs appear in [76, 77, 50]. The simplified proof provided here appears in [18], but it was first given in [56] and requires the following lemma from [18]

Lemma 2.5. *For a unitary matrix S and matrix $S\mathrm{e}^{\mathrm{i}k\mathbf{L}}$ with eigenvalues $\mathrm{e}^{\mathrm{i}\theta(k)}$ and corresponding normalized eigenvectors $\boldsymbol{u}(k)$,*

$$\frac{\mathrm{d}\theta}{\mathrm{d}k} = \langle \boldsymbol{u}(k), \mathbf{L}\boldsymbol{u}(k)\rangle \ . \tag{2.37}$$

Consequently, $\theta(k)$ is increasing as a function of k.

Theorem 2.6 (Weyl's Law for Quantum Graphs). *Let $N(a,b)$ be the algebraic counting function of a quantum graph with non-Robin boundary conditions. Then,*

$$N(a,b) = \frac{\mathcal{L}}{\pi}(b-a) + r \tag{2.38}$$

where $\mathcal{L} = L_1 + L_2 + \cdots + L_e$ and r is uniformly bounded in a, b.

Proof. Suppose that $0 \notin (a,b)$ and let $\mathrm{e}^{\mathrm{i}\theta_j(k)}$ be the eigenvalues of $S\mathrm{e}^{\mathrm{i}k\mathbf{L}}$. Then each eigenvalue of the quantum graph corresponds to a phase $\theta_j(k) = 2m\pi$ for some $m \in \mathbb{Z}$. These phases are increasing and we can count the eigenvalues from each of the j phases individually,

$$\frac{1}{2\pi}(\theta_j(b) - \theta_j(a)) - 1 \leq N_j(a,b) \leq \frac{1}{2\pi}(\theta_j(b) - \theta_j(a)) + 1 \ , \tag{2.39}$$

where $N_j(a,b)$ is the algebraic counting function associated to the phase $\theta_j(k)$. This difference of phases can be written as an integral,

$$|N_j(a,b)| \leq \frac{1}{2\pi}\int_a^b \frac{\mathrm{d}\theta_j}{\mathrm{d}k}\,\mathrm{d}k + 1\ , \tag{2.40}$$

so summing over all j phases,

$$\begin{aligned} |N(a,b)| &\leq \frac{1}{2\pi}\int_a^b \sum_{j=1}^{2E} \frac{\mathrm{d}\theta_j}{\mathrm{d}k}\,\mathrm{d}k + 2E \\ &\leq \frac{1}{2\pi}\int_a^b \sum_{j=1}^{2E} \langle \boldsymbol{u_j}, \mathbf{L}\boldsymbol{u_j}\rangle\,\mathrm{d}k + 2E \\ &\leq \frac{1}{2\pi}\int_a^b \mathrm{Tr}(\mathbf{L})\,\mathrm{d}k + 2E \\ &\leq \frac{\mathcal{L}}{\pi}(b-a) + 2E\ . \end{aligned} \tag{2.41}$$

Alternatively, we may write

$$N(a,b) = \frac{\mathcal{L}}{\pi}(b-a) + r \tag{2.42}$$

where r is an error term such that $|r| \leq 2E$. □

2.5 Quotient Graphs

In [7, 96] Band, Parzanchevski, and Ben-Shach introduced a method for constructing isospectral graphs using representations of symmetric groups acting on the graph. Joyner, Müller, and Sieber [68] applied this method to construct a quantum graph which displayed GSE statistics without introducing spin. This method will be used in chapter three (see 3.3.2) and extensively in chapter six.

2.5.1 Preliminaries

A *symmetry of a quantum graph* is an automorphism of the metric graph which preserves both the edge lengths and vertex conditions with respect to the symmetry group G. For a quantum graph with Neumann-like vertex conditions and

the Laplacian, we will denote the eigenspace of the graph with eigenvalue λ as

$$\Phi(\lambda) = \ker(\mathcal{H} - \lambda\mathbb{I}) \ . \tag{2.43}$$

A left action of the symmetry group G on $\mathcal{G}$ induces an action of G on the function space $\widetilde{H^2}(\mathcal{G})$ by

$$(\sigma f)(x) = f(\sigma^{-1}x) \ , \tag{2.44}$$

for all $\sigma \in G$. The eigenspace $\Phi(\lambda)$ can be decomposed into subspaces $\Phi_j(\lambda)$ each transforming according to an irreducible representation $\mathcal{R}_j$,

$$\Phi(\lambda) = \sum_{j=1}^{s} \Phi_j(\lambda) \ . \tag{2.45}$$

A *fundamental domain* is a subset of the graph which generates the whole graph under the action of the symmetry group. When determining the fundamental domain, it is sometimes useful to add *dummy vertices* to the graph. These are vertices of degree two with Neumann-like conditions which can be introduced at any point (usually the midpoint) of an interval without changing the graph spectrum. We let $\widetilde{\mathcal{G}}$ denote the graph $\mathcal{G}$ with added dummy vertices. A *quotient graph* $\mathcal{G}/\mathcal{R}$ with respect to some D-dimensional irreducible representation $\mathcal{R}$ of the symmetry group G is then constructed from D copies of the fundamental domain. Some identification among the vertices of the copies of the fundamental domain is done in such a way that the eigenspace of the quotient graph is isomorphic to the subspace of the eigenspace of $\mathcal{G}$ which transforms according to the representation $\mathcal{R}$.

2.5.2 Construction of a Quotient Graph

Let $\mathcal{G}$ be the graph given in figure 2.3(a) with Neumann-like vertex conditions and edge lengths L_1, L_2, and L_3, as shown. Consider the group of rotations of the

square generated by counterclockwise rotation by $\pi/2$, denoted σ,

$$G = \langle \sigma \rangle = \{\iota, \sigma, \sigma^2, \sigma^3\} \ , \tag{2.46}$$

where here ι is the group identity element. A one-dimensional representation $\mathcal{R}$ of G is

$$\mathcal{R} : \{\iota \mapsto (1), \quad \sigma \mapsto (\mathrm{i}), \quad \sigma^2 \mapsto (-1), \quad \sigma^3 \mapsto (-\mathrm{i})\} \ . \tag{2.47}$$

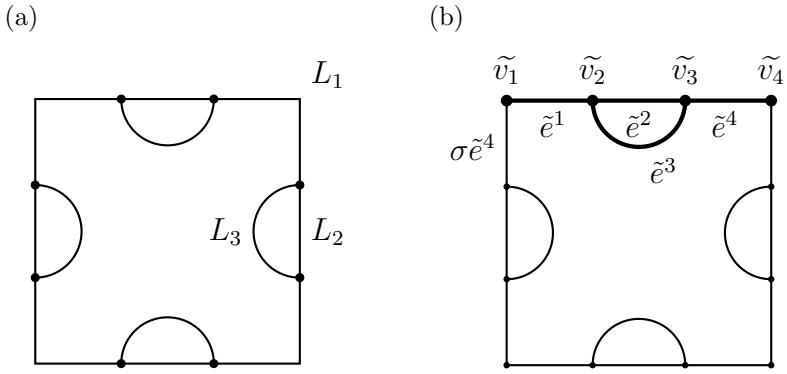

Figure 2.3. (a) The graph $\mathcal{G}$ with edge lengths L_1, L_2, and L_3; (b) the graph $\widetilde{\mathcal{G}}$ with fundamental domain shown in bold and representatives for the edge and vertex orbits.

We construct the quotient graph $\mathcal{G}/\mathcal{R}$, shown in figure 2.4, as follows. First, identify a fundamental domain under the group action of G on the graph. This will consist of one fourth of the graph $\widetilde{\mathcal{G}}$ with dummy vertices. For example, figure 2.3(b) depicts one option for a fundamental domain where dummy vertices have been added at the four corners of the square. For some $\lambda \in \mathbb{C}$, let $\widetilde{f}$ be a function on $\widetilde{\mathcal{G}}$ in the eigenspace of λ which transforms according to the irreducible representation $\mathcal{R}$, and consider the action of the elements of G on the function $\widetilde{f}$.

By (2.47), we know the group action of σ implies $\sigma\widetilde{f} = \mathrm{i}\widetilde{f}$. Neumann-like vertex conditions at $\widetilde{v_1}$ then imply that

$$\widetilde{f}_{\tilde{e}^1}(\widetilde{v_1}) = \widetilde{f}_{\sigma\tilde{e}^4}(\widetilde{v_1}) = \mathrm{i}\widetilde{f}_{\tilde{e}^4}(\widetilde{v_4}) \ , \tag{2.48}$$

$$\widetilde{f}'_{\tilde{e}^1}(\widetilde{v_1}) = \widetilde{f}'_{\sigma\tilde{e}^4}(\widetilde{v_1}) = \mathrm{i}\widetilde{f}'_{\tilde{e}^4}(\widetilde{v_4}) \ . \tag{2.49}$$

This suggests that we should identify $\widetilde{v_1}$ and $\widetilde{v_4}$ as the vertex v_1 in the quotient graph with vertex conditions,

$$f_{e^1}(v_1) = \mathrm{i}f_{e^4}(v_1) \ , \tag{2.50}$$

$$f'_{e^1}(v_1) + \mathrm{i}f'_{e^4}(v_1) = 0 \ , \tag{2.51}$$

where f is now a function on the quotient graph $\mathcal{G}/\mathcal{R}$. The vertices v_2 and v_3 retain the Neumann-like vertex conditions of their predecessors $\widetilde{v_2}$ and $\widetilde{v_3}$. The final form of the quotient graph $\mathcal{G}/\mathcal{R}$ is shown in figure 2.4. The edge e^2 has length L_2, the edge e^3 has length L_3, and the edges e^1 and e^4 have length $L_1/2$. Conditions at the vertex v_1 multiply by a phase factor of i, while the vertices v_2 and v_3 have standard Neumann-like vertex conditions.

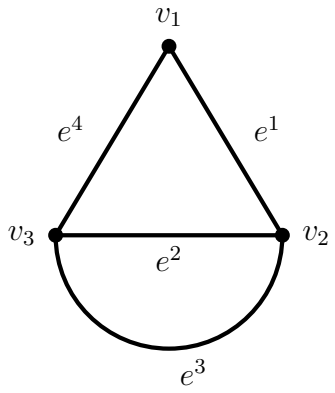

Figure 2.4. The quotient graph $\mathcal{G}/\mathcal{R}$.

2.6 Spectral Statistics

In 1977, Berry and Tabor [22] conjectured that the spectrum of a quantum system corresponding to a system with integrable classical dynamics behaves like a collection of independent random variables. More specifically, statistics of the spac-

ings between adjacent eigenvalues are modeled by a Poisson distribution. On the other hand, for systems whose classical dynamics are chaotic, the BGS conjecture [27] tells us that we should expect to see spectral statistics which match the predictions of random matrix theory.

Despite what one might expect, not all systems classify neatly into these two mutually exclusive categories. These conjectures are understood to hold generically, as there exist counter-examples for each case, see [22] for the former and [24, 87] for the latter. Additionally, there are many different systems which are said to exhibit *intermediate statistics*, as they fall somewhere between the extremes of Poisson and Gaussian statistics. One such example is the quantum star graph, which displays intermediate statistics of the same type as a rectangular billiard perturbed by a point singularity [12, 14]. In this section, we will give background on the basics of random matrix theory, which will be used in chapter four.

2.6.1 Random Matrices

A *random matrix* is a matrix whose elements are random variables. Generally, the elements are assumed to be independent and identically-distributed, but often conditions on the structure of the matrix, such as the requirement that the matrix be symmetric, will cause certain elements to be correlated. We are typically interested in considering a collection of random matrices whose elements are governed by the same probability distribution. This collection is referred to as a *random matrix ensemble*. There are many different ensembles studied in random matrix theory (RMT), see for example [91, 4], but in the study of quantum chaos, the three primary ensembles of interest are the Gaussian ensembles, so called because their elements are determined by a Gaussian distribution. It turns out, however, that the probability densities for these three ensembles can be entirely determined by considering two conditions on the set of matrices which arise from their applications to quantum physics [58]. These con-

ditions are independently distributed elements in the upper triangular portion of the matrix and an invariant probability distribution under some class of transformations.

To illustrate this, we will construct the probability density function $\rho(H)$ for a 2×2 matrix H in the Gaussian orthogonal ensemble, or GOE. In many respects, this is the simplest of the Gaussian ensembles and is also the one which we will be primarily considering in chapter four. We require H to be symmetric and have real-valued elements, H_{11}, H_{22}, and H_{12}. The construction relies entirely on the assumption that the three matrix elements are independent,

$$\rho(H) = \rho(H_{11})\rho(H_{22})\rho(H_{12}) \tag{2.52}$$

and that $\rho(H)$ is invariant under orthogonal transformation. That is, for some orthogonal matrix Q,

$$\rho(H) = \rho(QHQ^T) \ . \tag{2.53}$$

Let us consider an infinitesimal orthogonal matrix viewed as rotation by the infinitesimal angle Θ. More precisely, $\Theta = \mathrm{O}(\epsilon)$ where $\epsilon \ll 1$. So then

$$Q = \begin{pmatrix} 1+\mathrm{O}(\epsilon^2) & -\Theta+\mathrm{O}(\epsilon^2) \\ \Theta+\mathrm{O}(\epsilon^2) & 1+\mathrm{O}(\epsilon^2) \end{pmatrix} \tag{2.54}$$

and the transformation $\widetilde{H} = QHQ^T$ results in

$$\widetilde{H} = \begin{pmatrix} H_{11}-2\Theta H_{12}+\mathrm{O}(\epsilon^2) & H_{12}+\Theta(H_{11}-H_{22})+\mathrm{O}(\epsilon^2) \\ H_{12}+\Theta(H_{11}-H_{22})+\mathrm{O}(\epsilon^2) & H_{22}+2\Theta H_{12}+\mathrm{O}(\epsilon^2) \end{pmatrix} \ . \tag{2.55}$$

From equations (2.52)–(2.53), we see that

$$\rho(H) = \rho(\widetilde{H}) = \rho(\widetilde{H}_{11})\rho(\widetilde{H}_{22})\rho(\widetilde{H}_{12}) \ , \tag{2.56}$$

which implies

$$\rho(H) = \rho(H)\left\{1 - \Theta\left(2H_{12}\frac{\rho'(H_{11})}{\rho(H_{11})} - 2H_{12}\frac{\rho'(H_{22})}{\rho(H_{22})} - (H_{11} - H_{22})\frac{\rho'(H_{12})}{\rho(H_{12})}\right) + \mathrm{O}(\epsilon^2)\right\} . \tag{2.57}$$

The coefficient of Θ must vanish, which yields three differential equations for $\rho(H_{11})$, $\rho(H_{22})$, and $\rho(H_{12})$. Solving these gives a probability density function of the form

$$\rho(H) = C\exp(-A\,\mathrm{Tr}\,H^2) . \tag{2.58}$$

The $N \times N$ Gaussian orthogonal ensemble is described by the probability density function

$$\rho(H) = C\mathrm{e}^{-(N\,\mathrm{Tr}\,H^2)/4} , \tag{2.59}$$

with normalization constant C.

The Gaussian unitary ensemble (GUE) and the Gaussian symplectic ensemble (GSE) can be derived in a similar fashion, see [58]. The $N \times N$ Gaussian unitary ensemble is the space of $N \times N$ complex-valued Hermitian matrices governed by the probability density function

$$\rho(H) = C\mathrm{e}^{-(N\,\mathrm{Tr}\,H^2)/2} , \tag{2.60}$$

with normalization constant C. Matrices in the GUE are invariant under unitary transformations. The $N \times N$ Gaussian symplectic ensemble consists of $N \times N$ block matrices composed of quaternions. Matrices in this ensemble are invariant under symplectic transformation and are governed by the probability density function

$$\rho(H) = C\mathrm{e}^{-(N\,\mathrm{Tr}\,H^2)} , \tag{2.61}$$

with normalization constant C.

When comparing the spectral statistics of some quantum system to the various ensembles of random matrices, one is often interested in the distribution of the normalized spacings between eigenvalues. In order to compare the statistics for sets of eigenvalues with different average spacings, we unfold the spectra so that the mean spacing is one. One of the main statistics considered is the *nearest-neighbor spacing statistic*. This is the probability density of the distance between pairs of adjacent eigenvalues. Wigner computed this quantity for the 2×2 random matrix ensembles:

$$P_W(s) = \begin{cases} \frac{\pi}{2} s \mathrm{e}^{-s^2\pi/4} & \text{GOE matrices ,} \\ \frac{32}{\pi^2} s^2 \mathrm{e}^{-s^2 4/\pi} & \text{GUE matrices ,} \\ \frac{2^{18}}{3^6 \pi^3} s^4 \mathrm{e}^{-s^2 64/9\pi} & \text{GSE matrices .} \end{cases} \tag{2.62}$$

These are called the Wigner surmises [116] and are plotted in figure 2.5 along with the nearest-neighbor spacing distribution for a Poissonian random process. Wigner surmised that these were the actual density functions for all $N \times N$ Gaussian ensembles, but it was shown by Mehta [90] that this is not the case. Despite this, the Wigner surmises provide an excellent approximation, with an error less than 10^{-3} in the limit $N \to \infty$.

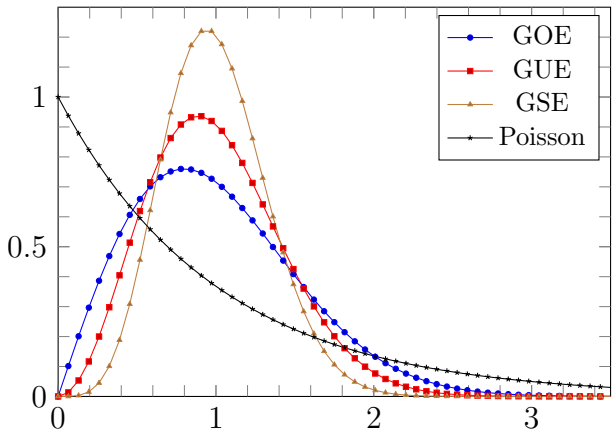

Figure 2.5. The Wigner surmises for the nearest-neighbor spacing distributions of the three Gaussian ensembles of random matrices and the Poisson distribution.

CHAPTER THREE

Quantum Circulant Graphs

3.1 Circulant Graphs

Circulant graphs, the Cayley graphs of cyclic groups, possess a high degree of symmetry which naturally extend the star graph examples introduced in the previous chapter. Although a secular equation for a quantum graph can be defined from the bond scattering matrix, equation (2.26), we can formulate an alternative secular equation using the vertex conditions directly, as we did for a quantum star graph in section 2.3.2.

There are several equivalent characterizations of circulant graphs, as seen in [37, 3, 23, 21, 114, 66, 92]. In a Cayley graph, every element of the group $\sigma \in G$ is assigned a vertex. Then, for some finite generating set Ω, edges correspond to the pairs of vertices $(\sigma, \sigma\tau)$ and $(\sigma, \sigma\tau^{-1})$ for $\sigma \in G$ and $\tau \in \Omega$. For a circulant graph with n vertices, we consider the group $\mathbb{Z}/n\mathbb{Z} = \mathbb{Z}_n$ as the set of integers $\{0, \ldots, n-1\}$ with group operation addition modulo n. For example, the circulant graphs in figure 3.1 are Cayley graphs of the cyclic groups $\mathbb{Z}_6$, $\mathbb{Z}_{10}$, and $\mathbb{Z}_{13}$, with generating sets $\{1, 2\}$, $\{2, 4, 5\}$, and $\{1, 3, 4\}$, respectively.

A second definition of a circulant graph is a graph that can be inscribed inside a regular polygon, such that the graph's vertices lie at the polygon's corners and every rotational symmetry of the polygon is also a symmetry of the inscribed graph. So a cyclic permutation of the vertices of a circulant graph is a graph automorphism. In figure 3.1, one sees that the first circulant graph can be inscribed in a regular 6-gon, the second in a regular 10-gon, and the third in a regular 13-gon.

Our primary definition of a circulant graph is more constructive and motivated by the one used in [89]. A circulant graph with n vertices, labeled $v = 1, \ldots, n$, is

defined by a vector $\boldsymbol{a} = (a_1, \ldots, a_d)$ such that

$$0 < a_1 < a_2 < \cdots < a_d < n/2 \; . \tag{3.1}$$

In general, it is possible that $a_d = n/2$, resulting in a double-edge, but we will assume this is not the case for circulant graphs that we study. For vertices $u, v \in \mathcal{V}$, we say that $u \sim v$ if and only if $|u - v| \equiv a_h \pmod{n}$ for some $a_h \in \boldsymbol{a}$. When $a_d < n/2$, each vertex v has d incoming edges, connecting to vertices $v - a_h \pmod{n}$, and d outgoing edges to vertices $v + a_h \pmod{n}$, so these circulant graphs are $2d$-regular. We use the notation $C_n(\boldsymbol{a})$ for a circulant graph with n vertices defined by the vector $\boldsymbol{a}$. Figure 3.1 shows the circulant graphs $C_6(1, 2)$, $C_{10}(2, 4, 5)$, and $C_{13}(1, 3, 4)$.

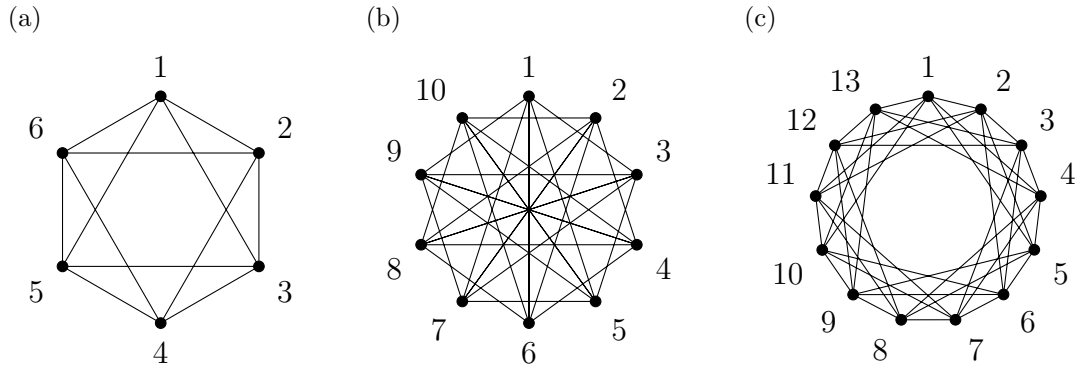

Figure 3.1. Examples of circulant graphs: (a) the circulant graph $C_6(1, 2)$; (b) the circulant graph $C_{10}(2, 4, 5)$ with double edge; (c) the circulant graph $C_{13}(1, 3, 4)$.

Without loss of generality, we will assume all circulant graphs that we study are connected. The following lemma gives a necessary and sufficient condition for circulant graphs to be connected.

Lemma 3.1. *$C_n(\boldsymbol{a})$ is connected if and only if* $\gcd(a_1, \ldots, a_d, n) = 1$.

Proof. For the purposes of this proof, we relabel the vertex n as 0, so the vertices of $C_n(\boldsymbol{a})$ are $\mathcal{V} = \{0, 1, \ldots, n-1\}$. Let $\gcd(a_1, \ldots, a_d, n) = g$. Then, by a generalization

of Bézout's identity (see for example [64]), there exist integers $x_0, x_1, \ldots, x_d$ such that

$$nx_0 + a_1x_1 + a_2x_2 + \cdots + a_dx_d = g \tag{3.2}$$

and g is the smallest integer of this form. Additionally, every number that can be written like the left-hand side of (3.2) is a multiple of g. By definition, a path in $C_n(\boldsymbol{a})$ from vertex u to vertex v must satisfy

$$v - u \equiv \sum_{h=1}^{d} \beta_h a_h \pmod{n} , \tag{3.3}$$

where β_h are integers. Note that, if $\beta_h = 0$ for all h, then $u = v$ and the path is closed.

Suppose that $g = 1$. Then for any v, there exist integers $x_0, x_1, \ldots, x_d$ such that

$$nx_0v + a_1x_1v + a_2x_2v + \cdots + a_dx_dv = v . \tag{3.4}$$

This is equivalent to (3.3) for $u = 0$ and $\beta_h = x_hv$, so there exists a path from 0 to any vertex v, since v was arbitrary. This implies that there exists a path from any vertex v_1 to any vertex v_2, as we can always choose the path through 0, so $C_n(\boldsymbol{a})$ is connected.

Suppose that $g \neq 1$. For an arbitrary vertex v, a path from 0 to v has the form (3.3), or equivalently

$$mn + \beta_1a_1 + \beta_2a_2 + \cdots + \beta_da_d = v . \tag{3.5}$$

Since this equation has the form of (3.2), v must be a multiple of g. For $C_n(\boldsymbol{a})$ to be connected, every $v = 1, \ldots, n-1$ must be a multiple of g, which is only possible if $g = 1$. □

Another significant characterization of circulant graphs involves their adjacency matrices. The adjacency matrix of a circulant graph is a circulant matrix [37].

Definition 3.2. An $N \times N$ *circulant matrix* C is uniquely determined by a row vector $\boldsymbol{c} = (c_1, \ldots, c_N)$, which becomes the first row of C. Every subsequent row of C is a cyclic permutation of $\boldsymbol{c}$, with each element moved one place to the right relative to the previous row,

$$C = \begin{pmatrix} c_1 & c_2 & \cdots & c_N \\ c_N & c_1 & \cdots & c_{N-1} \\ \vdots & \vdots & \ddots & \vdots \\ c_2 & c_3 & \cdots & c_1 \end{pmatrix} . \tag{3.6}$$

The highly symmetric and simple structure of circulant matrices gives them many useful properties. In particular, we can write the determinant of a circulant matrix as a product of polynomials whose coefficients are the elements of the row vector that uniquely defines the matrix. The following definitions and results are from [32].

Definition 3.3. The *representer* of a circulant matrix C, where C is uniquely defined by $\boldsymbol{c} = (c_1, \ldots, c_N)$, is the polynomial

$$p(z) = c_1 + c_2 z + \cdots + c_N z^{N-1} . \tag{3.7}$$

Theorem 3.4. *Let C be an $N \times N$ circulant matrix with representer $p(z)$ as in* (3.7)*. Then the determinant of C is given by*

$$\det C = \prod_{j=1}^{N} p\left(\omega^{j-1}\right) , \tag{3.8}$$

where $\omega = \exp(2\pi \mathrm{i}/N)$ is the N^{th} primitive root of unity.

When the circulant matrix is a real-valued matrix, as will be true in our case, this determinant formula simplifies further.

Corollary 3.5. *Let C be a circulant matrix as given in theorem 3.4. If the elements of $\boldsymbol{c}$ are real-valued, the determinant of C can be written as*

$$\det C = \begin{cases} p(1) \displaystyle\prod_{j=1}^{(N-1)/2} \left|p\left(\omega^j\right)\right|^2 & \text{when } N \text{ is odd}\ , \\ p(1)p(-1) \displaystyle\prod_{j=1}^{(N/2)-1} \left|p\left(\omega^j\right)\right|^2 & \text{when } N \text{ is even}\ . \end{cases} \tag{3.9}$$

Proof. Notice that $\omega^0 = 1$, so

$$\det C = p(1) \prod_{j=1}^{N-1} p\left(\omega^j\right)\ . \tag{3.10}$$

Suppose N is odd. Splitting the product at $j = (N-1)/2$ and letting $j' = N - j$,

$$\begin{aligned} \prod_{j=1}^{N-1} p\left(\omega^j\right) &= \prod_{j=1}^{(N-1)/2} p\left(\omega^j\right) \prod_{j=(N+1)/2}^{(N-1)} p\left(\omega^j\right) \\ &= \prod_{j=1}^{(N-1)/2} p\left(\omega^j\right) \prod_{j'=1}^{(N-1)/2} p\left(\omega^{N-j'}\right)\ . \end{aligned} \tag{3.11}$$

Since $\omega^{N-j'} = \overline{\omega^{j'}}$ and $p\left(\overline{\omega^{j'}}\right) = \overline{p\left(\omega^{j'}\right)}$ when the coefficients of p are real-valued, we have

$$\det C = p(1) \prod_{j=1}^{(N-1)/2} \left|p\left(\omega^j\right)\right|^2\ , \tag{3.12}$$

when N is odd. The case where N is even follows similarly. □

An undirected circulant graph can be given direction (see 2.1.1) in a very natural way. For $v - u \equiv a_h \pmod n$, $h \in \{1, \ldots, d\}$, denote the directed edge from u to v as (u, v). Assign the length $L_{u,v}$ to the edge $(u, v) \in \mathcal{E}$ so that $[0, L_{u,v}]$ is the associated interval. We choose an orientation on the edges which matches the direction of (u, v) described above. So then 0 corresponds to the vertex u and $L_{u,v}$ corresponds to v. A circulant graph endowed with this metric will be denoted $C_n(\boldsymbol{L}; \boldsymbol{a})$.

3.2 Quantum Circulant Graphs

We are interested in identifying the spectrum of quantum circulant graphs $C_n(\boldsymbol{L};\boldsymbol{a})$ equipped with the Laplace operator and Neumann-like vertex conditions (2.5)–(2.6). Our goal is to find a secular equation for quantum circulant graphs by directly applying the vertex conditions to solutions of the Laplace equation on each edge, analogously to the method outlined in section 2.3.2. The main results from the rest of this chapter appear in [62].

As seen in section 2.2, results on a quantum graph are frequently independent of the edge orientation, but we choose the orientation given in the previous section for the purposes of calculation. The Laplace equation on each oriented edge (u, v) of the graph reads

$$-\frac{\mathrm{d}^2 f_{u,v}}{\mathrm{d}x_{u,v}^2} = k^2 f_{u,v}(x_{u,v}) \ . \tag{3.13}$$

We can express the vertex conditions (2.5)–(2.6) at a particular vertex v using the directed circulant graph notation as

$$f_{u,v}(L_{u,v}) = \phi_v = f_{v,w}(0), \text{ for all } (u,v),(v,w) \in \mathcal{E} \ , \tag{3.14}$$

$$\sum_{(v,w)\in\mathcal{E}} f'_{v,w}(0) - \sum_{(u,v)\in\mathcal{E}} f'_{u,v}(L_{u,v}) = 0 \ , \tag{3.15}$$

where ϕ_v is the value of f at the vertex v, rather than a fixed constant.

3.2.1 Secular Equation for Generic Circulant Graphs

In this section, we apply a technique similar to the one used for star graphs (see 2.3.2) to construct a secular equation for a quantum circulant graph. Fix a vertex v and consider f restricted to the oriented edge (v, w), for some $w \sim v$. We write the solution to (3.13) on this edge as

$$f_{v,w}(x_{v,w}) = A_{v,w} \sin kx_{v,w} + B_{v,w} \cos kx_{v,w} \ , \tag{3.16}$$

which is analogous to (2.31) for star graphs. Since $f_{v,w}(0) = \phi_v$, we see that $B_{v,w} = \phi_v$. Assuming $\sin kL_{v,w} \neq 0$, we can use $f_{v,w}(L_{v,w}) = \phi_w$ to solve for $A_{v,w}$. Notice that $\sin kL_{v,w} = 0$ corresponds to eigenvalues in the Dirichlet spectrum (see 2.2.1). We will revisit this special case in section 3.4. So for $\sin kL_{v,w} \neq 0$, (3.16) written in terms of the values at the vertices is

$$f_{v,w}(x_{v,w}) = \left(\frac{\phi_w - \phi_v \cos kL_{v,w}}{\sin kL_{v,w}} \right) \sin kx_{v,w} + \phi_v \cos kx_{v,w} \ . \tag{3.17}$$

Differentiating (3.17) and evaluating at vertex v,

$$f'_{v,w}(0) = k \left[\phi_w \csc kL_{v,w} - \phi_v \cot kL_{v,w} \right] \ . \tag{3.18}$$

Now consider f restricted to the oriented edge (u, v) for some other vertex $u \sim v$ in the appropriately oriented way. Then (3.17) reads

$$f_{u,v}(x_{u,v}) = \left(\frac{\phi_v - \phi_u \cos kL_{u,v}}{\sin kL_{u,v}} \right) \sin kx_{u,v} + \phi_u \cos kx_{u,v} \ , \tag{3.19}$$

so

$$\begin{aligned} f'_{u,v}(L_{u,v}) &= k \left[\phi_v \cot kL_{u,v} - \phi_u \left(\frac{\cos^2 kL_{u,v}}{\sin kL_{u,v}} - \sin kL_{u,v} \right) \right] \\ &= k \left[\phi_v \cot kL_{u,v} - \phi_u \csc kL_{u,v} \right] \ . \end{aligned} \tag{3.20}$$

Combining (3.18) and (3.20), the vertex condition (3.15) reads

$$\begin{aligned} k \sum_{(v,w)\in\mathcal{E}} & (\phi_w \csc kL_{v,w} - \phi_v \cot kL_{v,w}) \\ & - k \sum_{(u,v)\in\mathcal{E}} (\phi_v \cot kL_{u,v} - \phi_u \csc kL_{u,v}) = 0 \ . \end{aligned} \tag{3.21}$$

As the edge lengths are independent of direction (see 2.1.2), we can combine (3.21) into a single sum over all vertices adjacent to v, independent of orientation. Since $k \neq 0$,

$$\sum_{w \sim v} (\phi_w \csc kL_{v,w} - \phi_v \cot kL_{v,w}) = 0 \ . \tag{3.22}$$

Each vertex $v \in \mathcal{V}$ will have an associated equation (3.22). This results in a system of n equations, one for each of the n vertices. Let $\boldsymbol{\phi} = \{\phi_1, \ldots, \phi_n\}$ be a vector of the values of f at each of the vertices. Then, the system of equations can be written in matrix form

$$M(k)\boldsymbol{\phi} = \mathbf{0}, \tag{3.23}$$

where $M(k)$ is the $n \times n$ matrix with

$$[M(k)]_{ii} = -\sum_{v \sim i} \cot kL_{i,v} \ , \tag{3.24}$$

$$[M(k)]_{ij} = \begin{cases} \csc kL_{i,j} & i \sim j \ , \\ 0 & i \not\sim j \ . \end{cases} \tag{3.25}$$

For a given value of k, $\boldsymbol{\phi}$ solves (3.23) if and only if it is an eigenvector of $M(k)$ corresponding to the eigenvalue 0. So, we have a solution to (3.23) if and only if k is a root of the secular equation

$$\det M(k) = 0 \ . \tag{3.26}$$

The multiplicity of a root of (3.26) will be the same as the algebraic multiplicity of 0 as an eigenvalue of $M(k)$. Since $M(k)$ is symmetric for all k, it is diagonalizable, so the multiplicity of the eigenvalue 0 is the same as the dimension of the null space of $M(k)$. The eigenfunctions of the Laplacian on $C_n(\boldsymbol{L}; \boldsymbol{a})$ are the vectors $\boldsymbol{f} = \{f_{u,v}\}_{(u,v) \in \mathcal{E}}$, where the $f_{u,v}$ are defined in (3.19). Thus each linearly independent $\boldsymbol{\phi}$ in the null

space of $M(k)$ uniquely defines a linearly independent eigenfunction $\boldsymbol{f}$ of the Laplacian with the eigenvalue k^2. This proves the following theorem, first given in [62].

Theorem 3.6. *Let $k \in \mathbb{R}$ such that $\sin kL_{u,v} \neq 0$, for all $L_{u,v} \in \boldsymbol{L}$. Then $\lambda = k^2$ is an eigenvalue of (3.13) on $C_n(\boldsymbol{L}; \boldsymbol{a})$ with q linearly independent eigenfunctions if and only if k is a root of (3.26) with multiplicity q.*

3.3 Symmetric Quantum Circulant Graphs

We will also consider a more specialized metric for $C_n(\boldsymbol{L}; \boldsymbol{a})$ which respects the underlying symmetry of $C_n(\boldsymbol{a})$. Fix a vector $\boldsymbol{l} = \{l_1, \ldots, l_h\}$ and assign edge lengths to $C_n(\boldsymbol{L}; \boldsymbol{a})$ such that the edge (u, v) has length l_h whenever $|u - v| \equiv a_h \pmod{n}$. We refer to this as a *symmetric quantum circulant graph* and let $C_n(\boldsymbol{l}; \boldsymbol{a})$ denote a circulant graph with this metric. In order to derive a secular equation for this type of graph, we use the characterization of a circulant graph as a graph with a circulant adjacency matrix (see section 3.1).

3.3.1 Secular Equation for Symmetric Circulant Graphs

For a symmetric quantum circulant graph $C_n(\boldsymbol{l}; \boldsymbol{a})$, the matrix $M(k)$ defined in (3.24)-(3.25) is

$$[M(k)]_{ii} = -2 \sum_{h=1}^{d} \cot kl_h \ , \tag{3.27}$$

$$[M(k)]_{ij} = \begin{cases} \csc kl_h & \text{if } |i - j| \equiv a_h \pmod{n} \ , \\ 0 & \text{otherwise} \ . \end{cases} \tag{3.28}$$

We show this matrix is a circulant matrix and utilize the properties of circulant matrices to evaluate $\det M(k)$ for a symmetric quantum circulant graph.

Lemma 3.7. *Let $C_n(\boldsymbol{l}; \boldsymbol{a})$ be a symmetric quantum circulant graph. Then $M(k)$ defined in (3.27)–(3.28) is a circulant matrix.*

Proof. For each $a_h \in \boldsymbol{a}$, let $\Gamma_h := C_n(a_h)$ be the subgraph of $C_n(\boldsymbol{a})$ containing only edges connected via a_h, and let J_h be its adjacency matrix. Each Γ_h is also a circulant graph, so each J_h is a circulant matrix. Then

$$M(k) = \left(-2 \sum_{h=1}^{d} \cot kl_h \right) \mathbb{I}_n + \sum_{h=1}^{d} (\csc kl_h) J_h \ , \tag{3.29}$$

where $\mathbb{I}_n$ is the $n \times n$ identity matrix. As a linear combination of circulant matrices is a circulant matrix [32], $M(k)$ is a circulant matrix. □

The representer, definition 3.3, of the matrix $M(k)$ is given in the following lemma.

Lemma 3.8. *The representer for the circulant matrix $M(k)$ of a symmetric quantum circulant graph is*

$$p(z) = \sum_{h=1}^{d} \left[-2\cot(kl_h) + \left(z^{a_h} + z^{n-a_h} \right) \csc(kl_h) \right] \ . \tag{3.30}$$

Proof. The first row of the matrix $M(k)$ is given by $\boldsymbol{m} = (m_1, \ldots, m_n)$, where $m_j = [M]_{1j}$ as defined in (3.27)-(3.28). Clearly, $m_1 = -2\sum_{h=1}^{d} \cot kl_h$. For each $a_h \in \boldsymbol{a}$, there are edges of length l_h connecting the vertex 1 to $1+a_h$ and $n+1-a_h$. Therefore $m_{a_h+1} = m_{n+1-a_h} = \csc kl_h$, and for all other j, $m_j = 0$. □

As shown in theorem 3.4, the determinant of a circulant matrix can be expressed using the representer evaluated at ω^j, where $\omega = \exp(2\pi \mathrm{i}/n)$ and $j = 0, \ldots n-1$. Since the secular equation is a function of k, we introduce functions $p_j(k)$ where $p_j(k) := p(\omega^j)$. Then,

$$p_j(k) = 2 \sum_{h=1}^{d} \left[-\cot(kl_h) + \left(\cos\left(\frac{2\pi j a_h}{n} \right) \right) \csc(kl_h) \right] \ . \tag{3.31}$$

When $j = 0$, $\cos(2\pi j a_h/n) = 1$, so this simplifies to

$$p_0(k) = 2\sum_{h=1}^{d} \tan\left(\frac{kl_h}{2}\right) \ , \tag{3.32}$$

and for n even, $j = n/2$ implies $\cos(2\pi j a_h/n) = (-1)^{a_h}$, so

$$p_{n/2}(k) = 2\left[\sum_{\substack{h=1 \\ a_h \text{ is even}}}^{d} \tan\left(\frac{kl_h}{2}\right) - \sum_{\substack{h=1 \\ a_h \text{ is odd}}}^{d} \cot\left(\frac{kl_h}{2}\right)\right] \ . \tag{3.33}$$

It is interesting to note the similarity between (3.32) and the standard secular equation for a star graph (2.36).

Applying corollary 3.5 to $M(k)$ gives the following result, which also appears in [62].

Theorem 3.9. *Let $C_n(\boldsymbol{l};\boldsymbol{a})$ be a symmetric quantum circulant graph, and let $p_j(k)$ be defined as in* (3.31)–(3.33). *Suppose that $k \neq m\pi/l_h$ for any $m \in \mathbb{Z}$ and any $l_h \in \boldsymbol{l}$.*

I. If n is odd and k is a q^{th} root of

$$p_0(k)\prod_{j=1}^{(n-1)/2} |p_j(k)|^2 = 0 \ , \tag{3.34}$$

then $\lambda = k^2$ is an eigenvalue of $C_n(\boldsymbol{l};\boldsymbol{a})$ with multiplicity q.

II. If n is even and k is a q^{th} root of

$$p_0(k)p_{n/2}(k)\prod_{j=1}^{(n/2)-1} |p_j(k)|^2 = 0 \ , \tag{3.35}$$

then $\lambda = k^2$ is an eigenvalue of $C_n(\boldsymbol{l};\boldsymbol{a})$ with multiplicity q.

3.3.2 Derivation of the Secular Equation Using Quotient Graphs

The secular equation derived in the previous section was obtained using the secular equation of a general quantum circulant graph, theorem 3.6. An alternative

method for obtaining the spectrum of a symmetric quantum circulant graph utilizes the quotient graph defined in section 2.5.

Recall that the quotient graph exploits the symmetry of a quantum graph to decompose its spectrum into subspectra whose eigenfunctions transform according to irreducible representations of the symmetry group. A circulant graph $C_n(\boldsymbol{l};\boldsymbol{a})$ is symmetric under a rotation of the vertex lables $\sigma(v) = v+1$. If $C_n(\boldsymbol{l};\boldsymbol{a})$ is embedded in the plane, as in figure 3.1, this is equivalent to rotation by $2\pi/n$. The cyclic group generated by σ is $\mathbb{Z}_n$ and has irreducible complex representations $\mathcal{R}_j$, $j = 0, \ldots, n-1$, where

$$\mathcal{R}_j(\sigma) = \mathrm{e}^{\mathrm{i}\theta_j} \tag{3.36}$$

for $\theta_j = 2\pi j/n$.

The left action of $\mathbb{Z}_n$ on an eigenfunction f of $C_n(\boldsymbol{l};\boldsymbol{a})$ is defined as

$$(\sigma f)(x) = f(\sigma^{-1}x)\ . \tag{3.37}$$

Then, f transforming according to the representation $\mathcal{R}_j$ is

$$(\sigma f)(x) = \mathcal{R}_j(\sigma)f(x) = \mathrm{e}^{\mathrm{i}\theta_j}f(x)\ . \tag{3.38}$$

The quotient graph for a symmetric quantum circulant graph $C_n(\boldsymbol{l};\boldsymbol{a})$ with given representation $\mathcal{R}_j$ can be constructed following the procedure defined in [7, 96] and outlined in section 2.5.2. To construct the quotient graph $C_n(\boldsymbol{l};\boldsymbol{a})/\mathcal{R}_j$, we introduce a dummy vertex of degree two with Neumann-like vertex conditions at the midpoint of each edge of the circulant graph. Recall that introducing such dummy vertices does not change the spectrum of the original graph (see 2.5.1), and a function on the graph is continuous with a continuous first derivative at the new vertices due to the Neumann-like conditions. For simplicity, we keep the original coordinates

when introducing the dummy vertices, so an edge corresponding to the interval $[0, l_h]$ is simply broken into subintervals $[0, l_h/2]$ and $[l_h/2, l_h]$ with a dummy vertex at $x = l_h/2$. Eigenfunctions on the original graph are obtained from eigenfunctions on the graph with dummy vertices by joining corresponding edge pairs. Figure 3.2(a) shows a circulant graph with dummy vertices.

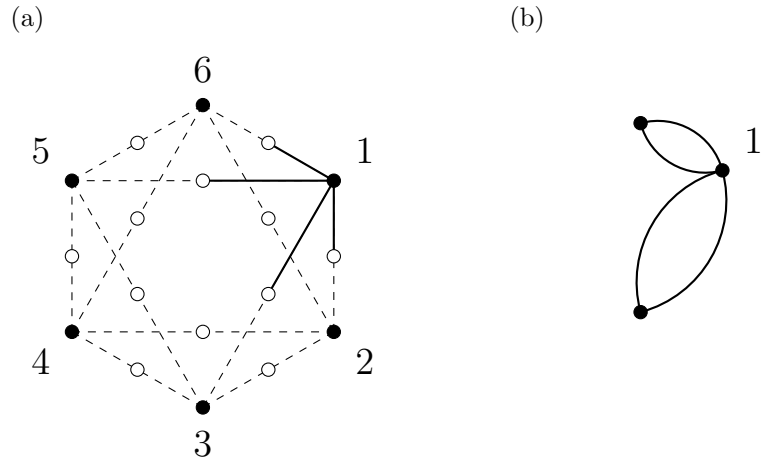

Figure 3.2. (a) The circulant graph, $C_6(\boldsymbol{l}; (1, 2))$, with dummy vertices. The dummy vertices are denoted by open dots, and edges in the fundamental domain are shown with solid lines. (b) The quotient graph $C_6(\boldsymbol{l}; (1, 2))/\mathcal{R}_j$ with respect to one of the irreducible representations given by $\mathcal{R}_j(\sigma) = \exp(\mathrm{i}\pi j/3)$.

The subgraph consisting of the vertex $v = 1$ with a pair of adjacent dummy vertices for each $h \in (1, \ldots, d)$ forms a fundamental domain containing two edges with length $l_h/2$ for each h. The quotient graph is constructed by identifying the two dummy vertices on edges of length $l_h/2$ in the fundamental domain, as depicted in figure 3.2(b). The quotient graph then has d vertices of degree two and a central vertex of degree $2d$. The central vertex retains the standard conditions (3.14)–(3.15) but we must introduce new vertex conditions at the other vertices which depend on the representation $\mathcal{R}_j$.

For a function f on the quotient graph, let f_{h-} denote the function on the interval $[0, l_h/2]$ and f_{h+} the function on $[l_h/2, l_h]$. Then at the h^{th} degree two ver-

tex, the vertex conditions for a function transforming according to the irreducible representation $\mathcal{R}_j$ take the form

$$f_{h-}(l_h/2) = \mathrm{e}^{\mathrm{i}a_h\theta_j} f_{h+}(l_h/2) \ , \tag{3.39}$$

$$f'_{h-}(l_h/2) = \mathrm{e}^{\mathrm{i}a_h\theta_j} f'_{h+}(l_h/2) \ . \tag{3.40}$$

The spectrum of the quotient graph is the subset of the spectrum of the circulant graph whose eigenfunctions transform according to the irreducible representation $\mathcal{R}_j$.

A solution to (3.13) on the pair of edges $h\pm$ can be written as a piecewise function defined on $[0, l_h/2) \cup (l_h/2, l_h]$,

$$f_h(x_h) = \begin{cases} A_h \sin(kx_h) + B_h \cos(kx_h) & \text{if } 0 \le x_h < l_h/2 \ , \\ A_h \mathrm{e}^{-\mathrm{i}a_h\theta_j} \sin(kx_h) + B_h \mathrm{e}^{-\mathrm{i}a_h\theta_j} \cos(kx_h) & \text{if } l_h/2 < x_h \le l_h \ . \end{cases} \tag{3.41}$$

Let ϕ be the value of an eigenfunction of the quotient graph at the central vertex. Assuming $k \neq m\pi/l_h$ for $m \in \mathbb{Z}$, then

$$f_h(x_h) = \begin{cases} \phi[\mathrm{e}^{\mathrm{i}a_h\theta_j} \csc(kl_h) - \cot(kl_h)] \sin(kx_h) & \\ \qquad + \phi \cos(kx_h) & \text{if } 0 \le x_h < l_h/2 \ , \\ \phi[\csc(kl_h) - \mathrm{e}^{-\mathrm{i}a_h\theta_j} \cot(kl_h)] \sin(kx_h) & \\ \qquad + \phi \mathrm{e}^{-\mathrm{i}a_h\theta_j} \cos(kx_h) & \text{if } l_h/2 < x_h \le l_h \ . \end{cases} \tag{3.42}$$

The vertex condition (3.15) at the central vertex requires,

$$\sum_{h=1}^{d} f'_h(0) - f'_h(l_h) = 0 \ , \tag{3.43}$$

so for $\phi \neq 0$,

$$2 \sum_{h=1}^{d} \cos(a_h\theta_j) \csc(kl_h) - \cot(kl_h) = 0 \ . \tag{3.44}$$

Notice that (3.44) is equivalent to $p_j(k) = 0$, for $p_j(k)$ defined in (3.31). Since the roots of (3.44) correspond to the eigenvalues of $C_n(\boldsymbol{l}; \boldsymbol{a})$ in the subspace transforming according to $\mathcal{R}_j$, for $k \neq m\pi/l_h$, we obtain the whole non-Dirichlet spectrum by taking the union over $j = 0, \ldots, n-1$. Therefore, a secular equation whose roots correspond to this union can be obtained by multiplying the equations in (3.44) for all j. This is equivalent to the secular equation obtained in theorem 3.9, since the determinant formula applied there is simplified from theorem 3.4.

3.4 Dirichlet Spectrum

We have considered Neumann-like vertex conditions on our quantum circulant graphs. However, in each of these cases, we have identified a secular equation which is only valid for $\sin kL_e \neq 0$. Recall that the roots of $\sin kL_e = 0$ correspond to eigenvalues of the quantum graph with an alternative set of vertex conditions for which the Laplace operator is self-adjoint, namely the Dirichlet conditions (2.7). Although finding the spectra of the graph with Dirichlet and Neumann-like vertex conditions are different problems, it is possible that eigenvalues in the Dirichlet spectrum may also appear in the Neumann spectrum. That is, we want to determine if there is a subset of eigenvalues under Neumann-like vertex conditions which also fall in the Dirichlet spectrum.

Consider a general quantum circulant graph $C_n(\boldsymbol{L}; \boldsymbol{a})$ with Neumann-like vertex conditions. If $k^2 = (m\pi/L_e)^2$ is in the spectrum for some edge e and some $m \in \mathbb{N}$, this Dirichlet eigenvalue can be removed by perturbing the edge lengths $\boldsymbol{L}$. So for almost all vectors of edge lengths $\boldsymbol{L}$, the Dirichlet spectrum and the Neumann spectrum do not overlap. Despite the fact that this is true in general, because of the additional edge-length symmetry present in $C_n(\boldsymbol{l}; \boldsymbol{a})$, some Dirichlet eigenvalues do appear under Neumann-like vertex conditions for the symmetric quantum circulant

graph. To determine which of these occur and with what multiplicity, it is useful to return to the quotient graph.

3.4.1 Symmetric Circulant Graphs

Fix some $a_g \in \boldsymbol{a}$ and consider $k = m\pi/l_g$ for some given $m \in \mathbb{N}$. Then, for $h \neq g$, solutions to (3.13) on the edge h of the quotient graph are given piecewise by (3.41). However, on the edge g we have

$$f_g(x_g) = \begin{cases} A_g \sin(\frac{m\pi}{l_g} x_g) + \phi \cos(\frac{m\pi}{l_g} x_g) & \text{if } 0 \leq x_g < l_g/2 \ , \\ A_g \mathrm{e}^{-\mathrm{i}a_g\theta_j} \sin(\frac{m\pi}{l_g} x_g) + \phi \mathrm{e}^{-\mathrm{i}a_g\theta_j} \cos(\frac{m\pi}{l_g} x_g) & \text{if } l_g/2 < x_g \leq l_g \ , \end{cases} \tag{3.45}$$

where ϕ is the value of the eigenfunction of the quotient graph at the central vertex.

By continuity at the central vertex, $f_g(l_g) = \phi$, which gives the restriction that

$$\phi \, \mathrm{e}^{-\mathrm{i}a_g\theta_j} (-1)^m = \phi \ . \tag{3.46}$$

This is always satisfied for $\phi = 0$, which yields the quotient graph eigenfunction

$$f_g(x_g) = \begin{cases} A_g \sin(\frac{m\pi}{l_g} x_g) & \text{if } 0 \leq x_g < l_g/2 \ , \\ A_g \mathrm{e}^{-\mathrm{i}a_g\theta_j} \sin(\frac{m\pi}{l_g} x_g) & \text{if } l_g/2 < x_g \leq l_g \ , \end{cases} \tag{3.47}$$

on the edge set $g\pm$, and $f_h(x_h) \equiv 0$ for $h \neq g$. If we apply the vertex condition (3.43) at the central vertex,

$$\frac{m\pi}{l_g} A_g \left[1 - \mathrm{e}^{-\mathrm{i}a_g\theta_j} (-1)^m \right] = 0 \ , \tag{3.48}$$

so either $A_g = 0$, which would be a trivial solution, or

$$\mathrm{e}^{\mathrm{i}a_g\theta_j} = (-1)^m \ . \tag{3.49}$$

Since $e^{i\theta_j}$ is the j^{th} primitive n^{th} root of unity, this requires ja_g to be a multiple of n when m is even and $2ja_g$ to be an odd multiple of n when m is odd.

We now consider (3.46) and assume that $\phi \neq 0$. Thus, $e^{ia_g\theta_j} = (-1)^m$ is now required to satisfy continuity at the central vertex,, which implies that $f_g'(0) = f_g'(l_g)$. Substituting this into the vertex condition (3.43), we obtain

$$\sum_{\substack{h=1 \\ h\neq g}}^{d} \cos(\theta_j a_h) \csc\left(\frac{m\pi l_h}{l_g}\right) - \cot\left(\frac{m\pi l_h}{l_g}\right) = 0 \ . \tag{3.50}$$

The derivative of the left hand side of equation (3.50) with respect to an edge length is non-zero. Hence if this condition is satisfied for some set of edge lengths a perturbation of any edge length will remove this. Thus, for edge lengths l_h chosen from $(1-\epsilon, 1+\epsilon)$, equation (3.50) is not satisfied for almost all choices of edge lengths. In this case, the only Dirichlet eigenvalues correspond to eigenfunctions which vanish at the central vertex.

Lemma 3.10. *Let $C_n(\boldsymbol{l}; \boldsymbol{a})$ be a symmetric quantum circulant graph ($d \geq 2$) equipped with the Laplace operator and satisfying Neumann-like vertex conditions. Then for almost every $\boldsymbol{l} \in (1-\epsilon, 1+\epsilon)^d$ and all for $m \in \mathbb{N}$, $m^2\pi^2/l_h^2$ is in the spectrum of the graph if some $j \in \{0, \ldots, n-1\}$ satisfies the condition:*

$$2ja_h = qn \text{ for some odd/even } q \text{ when } m \text{ is odd/even.} \tag{3.51}$$

The multiplicity of $m^2\pi^2/l_h^2$ is equal to the number of distinct j's under which (3.51) is satisfied, and the corresponding eigenfunctions are zero at the graph vertices.

Corollary 3.11. *Let $C_n(\boldsymbol{l}; \boldsymbol{a})$ be as in lemma 3.10. Then $(2p)^2\pi^2/l_h^2$ is in the spectrum of the graph for almost every $\boldsymbol{l} \in (1-\epsilon, 1+\epsilon)^d$ and all $p \in \mathbb{N}$.*

Proof. Since $m = 2p$ is even, condition (3.51) is always satisfied for $j, q = 0$. □

Corollary 3.12. *Let $C_n(\boldsymbol{l};\boldsymbol{a})$ be as in lemma 3.10 with n being odd. Then $(2p+1)^2\pi^2/l_h^2$ is not in the spectrum of the graph for almost any $\boldsymbol{l} \in (1-\epsilon, 1+\epsilon)^d$ and any $p \in \mathbb{N}$.*

Proof. Since $m = 2p+1$ is odd, q must be odd. A product of odd numbers is odd, so qn cannot equal $2ja_h$, which is even. Thus, condition (3.51) cannot be satisfied. □

3.5 Weyl Law for Symmetric Circulant Graphs

Recall from section 2.4 that the Weyl law gives the density of graph eigenvalues. To see that the Weyl law fits with the secular equations, we can estimate how many roots of the secular equation fall in a given interval. Recall that the spectrum of $C_n(\boldsymbol{l};\boldsymbol{a})$ is divided into subspectra whose eigenfunctions transform according to the irreducible representations $\mathcal{R}_j$ combined with the subset of the spectrum that intersects with the Dirichlet spectrum. To confirm that these are indeed all of the eigenvalues, we compare our results to the standard Weyl law for quantum graphs. We will do this by counting the number of roots found for each function $p_j(k)$ and then summing over all values of j, as well as including the appropriate parts of the Dirichlet spectrum.

Consider the function $p_j(k)$ and differentiate termwise with respect to k. The derivative is positive, so $p_j(k)$ is strictly increasing for all real values of k. Consequently, there is exactly one zero of $p_j(k)$ between each pair of adjacent asymptotes. By counting the asymptotes of $p_j(k)$ on a given interval (a,b), we will also have counted the roots of $p_j(k) = 0$ in that interval, up to a small error. We will denote the number of roots of $p_j(k) = 0$ on the interval (a,b) by the function $N_j(a,b)$.

For $p_0(k) = 0$ defined in (3.31), the spacing between asymptotes of $\tan(kl_h/2)$ is $2\pi/l_h$. So, the number of asymptotes in the interval (a,b) from a fixed h is approximately the length of the interval divided by the spacing of the asymptotes; that is, it falls between $(b-a)(l_h/2\pi)-1$ and $(b-a)(l_h/2\pi)+1$. Summing over all values of

h,

$$\frac{(b-a)}{2\pi}\sum_{h=1}^{d} l_h - d \leq \#\text{ of } p_0 \text{ asymptotes} \leq \frac{(b-a)}{2\pi}\sum_{h=1}^{d} l_h + d\ . \tag{3.52}$$

Since there is one root between each pair of asymptotes, the total number of roots in the interval (a,b) may be one less, the same as, or one more than the number of asymptotes in that interval, depending on where they fall in relation to the endpoints. So,

$$\frac{(b-a)\mathcal{L}}{2\pi n} - d - 1 \leq N_0(a,b) \leq \frac{(b-a)\mathcal{L}}{2\pi n} + d + 1\ , \tag{3.53}$$

where $\mathcal{L} = n\sum_{h=1}^{d} l_h$ is the total length of the graph. When n is even, we have the function $p_{n/2}(k)$, whose asymptotes are $(2q-1)\pi/l_h$ for even a_h and $2q\pi/l_h$ for odd a_h. In either case, the spacing between asymptotes is $2\pi/l_h$ and so the bounds in (3.53) are also bounds for $N_{n/2}(a,b)$.

For $1 \leq j \leq \lfloor (n-1)/2 \rfloor$, the asymptotes of $p_j(k)$ will be zeros of $\sin(kl_h)$ unless

$$2ja_h = 0 \pmod{n}\ . \tag{3.54}$$

First, let us consider a value of j that does not satisfy (3.54) for any $h = 1, \ldots, d$. In this case, the spacing between asymptotes for a fixed h is π/l_h. Summing over all values of h bounds the number of asymptotes,

$$\frac{(b-a)}{\pi}\sum_{h=1}^{d} l_h - d \leq \#\text{ of } p_j \text{ asymptotes} \leq \frac{(b-a)}{\pi}\sum_{h=1}^{d} l_h + d\ , \tag{3.55}$$

and counting the total number of roots as before gives

$$\frac{(b-a)\mathcal{L}}{\pi n} - d - 1 \leq N_j(a,b) \leq \frac{(b-a)\mathcal{L}}{\pi n} + d + 1\ . \tag{3.56}$$

Now suppose that a fixed j satisfies (3.54) for at least one value of h. This condition is equivalent to condition (3.51) for a given value of j in lemma 3.10. Consequently, every missing asymptote of $p_j(k)$ corresponds to an added Dirichlet eigenvalue. Instead of counting the total roots, $N_j(a,b)$, we count the total eigenvalues associated to $p_j(k)$, denoted $\widetilde{N}_j(a,b)$. This is bounded by

$$\frac{(b-a)\mathcal{L}}{\pi n} - d - 1 \leq \widetilde{N}_j(a,b) \leq \frac{(b-a)\mathcal{L}}{\pi n} + d + 1 \ . \tag{3.57}$$

Since there are no Dirichlet eigenvalues for the case where j does not satisfy (3.54), note that $\widetilde{N}_j(a,b) = N_j(a,b)$. So equation (3.57) holds for $j \in \{1, \ldots, \lfloor (n-1)/2 \rfloor\}$.

Finally, to obtain the Weyl law, we must sum the eigenvalues associated to each j. Recall that in theorem 3.9, each $p_j(k)$ for $1 \leq j \leq \lfloor (n-1)/2 \rfloor$ is squared, so eigenvalues associated to these j have multiplicity two and are counted twice. By corollary 3.11, every graph has the Dirichlet eigenvalues $2q\pi/l_h$ for $m \in \mathbb{N}$ and all $h = 1, \ldots, d$. Additionally, for graphs with an even number of vertices, $(2q+1)\pi/l_h$ is also included in the spectrum for all h. Consequently, we define

$$N_D(a,b) = \begin{cases} \#\text{ of } \dfrac{2q\pi}{l_h} \text{ in } (a,b), \forall h = 1, \ldots, d & \text{when } n \text{ is odd} \ , \\ \#\text{ of } \dfrac{m\pi}{l_h} \text{ in } (a,b), \forall h = 1, \ldots, d & \text{when } n \text{ is even} \ . \end{cases} \tag{3.58}$$

Then putting the bounds on the eigenvalues for each j together we obtain the following result.

Theorem 3.13. *Let $C_n(\boldsymbol{l}; \boldsymbol{a})$ be a symmetric quantum circulant graph equipped with the Laplace operator and satisfying Neumann-like vertex conditions. The number of eigenvalues in the interval (a,b) is*

$$N(a,b) = \frac{(b-a)\mathcal{L}}{\pi} + r \tag{3.59}$$

where $\mathcal{L} = n\sum_{h=1}^{d} l_h$ *is the total length of the graph, and* $|r| \leq nd + n + d$*, so it is uniformly bounded in the length of the interval.*

Proof. First, let n be odd. Then

$$N(a,b) = N_0(a,b) + N_D(a,b) + 2\sum_{j=1}^{(n-1)/2} \widetilde{N}_j(a,b) \ , \tag{3.60}$$

and so

$$\begin{aligned} |N(a,b)| &\leq \frac{(b-a)\mathcal{L}}{2\pi n} + d + 1 + \frac{(b-a)\mathcal{L}}{2\pi n} + d + 2\sum_{j=1}^{(n-1)/2}\left[\frac{(b-a)\mathcal{L}}{\pi n} + d + 1\right] \\ &\leq \frac{(b-a)\mathcal{L}}{\pi n} + \frac{(b-a)\mathcal{L}(n-1)}{\pi n} + 2d + 1 + d(n-1) + (n-1) \\ &\leq \frac{(b-a)\mathcal{L}}{\pi} + dn + d + n \ . \end{aligned} \tag{3.61}$$

When n is even,

$$N(a,b) = N_0(a,b) + N_{n/2}(a,b) + N_D(a,b) + 2\sum_{j=1}^{n/2-1} \widetilde{N}_j(a,b) \ . \tag{3.62}$$

Therefore,

$$\begin{aligned} |N(a,b)| &\leq \frac{(b-a)\mathcal{L}}{2\pi n} + d + 1 + \frac{(b-a)\mathcal{L}}{2\pi n} + d + 1 + \frac{(b-a)\mathcal{L}}{\pi n} + d \\ &\qquad + 2\sum_{j=1}^{n/2-1}\left[\frac{(b-a)\mathcal{L}}{\pi n} + d + 1\right] \\ &\leq \frac{2(b-a)\mathcal{L}}{\pi n} + \frac{(b-a)\mathcal{L}(n-2)}{\pi n} + 3d + 2 + d(n-2) + (n-2) \\ &\leq \frac{(b-a)\mathcal{L}}{\pi} + dn + d + n \ , \end{aligned} \tag{3.63}$$

which completes the proof. □

Comparing this result with theorem 2.6, we observe consistency with the established Weyl law for quantum graphs, although our bound r is not as good of a bound as in theorem 2.6.

CHAPTER FOUR

Spectral Statistics

One of the major applications of quantum graphs is the study of quantum chaos. Specifically, we look at statistics of the eigenvalues of a quantum circulant graph and compare their statistical properties to predictions for various classes of quantum systems that are classically chaotic. The analytic results in this chapter appear in [62], along with a sampling of the numerical results presented.

4.1 Nearest-Neighbor Spacing Statistics

The BGS conjecture states that the spectra of quantum systems which correspond to classically chaotic systems exhibit spectral fluctuations predicted by ensembles of random matrices [27]. Specifically, systems with time reversal invariance are proposed to match the probability distributions of the GOE. Kottos and Smilansky showed that quantum graphs serve as a model for quantum chaos [76], so we are interested in examining the nearest-neighbor spacing statistics of a quantum circulant graph and comparing it with the predictions of random matrix theory.

Consider a sequence of roots $\{k_j\}$ of the secular equation (3.26) so that $k_j^2 = \lambda_j$ is in the spectrum of the Laplace operator with Neumann-like conditions on $C_n(\boldsymbol{L}; \boldsymbol{a})$. To compare statistics of sequences whose average spacings differ, it is necessary to unfold the spectra so that the average spacing is 1. Since the average density of the k_j given by the Weyl law is $\pi/\mathcal{L}$ where $\mathcal{L}$ is the total length of the graph (see theorem 2.6 or theorem 3.13), setting $\hat{k}_j = k_j\mathcal{L}/\pi$ achieves this normalization. The nearest-neighbor spacings are then given by the sequence $s_j = \hat{k}_{j+1} - \hat{k}_j$ with probability distribution

$$P(x) = \lim_{N\to\infty} \frac{1}{N} \sum_{j=1}^{N} \delta(x - s_j) \ , \tag{4.1}$$

where δ is the Dirac delta function.

For an $N \times N$ random matrix from the GOE, the joint probability distribution function of its eigenvalues [91] is

$$\rho_N(x_1, \ldots, x_N) = \text{const} \times \exp\left(-\frac{1}{2}\sum_{j=1}^{N} x_j^2\right) \prod_{j<k} |x_j - x_k| \ . \tag{4.2}$$

For large N, the probability that a randomly chosen interval of length s contains no eigenvalues is then given by

$$\rho_E(s) = \lim_{N\to\infty} \int\cdots\int_{(-\infty,-\overline{s}s/2)\cup(\overline{s}s/2,\infty)} \rho_N(x_1, \ldots, x_N)\, \mathrm{d}x_1 \cdots \mathrm{d}x_N \ , \tag{4.3}$$

where here $\overline{s}$ is the mean spacing of eigenvalues, see [91]. To obtain the probability density for the nearest-neighbor spacings, $P(s)$, observe that $\rho_E(s) - \rho_E(s + \delta s)$ is the probability that the interval s is empty and the adjacent interval δs is not empty. The probability that δs will contain more than one eigenvalue is of second order or higher in δs. So taking the limit as $\delta s \to 0$ and dropping the higher order terms gives us that $-[\,\mathrm{d}\rho_E(s)/\,\mathrm{d}s]\,\delta s$ is the probability of s being empty and δs containing exactly one level. Analogous reasoning allows us to conclude that

$$P(s) = \frac{\mathrm{d}^2\rho_E}{\mathrm{d}s^2} \ . \tag{4.4}$$

In general, these distributions are difficult to work with, but a suitable approximation is given by the Wigner surmise. For the GOE, this is computed by letting $N = 2$ so that

$$P_W(s) = C \iint_{\mathbb{R}^2} \delta(s - |x_2 - x_1|) \times \mathrm{e}^{-(x_1+x_2)/2} \, \mathrm{d}x_1 \, \mathrm{d}x_n \ , \tag{4.5}$$

where C is such that $\int_0^\infty P_W(s) \, \mathrm{d}s = 1$ [91]. As a result,

$$P_W(s) = \frac{\pi s}{2} \mathrm{e}^{-\pi s^2/4} \ . \tag{4.6}$$

Interestingly, the deviation between the actual distribution and the Wigner surmise is quite small, according to [58] on the order of 10^{-4}, so we will use the simpler expression in our figures.

Another function of note is the integrated nearest-neighbor spacing distribution. This is defined as

$$I(s) = \int_0^s P(x) \, \mathrm{d}x \ , \tag{4.7}$$

and gives the probability that the spacing between nearest-neighbors is less than or equal to s. For the Wigner surmise for the GOE, the corresponding integrated distribution is

$$I_W(s) = 1 - \mathrm{e}^{-\pi s^2/4} \ . \tag{4.8}$$

4.1.1 Numerical Results for Generic Circulant Graphs

To compare our results with the statistical predictions, we chose a quantum circulant graph and computed its roots numerically using the secular equation (3.26) from the previous chapter. We evaluated (3.26) at evenly spaced values of k and found the sign changes. After removing sign changes resulting from asymptotes of the secular equation, we applied the secant method to find the roots. We numerically computed the k_j for several different sample circulant graphs up to $j \approx 50{,}000$ using this method. Then we plotted a histogram of the normalized spacings s_j against the Wigner surmise for the GOE (4.5).

The use of quantum graphs as a model for quantum chaos was first proposed by Kottos and Smilanksy in 1997 [76], who used a similar method to show numerical agreement between the statistics of quantum graphs and the predictions of the BGS conjecture [27]. As expected, we see this same agreement in figures 4.1, 4.2, and 4.3, further adding to the large body of evidence for this claim.

We also plotted the integrated spacings for these graphs, which is the accumulated total spacings less than a particular value. This is shown in figures 4.4, 4.5, and 4.6. The difference between the data and the random matrix prediction, shown in the inset, shows a systematic deviation which is due to the comparison with the Wigner surmise rather than the actual random matrix result.

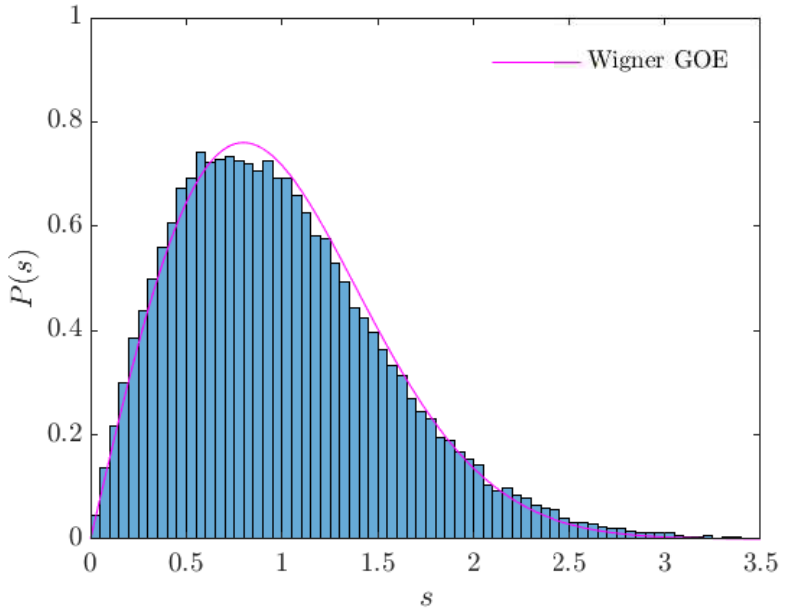

Figure 4.1. Histogram of the nearest-neighbor spacing distribution for the quantum circulant graph $C_{16}(\boldsymbol{L};(1,3,5,7))$ with incommensurate edge lengths for 50,009 eigenvalues plotted against the Wigner surmise for the GOE distribution.

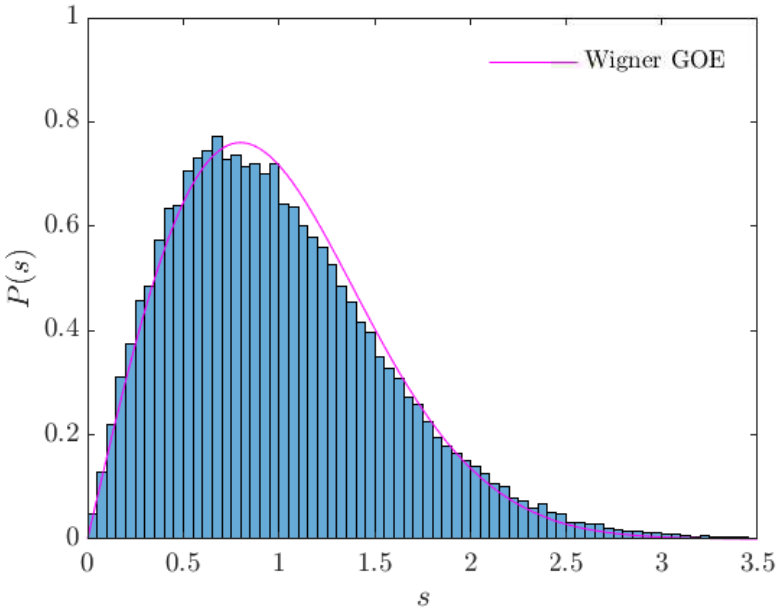

Figure 4.2. Histogram of the nearest-neighbor spacing distribution for the quantum circulant graph $C_{24}(\boldsymbol{L}; (1, 2, 3, 6))$ with incommensurate edge lengths for 50,011 eigenvalues plotted against the Wigner surmise for the GOE distribution.

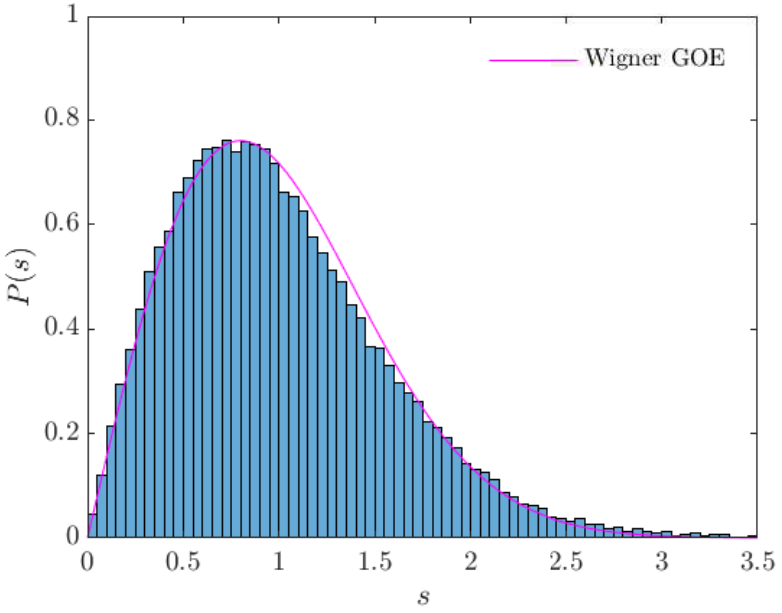

Figure 4.3. Histogram of the nearest-neighbor spacing distribution for the quantum circulant graph $C_{49}(\boldsymbol{L}; (3, 4, 9, 12, 15, 19, 20))$ with incommensurate edge lengths for 50,036 eigenvalues plotted against the Wigner surmise for the GOE distribution.

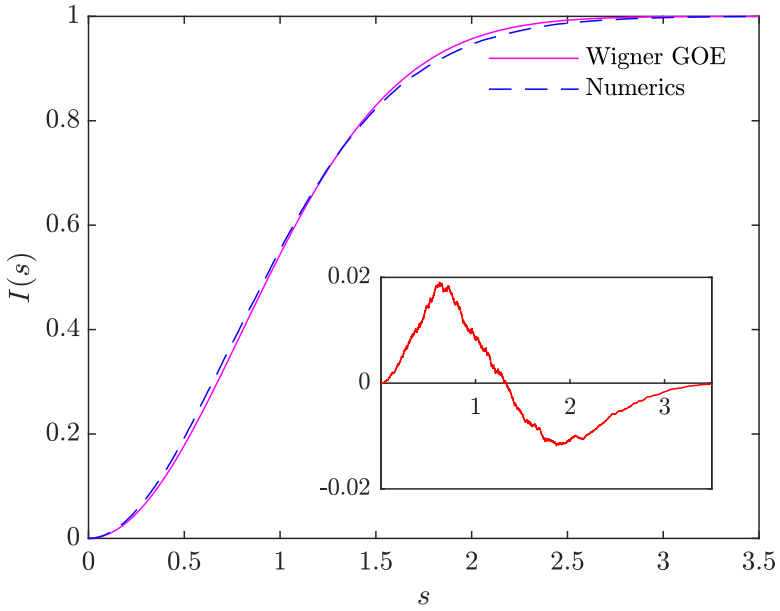

Figure 4.4. The integrated nearest-neighbor spacing distribution for the quantum circulant graph $C_{16}(\boldsymbol{L};(1,3,5,7))$ plotted against the GOE Wigner surmise. The inset shows the difference between the distribution and the numerical data.

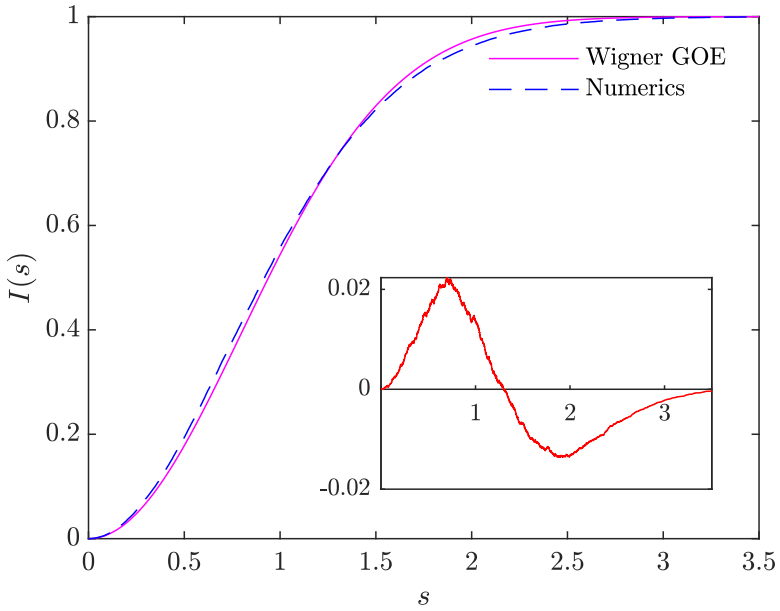

Figure 4.5. The integrated nearest-neighbor spacing distribution for the quantum circulant graph $C_{24}(\boldsymbol{L};(1,2,3,6))$ plotted against the GOE Wigner surmise. The inset shows the difference between the distribution and the numerical data.

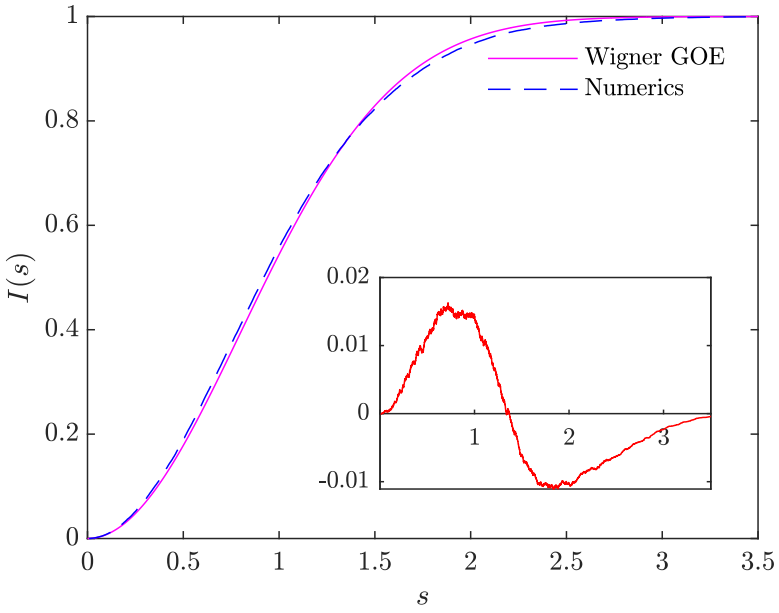

Figure 4.6. The integrated nearest-neighbor spacing distribution for the quantum circulant graph $C_{49}(\boldsymbol{L}; (3, 4, 9, 12, 15, 19, 20))$ plotted against the GOE Wigner surmise. The inset shows the difference between the distribution and the numerical data.

4.2 Intermediate Statistics

In the case of symmetric quantum circulant graphs, the spectrum decomposes into subspectra whose eigenfunctions transform according to irreducible representations of the cyclic group (see 3.3.2). As we will see, these subspectra do not follow the spectral statistics of random matrix theory as proposed by the BGS conjecture. In fact, these spectral statistics fall into a class known as intermediate statistics.

Classically chaotic quantum systems are conjectured to have spectral statistics in agreement with the predictions of the Gaussian ensembles of random matrices. In contrast, classically integrable systems typically give rise to Poisson statistics, indicating an uncorrelated spectrum. Between these two extremes lie a variety of examples of intermediate statistics.

A prototypical example of a system giving rise to intermediate statistics is the Šeba billiard. This is a rectangular quantum billiard (integrable system) perturbed by

a point singularity. The well-studied star graph also belongs to this same class [14, 12]. Despite what one might wish to believe, intermediate statistics are by no means universal [55]. Harrison and Winn [63] found a type of intermediate statistics distinct from the star graph for the *Dirac rose graph*, a single vertex with d loops equipped with the Dirac operator. This in turn was adapted from methods of Bogomolny, Gerland, and Schmit in [26].

4.2.1 Two-Point Correlation Function

As seen in figure 3.2, the quotient graph of a symmetric quantum circulant graph is topologically a rose graph. For symmetric circulant graphs, we can obtain predictions for the two-point correlation function of the subspectra transforming according to an irreducible representation $\mathcal{R}_j$ by applying arguments developed in [25, 26]. The *two-point correlation function* is defined as

$$R_2(x) = \lim_{N\to\infty} \frac{1}{N} \sum_{n=1}^{N} \sum_{m=1}^{N} \delta(x - (\hat{k}_n - \hat{k}_m)) \ . \tag{4.9}$$

Notice that $R_2(x)$ is not a probability distribution, since it contains two sums from 1 to N but has a normalization factor of $1/N$.

To analyze the spectral statistics of a symmetric quantum circulant graph, we consider both small and large parameter asymptotics of the two-point correlation function. That is, we examine how $R_2(x)$ behaves as $x \to 0$ and $x \to \infty$, respectively. After obtaining suitable estimates, we compare these with numerical results in section 4.2.4.

4.2.2 Small Spacing Asymptotic Estimate

The method follows from [63] but will be reproduced here for completeness. Recall the secular equation for the subspectra of a symmetric quantum circulant graph transforming according to an irreducible representation $\mathcal{R}_j$ in section 3.3.2, and define

$$p_j(k) = 2\sum_{h=1}^{d} \cos(a_h\theta_j)\csc(kl_h) - \cot(kl_h) \ , \tag{4.10}$$

so that $p_j(k) = 0$ corresponds to (3.44). The dominant behavior of $R_2(x)$ for small x comes from closely spaced roots. To analyze these statistics, we can approximate with the zeros of a function with three randomly-distributed poles,

$$\frac{r_1}{k-c_1} + \frac{r_2}{k-c_2} + \frac{r_3}{k-c_3} = 0 \ . \tag{4.11}$$

where r_1, r_2, r_3 are random residues and c_1, c_2, c_3 are random poles.

Rearranging (4.11) gives the quadratic equation,

$$\begin{aligned}(r_1+r_2+r_3)k^2 - (r_1(c_2+c_3) + r_2(c_1+c_3) + r_3(c_1+c_2))k \\ + r_1c_2c_3 + r_2c_1c_3 + r_3c_1c_2 = 0 \ ,\end{aligned} \tag{4.12}$$

whose two solutions are

$$k_\pm = \frac{r_1(c_2+c_3) + r_2(c_1+c_3) + r_3(c_1+c_2) \pm \sqrt{\mathcal{D}}}{2(r_1+r_2+r_3)} \ , \tag{4.13}$$

with

$$\begin{aligned}\mathcal{D} = (r_1(c_2+c_3) + r_2(c_1+c_3) + r_3(c_1+c_2))^2 \\ - 4(r_1c_2c_3 + r_2c_1c_3 + r_3c_1c_2)(r_1+r_2+r_3) \ .\end{aligned} \tag{4.14}$$

Shifting all the poles by any constant C, so $(c_1, c_2, c_3) \mapsto (c_1+C, c_2+C, c_3+C)$, also shifts both zeros by C so that the spacing $k_+ - k_-$ is unchanged. Thus, we choose coordinates such that

$$(r_1(c_2+c_3) + r_2(c_1+c_3) + r_3(c_1+c_2)) = 0 \ , \tag{4.15}$$

which simplifies (4.14) to

$$\begin{aligned}\mathcal{D} &= -4(r_1c_2c_3 + r_2c_1c_3 + r_3c_1c_2)(r_1 + r_2 + r_3) \\ &= 4(r_1 + r_2 + r_3)\left(\frac{r_2(r_2 + r_3)}{r_1 + r_2}c_1^2 + \frac{r_1(r_1 + r_3)}{r_1 + r_2}c_2^2 + \frac{2r_1r_2}{r_1 + r_2}c_1c_2\right) \ .\end{aligned} \tag{4.16}$$

Averaging over the poles c_1, c_2 and the residues r_1, r_2, r_3 gives the main contribution to the two-point correlation function,

$$\mathrm{E}[R_2(x)] \approx \frac{1}{2}\mathrm{E}\left[\int_{-\infty}^{\infty}\int_{-\infty}^{\infty}\delta(x - \Delta k)\,\mathrm{d}e_1\,\mathrm{d}e_2\right] \ , \tag{4.17}$$

where

$$\Delta k = k_+ - k_- = \frac{\sqrt{\mathcal{D}}}{r_1 + r_2 + r_3} \ , \tag{4.18}$$

and with $\mathcal{D}$ as in (4.16). To evaluate (4.17), transform to polar coordinates by defining

$$e_1 = \sqrt{\frac{r_1 + r_2}{r_2(r_2 + r_3)}}\rho\cos\phi \ , \tag{4.19}$$

$$e_2 = \sqrt{\frac{r_1 + r_2}{r_1(r_1 + r_3)}}\rho\sin\phi \ , \tag{4.20}$$

so (4.17) becomes

$$\begin{aligned}\mathrm{E}[R_2(x)] \approx \frac{1}{2}\mathrm{E}\Bigg[\int_0^{2\pi}\int_0^{\infty} &\frac{(r_1 + r_2)\rho}{\sqrt{r_1r_2(r_1 + r_3)(r_2 + r_3)}}\times \\ &\delta\left(x - \frac{2\rho}{\sqrt{r_1 + r_2 + r_3}}\left(1 + \frac{2\sqrt{r_1r_2}\cos\phi\sin\phi}{\sqrt{(r_1 + r_3)(r_2 + r_3)}}\right)^{1/2}\right)\,\mathrm{d}\rho\,\mathrm{d}\phi\Bigg] \ .\end{aligned} \tag{4.21}$$

Rescaling $\delta(x - \alpha\rho) = \delta(x - \rho)/|\alpha|^2$, where

$$\alpha = \frac{2}{\sqrt{r_1 + r_2 + r_3}}\left(1 + \frac{2\sqrt{r_1r_2}\cos\phi\sin\phi}{\sqrt{(r_1 + r_3)(r_2 + r_3)}}\right)^{1/2} \ , \tag{4.22}$$

yields

$$\begin{aligned}\mathrm{E}[R_2(x)] \approx & \frac{1}{2}\mathrm{E}\left[\frac{(r_1+r_2)}{\sqrt{r_1r_2(r_1+r_3)(r_2+r_3)}}\frac{r_1+r_2+r_3}{4}\times\right. \\ & \left.\int_0^{2\pi}\left(1+\frac{2\sqrt{r_1r_2}\cos\phi\sin\phi}{\sqrt{(r_1+r_3)(r_2+r_3)}}\right)^{-1}\mathrm{d}\phi\int_0^{\infty}\delta\left(x-\rho\right)\rho\,\mathrm{d}\rho\right] .\end{aligned} \tag{4.23}$$

To evaluate the integral over ϕ, we use the integral formula

$$\int_0^{2\pi}\frac{\mathrm{d}\phi}{1+a\cos\phi\sin\phi}=\frac{2\pi}{\sqrt{1-a^2/4}}\ , \tag{4.24}$$

applicable when $|a|<2$. So,

$$\begin{aligned}\int_0^{2\pi}\left(1+\frac{2\sqrt{r_1r_2}\cos\phi\sin\phi}{\sqrt{(r_1+r_3)(r_2+r_3)}}\right)^{-1}\mathrm{d}\phi &= 2\pi\left(1-\frac{r_1r_2}{(r_1+r_3)(r_2+r_3)}\right)^{-1/2} \\ &= 2\pi\frac{\sqrt{(r_1+r_3)(r_2+r_3)}}{(r_3)^{1/2}\sqrt{(r_1+r_2+r_3)}}\ ,\end{aligned} \tag{4.25}$$

which when substituted into (4.23),

$$\begin{aligned}\mathrm{E}[R_2(x)] &\approx \frac{\pi}{4}\mathrm{E}\left[\frac{(r_1+r_2)\sqrt{(r_1+r_2+r_3)}}{\sqrt{r_1r_2r_3}}\int_0^{\infty}\delta\left(x-\rho\right)\rho\,\mathrm{d}\rho\right] \\ &\approx \frac{\pi x}{4}\mathrm{E}\left[\frac{(r_1+r_2)\sqrt{(r_1+r_2+r_3)}}{\sqrt{r_1r_2r_3}}\right] .\end{aligned} \tag{4.26}$$

Assuming the r_j are identically distributed gives the symmetrized form

$$\mathrm{E}[R_2(x)] \approx \frac{\pi x}{6}\mathrm{E}\left[\sqrt{\frac{(r_1+r_2+r_3)^3}{r_1r_2r_3}}\right] . \tag{4.27}$$

Now to determine the r_j, consider the function $\psi(x,\theta)=\cos\theta\csc x-\cot x$, so that (4.10) becomes

$$p_j(k) = \sum_{h=1}^{d} \psi(kl_h, a_h\theta_j) \ . \tag{4.28}$$

We can rewrite $\psi(x,\theta)$ as a Laurent series by observing

$$\cot x = \frac{1}{x} + 2\sum_{m=1}^{\infty} \frac{x}{x^2 - m^2\pi^2} \ , \tag{4.29}$$

and

$$\csc x = \frac{1}{x} + 2\sum_{m=1}^{\infty} \frac{(-1)^m x}{x^2 - m^2\pi^2} \ , \tag{4.30}$$

so that

$$\psi(x,\theta) = \sum_{m=-\infty}^{\infty} ((-1)^m \cos\theta - 1)\left(\frac{1}{x+m\pi} - \frac{m\pi}{1+m^2\pi^2}\right) \ . \tag{4.31}$$

This shows that $p_j(k)$ has a sequence of poles at $k = m\pi/l_h$, for $h = 1, \ldots, d$ with residues $r = (-1)^m \cos(a_h\theta_j) - 1$. For a fixed h, the poles of $p_j(k)$ are evenly spaced, so closely spaced poles must come from different h.

For a given circulant graph $C_n(\boldsymbol{l};\boldsymbol{a})$ and a fixed representation $\mathcal{R}_j$, the values $a_h\theta_j$ are a finite set of integer multiples of $2\pi j/n$ distributed in $[0, \pi j]$. We can treat $a_h\theta_j$ as a discrete random variable if we randomly generate the circulant graph. This is done by performing a Bernoulli trial on each *possible* value of $a_h \in \{1, \ldots, \lfloor (n-1)/2 \rfloor\}$. As n grows large, $a_h\theta_j$ can be approximated by a continuous, uniformly distributed random variable in $[0, \pi]$. To avoid the presence of any Dirichlet eigenvalues (see section 3.4), which are regularly spaced and would therefore affect the statistics, we will assume that n is a large prime, so that n and j have no common factors.

The next part of the method relies on an argument in [26]. Returning to (4.27), we will consider the random residues

$$r_i = 1 - \cos\theta_i \ , \tag{4.32}$$

where θ_i is uniformly distributed in $[0, \pi]$. As described above, θ_i will serve as a model for $a_h\theta_j$, so that r_i will correspond to the residues given in (4.31). The expectation in (4.27) clearly diverges when r is small, but its leading behavior is

$$\mathrm{E}\left[\sqrt{\frac{(r_1+r_2+r_3)^3}{r_1r_2r_3}}\right] \to 3\mathrm{E}\left[r\right]\mathrm{E}\left[\frac{1}{\sqrt{r}}\right]^2 \ . \tag{4.33}$$

Evaluating

$$\mathrm{E}\left[r\right] = \frac{1}{\pi}\int_0^\pi (1-\cos\phi)\,\mathrm{d}\phi = 1 \ , \tag{4.34}$$

we see that the divergence stems from $\mathrm{E}\left\{1/\sqrt{r}\right\}$. To remedy this, we introduce a cutoff ϕ_0 at zero, so

$$\mathrm{E}\left[\frac{1}{\sqrt{r}}\right] = \frac{1}{\pi}\int_{\phi_0}^\pi \frac{\mathrm{d}\phi}{\sqrt{1-\cos\phi}} \approx -\frac{\sqrt{2}}{\pi}\ln\phi_0 \ . \tag{4.35}$$

The value ϕ_0 is proportional to x with logarithmic accuracy, so $\phi_0 \to x/c$ for some constant c. Therefore, plugging (4.34) and (4.35) into (4.33),

$$\mathrm{E}[R_2(x)] \approx \frac{1}{4\pi}\ln^2\left(\frac{x}{c}\right)x \ , \tag{4.36}$$

which gives an estimate for the asymptotic behavior of $R_2(x)$ for small x [62].

4.2.3 Large Spacing Asymptotic Estimate

To examine the large parameter asymptotics, we study the Fourier transform of the two-point correlation function, $R_2(x)$, called the *form factor* $K(\tau)$. Considering the small parameter asymptotics of $K(\tau)$ will determine the large parameter asymptotics of $R_2(x)$. To do this, we write $K(\tau)$ in terms of periodic orbits using the trace formula. This technique is adapted from a method used in [14, 63].

Before introducing the form factor, we must include some necessary terminology regarding periodic orbits on graphs. A *periodic orbit* p is an equivalence class of closed

paths with respect to cyclic shifts. That is,

$$p = [e_1 e_2 \dots e_{m-1} e_m] \cong [e_2 e_3 \dots e_m e_1] \cong \dots \cong [e_m e_1 \dots e_{m-2} e_{m-1}] \ . \tag{4.37}$$

We will generally omit the brackets.

The *topological length* of a periodic orbit is the number of edges in the periodic orbit. For example, the periodic orbit p in (4.37) has topological length m. The set of all periodic orbits of topological length m is denoted $\mathcal{P}_m$. In a metric graph, the *metric length* L_p of a periodic orbit p is the sum of the lengths of all the edges in p, so

$$L_p = L_{e_1} + L_{e_2} + \dots + L_{e_{m-1}} + L_{e_m} = \sum_{e_j \in p} L_{e_j} \ , \tag{4.38}$$

where L_{e_j} is the metric length of the edge e_j.

A *primitive periodic orbit* is one which is not a repetition of a shorter orbit. Suppose the orbit p of topological length m is a repetition of the primitive periodic orbit p' with topological length m'. Then, the *repetition number* of p is $r_p = m/m'$.

Finally, A_p is the *stability amplitude* of the periodic orbit p. This is the product of the elements of the scattering matrices of all the vertices in the periodic orbit. Recall that $\sigma^{(v)}$ is the vertex scattering matrix at the vertex v 2.13 where $\sigma^{(v)}_{e',e}$ gives the coefficient when scattering from e to e'. So we have

$$A_p = \sigma^{(v_{i_1})}_{e_2,e_1} \sigma^{(v_{i_2})}_{e_3,e_2} \cdots \sigma^{(v_{i_{m-1}})}_{e_m,e_{m-1}} \sigma^{(v_{i_m})}_{e_1,e_m} \ , \tag{4.39}$$

where $v_{i_j} = t(e_j)$ for $j = 1, \dots, m$.

As in [18], the form factor of a quantum graph is

$$K(\tau) = \frac{1}{4\mathcal{L}^2} \sum_{n=1}^{\infty} \sum_{p,q \in \mathcal{P}_n} \frac{A_p A_q L_p L_q}{r_p r_q} \delta\left(\tau - \frac{L_p}{2\mathcal{L}}\right) \delta_{L_p, L_q} \ . \tag{4.40}$$

If we choose the distinct edge lengths to be incommensurate, then δ_{L_p,L_q} ensures that any pair of orbits which contribute to the form factor visit each edge the same number of times, so they must have the same topological length n. So if $\mathcal{P}$ is the set of all periodic orbits on the graph, we can rewrite the form factor as

$$K(\tau) = \frac{1}{4\mathcal{L}^2} \sum_{p,q\in\mathcal{P}} \frac{A_p A_q L_p L_q}{r_p r_q} \delta\left(\tau - \frac{L_p}{2\mathcal{L}}\right) \delta_{L_p,L_q} \ . \tag{4.41}$$

Let $\mathfrak{L}$ be the set of all possible lengths of periodic orbits. A periodic orbit with length $L \in \mathfrak{L}$ is a member of the *degeneracy class* associated to that length. Sorting (4.41) by degeneracy class,

$$K(\tau) = \frac{1}{4\mathcal{L}^2} \sum_{L\in\mathfrak{L}} L^2 \delta\left(\tau - \frac{L}{2\mathcal{L}}\right) \left(\sum_{\substack{p\in\mathcal{P}\\ L_p=L}} \frac{A_p}{r_p}\right)^2 \ . \tag{4.42}$$

Let $\mathcal{P}_t$ be the set of periodic orbits of topological length t. Then we define

$$\tilde{K}(t,E) = \frac{E}{2\mathcal{L}^2} \sum_{L\in\mathfrak{L}} L^2 \left(\sum_{\substack{p\in\mathcal{P}_t\\ L_p=L}} \frac{A_p}{r_p}\right)^2 \ , \tag{4.43}$$

where $E = |\mathcal{E}|$ is the number of edges, so that $\tilde{K}(t,E) \to K(\tau)$ weakly as $E \to \infty$ if $t/2E \to \tau$ as $E \to \infty$.

Recall the quotient graph of a symmetric circulant graph $C_n(\boldsymbol{l};\boldsymbol{a})$, section 3.3.2. The quotient graph has d edges, one corresponding to each element of the vector $\boldsymbol{a}$, and its metric length is $\mathcal{L}_Q = \sum_{h=1}^{d} l_h$, so (4.43) becomes

$$\tilde{K}(t,d) = \frac{d}{2(\mathcal{L}_Q)^2} \sum_{L\in\mathfrak{L}} L^2 \left(\sum_{\substack{p\in\mathcal{P}_t\\ L_p=L}} \frac{A_p}{r_p}\right)^2 \ . \tag{4.44}$$

Now, define

$$\tilde{K}_j(t,d) = \frac{d}{2(\mathcal{L}_Q)^2} \sum_{\substack{L \text{ restricted} \\ \text{to } j \text{ edges}}} L^2 \mathrm{E}\left[\sum_{\substack{p\in\mathcal{P}_t \\ L_p = L}} \frac{A_p}{r_p} \right]^2 , \tag{4.45}$$

which is the expectation of $\tilde{K}(t,d)$ restricted to j edges and averaged over random phases θ_i from the previous section. So then,

$$\mathrm{E}\left[K(\tau)\right] = \lim_{\substack{d\to\infty \\ t/2d\to\tau}} \sum_{j=1}^{d} \tilde{K}_j(t,d) \ . \tag{4.46}$$

To approximate $\mathrm{E}\left[K(\tau)\right]$, we will select terms from (4.45) whose orbits give the largest contribution as the number of edges increases to infinity. This turns out to be those orbits who exhibit maximal back-scattering. To see why, consider the vertex scattering matrix for the vertex v with degree d_v and Neumann-like conditions,

$$\sigma^{(v)} = \frac{2}{d_v}\mathbb{E} - \mathbb{I} \ , \tag{4.47}$$

where $\mathbb{E}$ is the $d_v \times d_v$ matrix of ones and $\mathbb{I}$ is the $d_v \times d_v$ identity matrix. In the quotient graph, $d_v = 2d$ at the central vertex, so the contribution from back-scattering is increasingly more significant as $d \to \infty$.

4.2.3.1 Orbits restricted to one edge. We first consider the case where $j = 1$, that is periodic orbits restricted to a single edge e. When t, the topological length of p, is even, maximal back-scattering is achieved by repeated transitions from e to $\bar{e}$ and back to e, where $\bar{e}$ is the reversal of e. So, the contributing orbits take the form

$$p = e\bar{e}e\bar{e}\cdots e\bar{e}e\bar{e} \ . \tag{4.48}$$

Since the the transition from e to $\bar{e}$ involves back-scattering at the central vertex v, the scattering coefficient $\sigma^{(v)}_{\bar{e},e} = (1/d - 1)\mathrm{e}^{\mathrm{i}\theta_e}$, where $\mathrm{e}^{\mathrm{i}\theta_e}$ is the phase factor

picked up at the midpoint dummy vertex. On the other hand, $\sigma^{(v)}_{e,\bar{e}} = (1/d-1)\mathrm{e}^{-\mathrm{i}\theta_e}$, since traversing the edge e in the opposite direction picks up the inverse factor $\mathrm{e}^{-\mathrm{i}\theta_e}$. The stability amplitude (4.39) is the product of these coefficients,

$$A_p = \left(\frac{1}{d} - 1\right)^t \ . \tag{4.49}$$

The repetition number of p is $r_p = t/2$, as there are $t/2$ copies of $e\bar{e}$. We choose edge lengths $l \in (1-1/d, 1+1/d)$ so that $l \to 1$ as $d \to \infty$. Thus, we can approximate $L \approx t$ and $\mathcal{L}_Q \approx d$. Because there are d choices for the edge e, we have

$$\begin{aligned} \tilde{K}_1(t,d) &\approx (d)_1 \frac{d}{2d^2} t^2 \left(\frac{\left(1-\frac{1}{d}\right)^t}{t/2}\right)^2 \\ &\approx 2\left(1-\frac{1}{d}\right)^{2t} \ , \end{aligned} \tag{4.50}$$

where $(d)_1 = d!/(d-1)!$ is the Pochhammer symbol, or falling factorial. Letting $t \to 2d\tau$ as $d \to \infty$,

$$\begin{aligned} \lim_{\substack{d\to\infty \\ t/2d\to\tau}} \tilde{K}_1(t,d) &\approx \lim_{d\to\infty} 2\left(1-\frac{1}{d}\right)^{4d\tau} \\ &= 2\mathrm{e}^{-4\tau} \ , \end{aligned} \tag{4.51}$$

which is the same result obtained for $j = 1$ and even t for rose graphs in [63].

When t is odd, there are two possible orbits restricted to one edge that achieve maximal back-scattering, corresponding to a transition ee or $\bar{e}\bar{e}$,

$$p = \begin{cases} \bar{e}e\bar{e}e\cdots\bar{e}ee \ , \\ e\bar{e}e\bar{e}\cdots e\bar{e}\bar{e} \ . \end{cases} \tag{4.52}$$

As before, there are $(t-1)/2$ repetitions of $e\bar{e}$, resulting in a contribution of $(1/d-1)^{t-1}$. The remaining scattering coefficients are $\sigma^{(v)}_{e,e} = (1/d)\mathrm{e}^{\mathrm{i}\theta_e}$ and $\sigma^{(v)}_{\bar{e},\bar{e}} = (1/d)\mathrm{e}^{-\mathrm{i}\theta_e}$, so (4.39) is

$$A_p = \begin{cases} \left(\frac{1}{d}-1\right)^{t-1} \frac{1}{d}\mathrm{e}^{\mathrm{i}\theta_e} \ , \\ \left(\frac{1}{d}-1\right)^{t-1} \frac{1}{d}\mathrm{e}^{-\mathrm{i}\theta_e} \ , \end{cases} \tag{4.53}$$

respectively.

Finally, both orbits are primitive, so $r_p = 1$. Choosing appropriate edge lengths and approximating $\mathcal{L}$ and L as before, we have

$$\begin{aligned} \tilde{K}_1(t,d) &\approx (d)_1 \frac{t^2}{2d}\left(1-\frac{1}{d}\right)^{2t-2}\left(\frac{1}{d}\right)^2 \mathrm{E}\left[(\mathrm{e}^{\mathrm{i}\theta_e}+\mathrm{e}^{-\mathrm{i}\theta_e})^2\right] \\ &\approx \frac{t^2}{2d^2}\left(1-\frac{1}{d}\right)^{2t-2} \mathrm{E}\left[4\cos^2\theta_e\right] \ . \end{aligned} \tag{4.54}$$

Consequently,

$$\lim_{\substack{d\to\infty \\ t/2d\to\tau}} \tilde{K}_1(t,d) \approx \lim_{d\to\infty} 8\tau^2\left(1-\frac{1}{d}\right)^{4d\tau-2} \mathrm{E}\left[\cos^2\theta_e\right] = 4\tau^2\mathrm{e}^{-4\tau} \ . \tag{4.55}$$

Since odd and even values of t are equally distributed, the total contribution to (4.46) for $j=1$ is the average of (4.51) and (4.55):

$$(1+2\tau^2)e^{-4\tau} \ . \tag{4.56}$$

4.2.3.2 Orbits restricted to two edges. To better understand the general case, we first consider the case where $j=2$. We will denote the two edges on which the orbit lives as e_1 and e_2. To achieve maximal back-scattering, we split the topological length t into an orbit of length t_1 on e_1 and an orbit of length t_2 on e_2 such that $t = t_1 + t_2$. There are $2^2 = 4$ possibilities for t_1 and t_2 to be even or odd, each with a weight of approximately $t/4$:

1. t_1 is odd and t_2 is odd, so t is even. $\left(\frac{t}{2} \text{ possibilities}\right)$

   Here, there are $2^2 = 4$ members of the degeneracy class, given by

$$p = \begin{cases} e_1\bar{e_1}e_1\bar{e_1}\cdots e_1\bar{e_1}e_1e_2\bar{e_2}e_2\cdots\bar{e_2}e_2, & (\text{transitions: } e_1e_2, e_2e_1) \\ \bar{e_1}e_1\bar{e_1}e_1\cdots\bar{e_1}e_1\bar{e_1}e_2\bar{e_2}e_2\cdots\bar{e_2}e_2, & (\text{transitions: } \bar{e_1}e_2, e_2\bar{e_1}) \\ e_1\bar{e_1}e_1\bar{e_1}\cdots e_1\bar{e_1}e_1\bar{e_2}e_2\bar{e_2}\cdots e_2\bar{e_2}, & (\text{transitions: } e_1\bar{e_2}, \bar{e_2}e_1) \\ \bar{e_1}e_1\bar{e_1}e_1\cdots\bar{e_1}e_1\bar{e_1}\bar{e_2}e_2\bar{e_2}\cdots e_2\bar{e_2}, & (\text{transitions: } \bar{e_1}\bar{e_2}, \bar{e_2}\bar{e_1}) \end{cases} \tag{4.57}$$

   which yield stability amplitudes (4.39),

$$A_p = \begin{cases} \left(\frac{1}{d} - 1\right)^{t-2} \frac{\exp(\mathrm{i}\theta_{e_1})\exp(\mathrm{i}\theta_{e_2})}{d^2} \\ \left(\frac{1}{d} - 1\right)^{t-2} \frac{\exp(-\mathrm{i}\theta_{e_1})\exp(\mathrm{i}\theta_{e_2})}{d^2} \\ \left(\frac{1}{d} - 1\right)^{t-2} \frac{\exp(\mathrm{i}\theta_{e_1})\exp(-\mathrm{i}\theta_{e_2})}{d^2} \\ \left(\frac{1}{d} - 1\right)^{t-2} \frac{\exp(-\mathrm{i}\theta_{e_1})\exp(-\mathrm{i}\theta_{e_2})}{d^2} \end{cases} \tag{4.58}$$

   respectively.

2. t_1 is odd and t_2 is even, so t is odd. $\left(\frac{t-1}{2} \text{ possibilities}\right)$

   Here, there are $2^2 = 4$ members of the degeneracy class, given by

$$p = \begin{cases} e_1\bar{e_1}e_1\bar{e_1}\cdots e_1\bar{e_1}e_1e_2\bar{e_2}\cdots e_2\bar{e_2}, & (\text{transitions: } e_1e_2, \bar{e_2}e_1) \\ \bar{e_1}e_1\bar{e_1}e_1\cdots\bar{e_1}e_1\bar{e_1}e_2\bar{e_2}\cdots e_2\bar{e_2}, & (\text{transitions: } \bar{e_1}e_2, \bar{e_2}\bar{e_1}) \\ e_1\bar{e_1}e_1\bar{e_1}\cdots e_1\bar{e_1}e_1\bar{e_2}e_2\cdots\bar{e_2}e_2, & (\text{transitions: } e_1\bar{e_2}, e_2e_1) \\ \bar{e_1}e_1\bar{e_1}e_1\cdots\bar{e_1}e_1\bar{e_1}\bar{e_2}e_2\cdots\bar{e_2}e_2, & (\text{transitions: } \bar{e_1}\bar{e_2}, e_2\bar{e_1}) \end{cases} \tag{4.59}$$

   which yield stability amplitudes (4.39),

$$A_p = \begin{cases} \left(\frac{1}{d} - 1\right)^{t-2} \frac{\exp(\mathrm{i}\theta_{e_1})}{d^2} \\ \left(\frac{1}{d} - 1\right)^{t-2} \frac{\exp(-\mathrm{i}\theta_{e_1})}{d^2} \\ \left(\frac{1}{d} - 1\right)^{t-2} \frac{\exp(\mathrm{i}\theta_{e_1})}{d^2} \\ \left(\frac{1}{d} - 1\right)^{t-2} \frac{\exp(-\mathrm{i}\theta_{e_1})}{d^2} \end{cases} \tag{4.60}$$

respectively.

3. t_1 is even and t_2 is odd, so t is odd. $\left(\frac{t-1}{2} \text{ possibilities}\right)$

   Here, there are $2^2 = 4$ members of the degeneracy class, given by

$$p = \begin{cases} \bar{e_1} e_1 \bar{e_1} e_1 \cdots \bar{e_1} e_1 e_2 \bar{e_2} e_2 \cdots \bar{e_2} e_2, & (\text{transitions: } e_1 e_2, e_2 \bar{e_1}) \\ e_1 \bar{e_1} e_1 \bar{e_1} \cdots e_1 \bar{e_1} e_2 \bar{e_2} e_2 \cdots \bar{e_2} e_2, & (\text{transitions: } \bar{e_1} e_2, e_2 e_1) \\ \bar{e_1} e_1 \bar{e_1} e_1 \cdots \bar{e_1} e_1 \bar{e_2} e_2 \bar{e_2} \cdots e_2 \bar{e_2}, & (\text{transitions: } e_1 \bar{e_2}, \bar{e_2} \bar{e_1}) \\ e_1 \bar{e_1} e_1 \bar{e_1} \cdots e_1 \bar{e_1} \bar{e_2} e_2 \bar{e_2} \cdots e_2 \bar{e_2}, & (\text{transitions: } \bar{e_1} \bar{e_2}, \bar{e_2} e_1) \end{cases} \tag{4.61}$$

   which yield stability amplitudes (4.39),

$$A_p = \begin{cases} \left(\frac{1}{d} - 1\right)^{t-2} \frac{\exp(\mathrm{i}\theta_{e_2})}{d^2} \\ \left(\frac{1}{d} - 1\right)^{t-2} \frac{\exp(\mathrm{i}\theta_{e_2})}{d^2} \\ \left(\frac{1}{d} - 1\right)^{t-2} \frac{\exp(-\mathrm{i}\theta_{e_2})}{d^2} \\ \left(\frac{1}{d} - 1\right)^{t-2} \frac{\exp(-\mathrm{i}\theta_{e_2})}{d^2} \end{cases} \tag{4.62}$$

   respectively.

4. t_1 is even and t_2 is even, so t is even. $\left(\frac{t-2}{2} \text{ possibilities}\right)$

   Here, there are $2^2 = 4$ members of the degeneracy class, given by

$$p = \begin{cases} e_1\bar{e_1}e_1\bar{e_1}\cdots e_1\bar{e_1}e_2\bar{e_2}\cdots e_2\bar{e_2}, & (\text{transitions: } \bar{e_1}e_2, \bar{e_2}e_1) \\ \bar{e_1}e_1\bar{e_1}e_1\cdots \bar{e_1}e_1\bar{e_2}e_2\cdots \bar{e_2}e_2, & (\text{transitions: } e_1\bar{e_2}, e_2\bar{e_1}) \\ e_1\bar{e_1}e_1\bar{e_1}\cdots e_1\bar{e_1}\bar{e_2}e_2\cdots \bar{e_2}e_2, & (\text{transitions: } \bar{e_1}\bar{e_2}, e_2e_1) \\ \bar{e_1}e_1\bar{e_1}e_1\cdots \bar{e_1}e_1e_2\bar{e_2}\cdots e_2\bar{e_2}, & (\text{transitions: } e_1e_2, \bar{e_2}\bar{e_1}) \end{cases} \tag{4.63}$$

which yield (4.39), in all cases,

$$A_p = \left(\frac{1}{d} - 1\right)^{t-2} \frac{1}{d^2} \ . \tag{4.64}$$

In each of the above possibilities, the orbit is primitive, so the repetition number is $r_p = 1$. As in the previous section, we choose edge lengths to approximate $L \approx t$ and $\mathcal{L} \approx d$, which gives

$$\begin{aligned} \tilde{K}_2(t,d) \approx & \ \frac{(d)_2}{2}\frac{t^2}{2d}\left(1-\frac{1}{d}\right)^{2t-4}\left(\frac{1}{d}\right)^4 \frac{t}{4}\mathrm{E}[4 + 2\mathrm{e}^{\mathrm{i}\theta_{e_1}} + 2\mathrm{e}^{-\mathrm{i}\theta_{e_1}} + 2\mathrm{e}^{\mathrm{i}\theta_{e_2}} \\ & + 2\mathrm{e}^{-\mathrm{i}\theta_{e_2}} + \mathrm{e}^{\mathrm{i}\theta_{e_1}}\mathrm{e}^{\mathrm{i}\theta_{e_2}} + \mathrm{e}^{-\mathrm{i}\theta_{e_1}}\mathrm{e}^{\mathrm{i}\theta_{e_2}} + \mathrm{e}^{\mathrm{i}\theta_{e_1}}\mathrm{e}^{-\mathrm{i}\theta_{e_2}} + \mathrm{e}^{-\mathrm{i}\theta_{e_1}}\mathrm{e}^{-\mathrm{i}\theta_{e_2}}]^2 \\ \approx & \ \frac{t^3}{16d^3}\left(1-\frac{1}{d}\right)^{2t-4}\Big(16 + \mathrm{E}[16\cos^2\theta_{e_1}] + \mathrm{E}[16\cos^2\theta_{e_2}] \\ & + \mathrm{E}\left[\mathrm{e}^{\mathrm{i}(\theta_{e_1}+\theta_{e_2})} + \mathrm{e}^{\mathrm{i}(\theta_{e_2}-\theta_{e_1})} + \mathrm{e}^{\mathrm{i}(\theta_{e_1}-\theta_{e_2})} + \mathrm{e}^{-\mathrm{i}(\theta_{e_1}+\theta_{e_2})}\right]^2\Big) \\ \approx & \ \frac{t^3}{16d^3}\left(1-\frac{1}{d}\right)^{2t-4}\Big(16+8+8+4\Big) \\ \approx & \ \frac{18t^3}{(2d)^3}\left(1-\frac{1}{d}\right)^{2t-4} \ . \end{aligned} \tag{4.65}$$

Letting $t \to 2d\tau$ as $d \to \infty$,

$$\begin{aligned} \lim_{\substack{d\to\infty \\ t/2d\to\tau}} \tilde{K}_2(t,d) &\approx \lim_{d\to\infty} 18\tau^3\left(1-\frac{1}{d}\right)^{4d\tau-4} \\ &= 18\tau^3\mathrm{e}^{-4\tau} \ . \end{aligned} \tag{4.66}$$

4.2.3.3 Orbits restricted to j edges. In general, if an orbit is restricted to j edges of the graph, $e_1, \ldots, e_j$, maximizing back-scattering requires minimizing transitions between edges. So think of splitting the orbit into j orbits, each living on a single edge such that

$$t_1 + \cdots + t_j = t \ , \tag{4.67}$$

where t_l is the length of the orbit living on e_l for $l = 1, \ldots, j$. This limits the number of transitions to j, so there are $t - j$ back-scatterings.

To weight the various contributions to the form factor, we must consider both the number of ways to decompose the sum in (4.67) and the relative density of odd and even t_l. Despite the fact that these are not independent, since even and odd t_l are evenly distributed, we may represent this weight for large t by the product

$$\frac{1}{2^j}\binom{t-1}{j-1} \sim \frac{t^{j-1}}{2^j(j-1)!} \ . \tag{4.68}$$

In the above expression, $1/2^j$ gives the relative density of j different odd and even t_l, $\binom{t-1}{j-1}$ gives the number of possible ways to choose transition points in (4.67), and $(t-1)!/(t-j)! \sim t^{j-1}$.

As we have seen in the previous cases, it is only odd values of t_l that contribute phases $\exp(\pm \mathrm{i}\theta_{e_l})$ to the scattering amplitude since the even values cause the terms to cancel. So, suppose there are r indices $\{i_1, \ldots, i_r\}$ for which t_{i_l} is odd. Then,

$$A_p = \left(\frac{1}{d} - 1\right)^{t-j} \frac{1}{d^j} \omega_{e_{i_1}}^{\alpha_{i_1}} \cdots \omega_{e_{i_r}}^{\alpha_{i_r}} \ , \tag{4.69}$$

where $\omega_{e_{i_l}} = \exp(\mathrm{i}\theta_{e_l})$ and $\alpha_{i_l} = \pm 1$. There are 2^j members of each degeneracy class, corresponding to j choices of e_l or $\bar{e}_l$, and there are 2^r possibilities for $\alpha_{i_l} = \pm 1$. For a given r, there are $\binom{j}{r}$ ways to choose r odd indicies, and we sum over all possible values of r. Since $r_p = 1$ in all cases,

$$
\begin{aligned}
\mathrm{E}\left[\sum_{\substack{p\in\mathcal{P}_t\\ L_p=L}} A_p\right]^2 &= \sum_{r=0}^{j}\binom{j}{r}\mathrm{E}\left[\left(\frac{1}{d}-1\right)^{t-j}\frac{1}{d^j}\sum_{\alpha_{i_l}=\pm 1} 2^{j-r}\left(\omega_{e_{i_1}}^{\alpha_{i_1}}\cdots\omega_{e_{i_r}}^{\alpha_{i_r}}\right)\right]^2 \\
&= \left(\frac{1}{d}-1\right)^{2t-2j}\frac{1}{d^{2j}}\sum_{r=0}^{j}\left\{\binom{j}{r}2^{2j-2r}\right. \\
&\qquad \left.\times\mathrm{E}\left[2^{2r}\cos^2\theta_{e_{i_1}}\cdots\cos^2\theta_{e_{i_r}}\right]\right\}
\end{aligned}
\tag{4.70}
$$

which simplifies to

$$
\mathrm{E}\left[\sum_{\substack{p\in\mathcal{P}_t\\ L_p=L}} A_p\right]^2 = \left(\frac{1}{d}-1\right)^{2t-2j}\frac{1}{d^{2j}}\sum_{r=0}^{j}\binom{j}{r}2^{2j-r} \tag{4.71}
$$

Finally, there are $(d)_j/j$ number of ways to choose j bonds on which the orbit is restricted, where the $1/j$ factor removes cyclic permutations. Combining all this into (4.45) and approximating $L \approx t$ and $\mathcal{L} \approx d$ results in

$$
\begin{aligned}
\tilde{K}_j(t,d) &\approx \frac{(d)_j}{j}\frac{t^2}{2d}\left(1-\frac{1}{d}\right)^{2t-2j}\frac{1}{d^{2j}}\frac{t^{j-1}}{2^j(j-1)!}\left\{\sum_{r=0}^{j}\binom{j}{r}2^{2j-r}\right\} \\
&\approx \frac{t^{j+1}}{(2d)^{j+1}j!}\left(1-\frac{1}{d}\right)^{2t-2j}\{6^j\}\ .
\end{aligned}
\tag{4.72}
$$

Letting $d\to\infty$ as $t/2d\to\tau$,

$$
\lim_{\substack{d\to\infty\\ t/2d\to\tau}}\tilde{K}_j(t,d) \approx \lim_{d\to\infty}\frac{\tau^{j+1}6^j}{j!}\left(1-\frac{1}{d}\right)^{4d\tau-2j} \approx \tau^{j+1}\mathrm{e}^{-4\tau}\frac{6^j}{j!}\ . \tag{4.73}
$$

Notice that substituting $j=2$ equals the result in (4.66), as expected.

To find the expected value for the form factor $K(\tau)$, we substitute (4.56) and (4.73) into (4.46),

$$\begin{aligned} \mathrm{E}\left[K(\tau)\right] &\approx (1+2\tau^2)\mathrm{e}^{-4\tau} + \tau\mathrm{e}^{-4\tau}\sum_{j=2}^{\infty}\frac{6^j}{j!}\tau^j \\ &= \left(1-\tau-4\tau^2\right)\mathrm{e}^{-4\tau} + \tau\mathrm{e}^{2\tau} \ . \end{aligned} \tag{4.74}$$

So, for small τ, we approximate (4.74) by its Maclaurin series,

$$\mathrm{E}\left[K(\tau)\right] \approx 1 - 4\tau + 10\tau^2 - \frac{2}{3}\tau^3 - \frac{28}{3}\tau^4 + \mathrm{O}(\tau^5) \ . \tag{4.75}$$

Since $K(\tau)$ is the Fourier transform of $R_2(x)$, the small asymptotic behavior of τ will determine the large asymptotic behavior of x. Specifically, if

$$1 - k(\tau) = \int_{-\infty}^{\infty}(1-r(x))\mathrm{e}^{2\pi\mathrm{i}x\tau}\,\mathrm{d}x \ , \tag{4.76}$$

holds for some functions $k(\tau)$ and $r(x)$, then for even $k(\tau)$ such that

$$k(\tau) \sim 1 + \sum_{l=1}^{\infty} a_l\tau^l \ , \tag{4.77}$$

we have

$$r(x) \sim 1 + 2\Re\left\{\sum_{l=1}^{\infty}\left(\frac{-\mathrm{i}}{2\pi}\right)^{l+1}\frac{a_l l!}{x^{l+1}}\right\} \ . \tag{4.78}$$

So, using the coefficients of (4.75) applied to the previous equation gives the approximation

$$\mathrm{E}[R_2(x)] \sim 1 + \frac{2}{\pi^2x^2} - \frac{1}{2\pi^4x^4} + \mathrm{O}\left(\frac{1}{x^6}\right) \ . \tag{4.79}$$

This result [62] is similar to the corresponding asymptotic approximations for the two-point correlation functions of the star graph and the Dirac operator on a rose graph. For the star graph, the full series expansion is [14, 12]

$$R_2(x) \sim 1 + \frac{2}{\pi^2x^2} + \frac{76}{\pi^4x^4} + \mathrm{O}\left(\frac{1}{x^6}\right) \ , \tag{4.80}$$

and for the rose graph, it is [63]

$$R_2(x) \sim 1 + \frac{2}{\pi^2 x^2} - \frac{13}{8\pi^4 x^4} + \mathrm{O}\left(\frac{1}{x^6}\right) \ . \tag{4.81}$$

The main distinction between these three cases is the difference in the coefficient of the third term. Whereas for the star graph, it is $76/\pi^4$, for the rose graph and the symmetric quantum circulant quotient graph, the coefficient is negative: $-13/8\pi^4$ in the former and $-1/2\pi^4$ in the latter.

4.2.4 Numerical Analysis of Two-Point Correlation Function

When comparing the numerical statistics to the estimates (4.36) and (4.79), we considered the subspectra for a symmetric quantum circulant graph separately, as well as looking at the average over all the subspectra. We numerically computed the eigenvalues corresponding to each of the irreducible representations $\mathcal{R}_j$ for several different symmetric quantum circulant graphs. To avoid a large number of Dirichlet eigenvalues in the spectrum, we primarily considered symmetric quantum circulant graphs with a prime number of vertices.

For a given graph $C_n(\boldsymbol{l};\boldsymbol{a})$, the vector $\boldsymbol{a}$ was randomly generated by using a Bernoulli trial on each integer in $\{1,\ldots,(n-1)/2\}$, with probability $1/2$. We then chose a handful of its representations $\mathcal{R}_j$ and evaluated $\approx$ 20,000,000 roots for each by using the functions $p_j(k)$ (3.31). To numerically evaluate $R_2(x)$, we approximated the Dirac delta function in (4.9) by the boxcar function,

$$g(x) = \begin{cases} \dfrac{1}{\varepsilon} & x \in [-\varepsilon/2, \varepsilon/2] \ , \\ 0 & \text{otherwise} \ , \end{cases} \tag{4.82}$$

so that, for small ε and large N,

$$R_2(x) \approx \frac{1}{N} \sum_{n=1}^{N} \sum_{m=1}^{N} g(x - (a_n - a_m)) \ . \tag{4.83}$$

In our case, this amounted to dividing the interval $[0, 4]$ into sub-intervals of length $\varepsilon = 0.04$, counting the number of total spacings that fell into each interval, and multiplying this by a factor of about 25/20,000,000.

Figure 4.7 shows the numerically computed two-point correlation function for the subspectra corresponding to the representations $\mathcal{R}_{401}$ and $\mathcal{R}_{2051}$ of a symmetric quantum circulant graph with 7919 vertices. These statistics are plotted against the small (4.36) and large (4.79) parameter asymptotic approximations computed in the previous sections. The constant in (4.36) was computed to be $c \approx 5.514$ for $\mathcal{R}_{401}$ and $c \approx 5.507$ for $\mathcal{R}_{2051}$ by using a least squares curve fitting algorithm for $x < 0.55$.

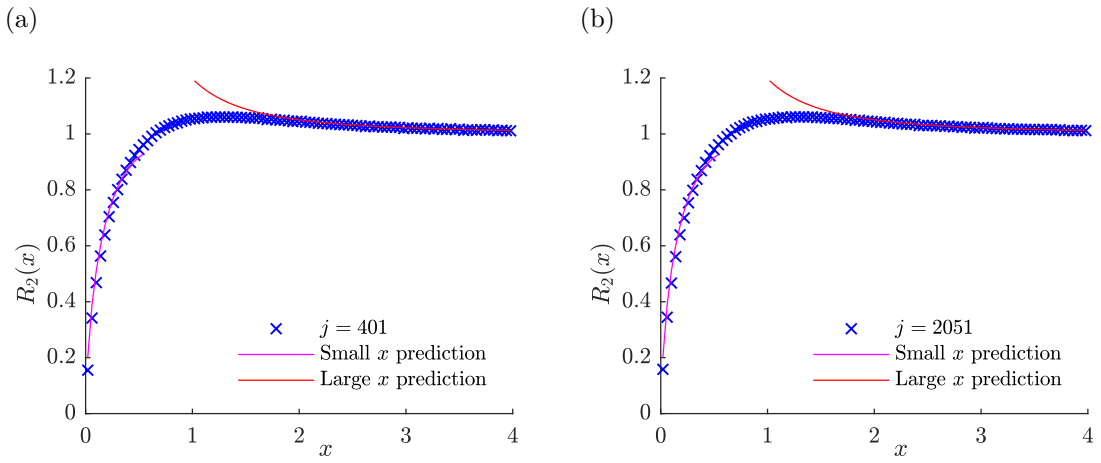

Figure 4.7. Two-point correlation functions for the subspectra of the symmetric quantum circulant graph $C_{7919}(\boldsymbol{l}; \boldsymbol{a})$ transforming according to two different irreducible representations. Both are plotted along with predictions for the small and large parameter asymptotics: (a) the two-point correlation function plotted for 20,000,089 eigenvalues from the subspectrum transforming according to $\mathcal{R}_{401}$; (b) the two-point correlation function plotted for 20,000,553 eigenvalues from the subspectrum transforming according to $\mathcal{R}_{2051}$.

Using a graph with the same number of vertices, we wanted to compute the two-point correlation function averaged over all the non-trivial irreducible representations, since the predictions are the same for all irreducible representations without

Dirichlet eigenvalues. The trivial representation, corresponding to $j = 0$ was omitted from these averages due to the presence of Dirichlet eigenvalues. To get comparable statistics, we calculated around 5,000 eigenvalues for each representation $\mathcal{R}_j$ for a total of about 20,000,000 roots. The $R_2(x)$ estimates were obtained individually for each representation $\mathcal{R}_j$ and then averaged over all the j. These are also plotted against the asymptotic estimates, shown in figure 4.8. The constant $c \approx 5.367$ was computed using the same method.

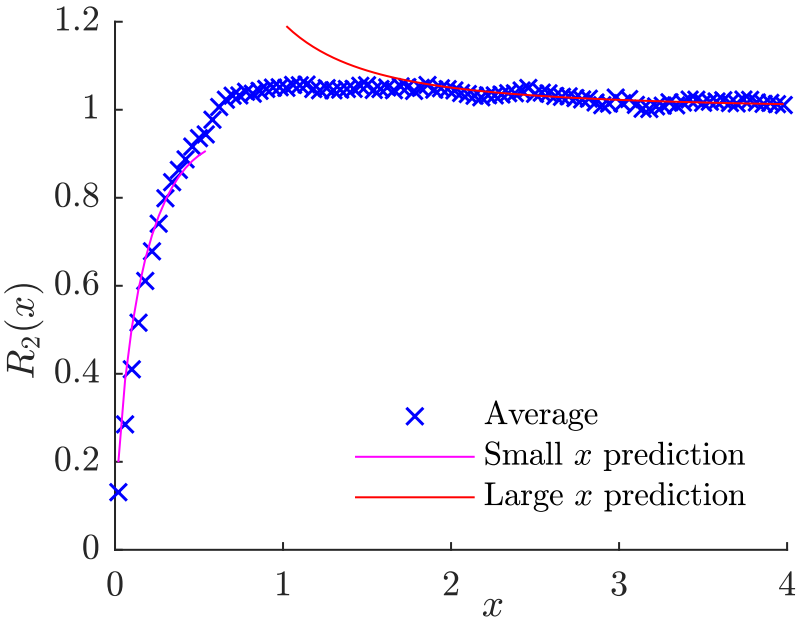

Figure 4.8. The two-point correlation function plotted for 5,362 eigenvalues from each of the subspectra of the symmetric quantum circulant graph $C_{7919}(\boldsymbol{l}; \boldsymbol{a})$ transforming according to the irreducible representations $\mathcal{R}_j$, averaged over $j = 1, \ldots, 3959$.

For completeness, we also considered the statistics of the quantum circulant graph $C_{4409}(\boldsymbol{l}; \boldsymbol{a})$. The numerically computed two-point correlation function for the subspectra corresponding to the representations $\mathcal{R}_{1796}$ and $\mathcal{R}_{1095}$ are shown in figure 4.9, along with the small (4.36) and large (4.79) parameter asymptotic approximations. We again used a least squares curve fitting algorithm for $x < 0.55$ to find c in (4.36). For $\mathcal{R}_{1796}$, we found $c \approx 5.4976$ and for $\mathcal{R}_{1095}$, we found $c \approx 5.4862$. The aver-

aged two-point correlation function for $C_{4409}(\boldsymbol{l};\boldsymbol{a})$ over all the non-trivial irreducible representations, plotted against the asymptotic estimates, is shown in figure 4.10, with constant $c \approx 5.7756$ computed using the same method. These figures, along with figures 4.7 and 4.8 demonstrate agreement between the numerical statistics for a symmetric quantum circulant graph and the asymptotics we derived. This shows that symmetric circulant graphs serve as an example of intermediate statistics.

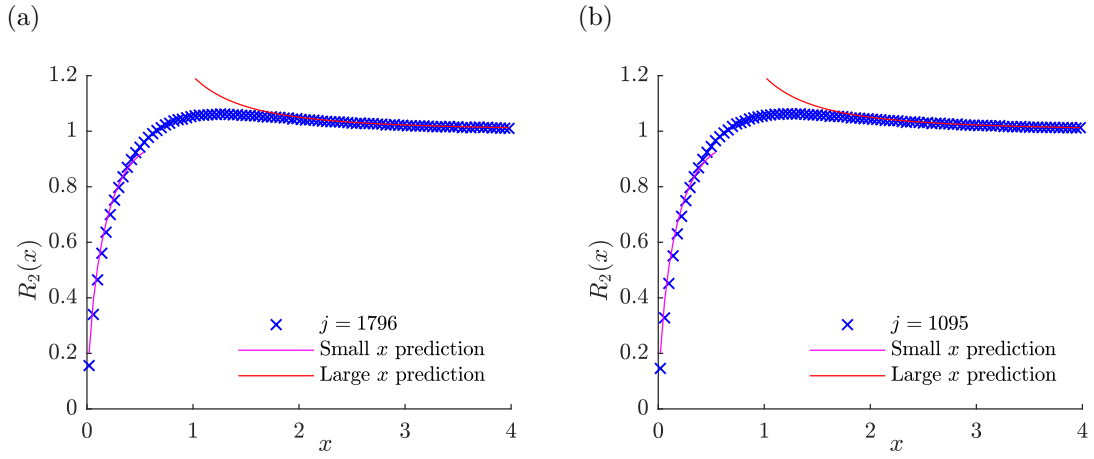

Figure 4.9. Two-point correlation functions for the subspectra of the symmetric quantum circulant graph $C_{4409}(\boldsymbol{l};\boldsymbol{a})$ transforming according to two different irreducible representations. Both are plotted along with predictions for the small and large parameter asymptotics: (a) the two-point correlation function plotted for 20,000,191 eigenvalues from the subspectrum transforming according to $\mathcal{R}_{1796}$; (b) the two-point correlation function plotted for 19,999,975 eigenvalues from the subspectrum transforming according to $\mathcal{R}_{1095}$.

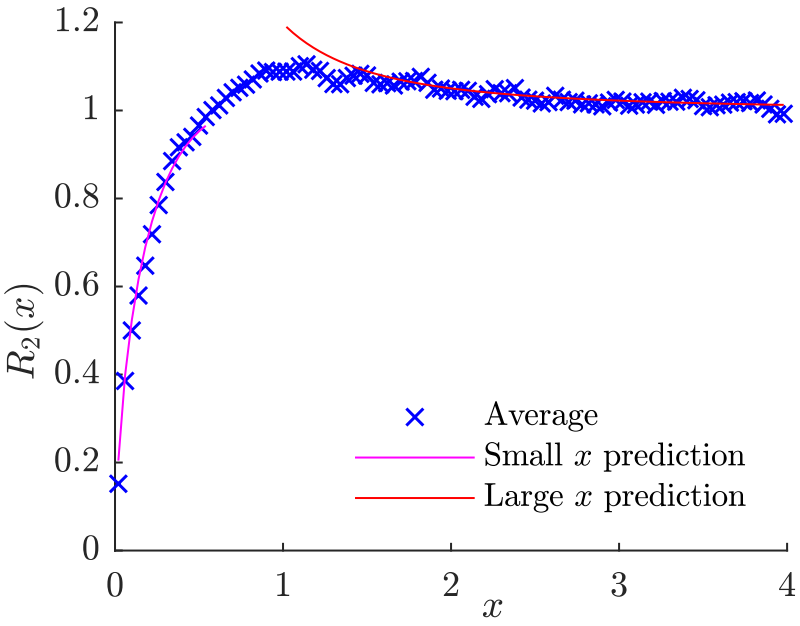

Figure 4.10. The two-point correlation function for 5,368 eigenvalues from each of the subspectra of the symmetric quantum circulant graph $C_{4409}(\boldsymbol{l};\boldsymbol{a})$ transforming according to the irreducible representations $\mathcal{R}_j$, averaged over $j = 1, \ldots, 2204$.

CHAPTER FIVE

Spectral Zeta Function

The spectral zeta function of a quantum graph is a generalization of the Riemann zeta function; instead of summing over the integers, one sums over the eigenvalues of the graph. For the Laplace operator on a quantum graph with Neumann-like vertex conditions, its spectrum will be non-negative [75, 9]. So ordering the spectrum, $0 \leq \lambda_0 \leq \lambda_1 \leq \lambda_2 \leq \cdots$, with $\lambda_i = k_i^2$, the associated spectral zeta function is defined as

$$\zeta(s) = \sum_{i=0}^{\infty}{}' k_i^{-2s}, \tag{5.1}$$

where the prime indicates that any eigenvalues of zero are omitted from the sum. We will see that the spectral zeta function encodes many of quantum graph's spectral properties. In [60, 61], the spectral zeta function for a quantum graph with general vertex conditions was constructed for the Laplace and Schrödinger operators. We construct the spectral zeta function for quantum circulant graphs using a contour integral technique introduced in [71, 72]. The results presented here for quantum circulant graphs first appeared in [62].

5.1 Symmetric Circulant Graph Zeta Function

For a symmetric quantum circulant graph, the secular equation is given as a product of functions $p_j(k)$ defined in (3.31)–(3.33). The spectrum of the quantum graph decomposes into subspectra whose eigenfunctions transform according to the irreducible representations $\mathcal{R}_j$ (see 3.3.2). Additionally, the eigenvalues in these subspectra which are not Dirichlet eigenvalues correspond to the zeros of $p_j(k)$. For each $j \in \{0, \ldots, \lfloor n/2 \rfloor\}$, we define a spectral zeta function consisting of the subspectrum associated to that value of j. Let $0 < k_{j_0} \leq k_{j_1} \leq k_{j_2} \leq \cdots$ be the positive zeros of

$p_j(k)$ for each j. Then for $\Re(s) > 1$,

$$\zeta_j(s) = \zeta_{j_D}(s) + \sum_{i=0}^{\infty}{}' k_{j_i}^{-2s} \ . \tag{5.2}$$

The term $\zeta_{j_D}(s)$ in (5.2) is the sum over the Dirichlet eigenvalues corresponding to eigenfunctions transforming according to the irreducible representation $\mathcal{R}_j$ for $j = 1, \ldots, n/2$. For $j = 0$, $\zeta_{0_D}(s)$ includes those Dirichlet eigenvalues which are present for every symmetric quantum circulant graph, corollary 3.11, namely $2m\pi/l_h$ for all $h = 1, \ldots, d$. This is because these are precisely the Dirichlet eigenvalues whose eigenfunctions transform according to the trivial representation. Then

$$\zeta(s) = \begin{cases} \zeta_0(s) + 2\sum_{j=1}^{(n-1)/2} \zeta_j(s) & \text{when } n \text{ is odd} \ , \\ \zeta_0(s) + \zeta_{n/2}(s) + 2\sum_{j=1}^{(n/2)-1} \zeta_j(s) & \text{when } n \text{ is even} \ , \end{cases} \tag{5.3}$$

is the spectral zeta function for a symmetric quantum circulant graph.

5.1.1 Integral Representation of $\zeta_0(s)$

We describe a procedure to produce an integral representation of $\zeta_0(s)$ valid for $\Re(s) < 1$. We will then be able to obtain the other $\zeta_j(s)$ in a similar fashion. The method for constructing $\zeta_0(s)$ begins by defining a complex-valued function $f_0(z)$ whose zeros on the positive real-axis correspond to the zeros of the $p_0(k)$. Recall that $p_0(k) = 2\sum_{h=1}^{d} \tan(kl_h/2)$ (3.32) and define

$$f_0(z) = \frac{1}{z}\sum_{h=1}^{d} \tan\left(\frac{zl_h}{2}\right) \ , \tag{5.4}$$

where $z = k + \mathrm{i}t \in \mathbb{C}$. Note that the zeros of f_0 are zeros of p_0, except that the zero at the origin has been removed by multiplication by $1/z$. We now choose a contour $\mathcal{C}$

which encloses the zeros of $f_0(z)$ on the positive real axis and avoids its poles. Figure 5.1 gives an example of such a contour. By the argument principle,

$$\frac{1}{2\pi \mathrm{i}} \int_{\mathcal{C}} z^{-2s} \frac{f'(z)}{f(z)} \, \mathrm{d}z = \sum_{i=0}^{\infty}{}' \left(k_{0_i}\right)^{-2s} \ , \tag{5.5}$$

where the k_{0_i} are the zeros of $f_0(z)$. So,

$$\zeta_0(s) = \zeta_{0_D}(s) + \frac{1}{2\pi \mathrm{i}} \int_{\mathcal{C}} z^{-2s} \frac{\mathrm{d}}{\mathrm{d}z} \log f_0(z) \, \mathrm{d}z \ . \tag{5.6}$$

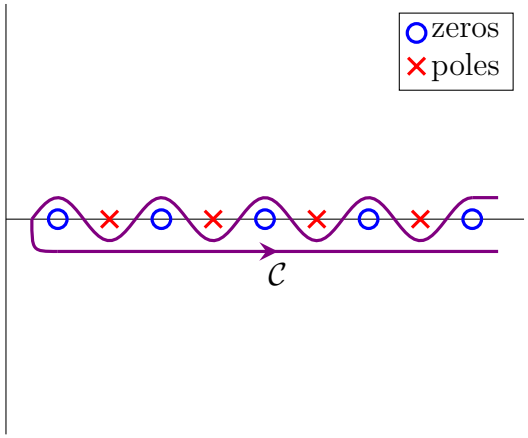

Figure 5.1. A contour $\mathcal{C}$, which encloses the zeros of $f(z)$ on the positive real axis and avoids its poles.

To obtain an analytic continuation of (5.6), we perform a contour transformation from $\mathcal{C}$ to a contour $\mathcal{C}'$, so that $\mathcal{C}'$ lies along the imaginary axis with a loop around each pole of $f_0(z)$, as shown in figure 5.2. We may then write

$$\zeta_0(s) = \zeta_{0_D}(s) + \zeta_{0_P}(s) + \zeta_{0_I}(s) \ , \tag{5.7}$$

where $\zeta_{0_I}(s)$ is the integral along the imaginary axis and $\zeta_{0_P}(s)$ is the contribution from the poles of $f_0(z)$.Since $\zeta_{0_D}(s)$ is the sum over Dirichlet eigenvalues associated

to $p_0(k)$,

$$\zeta_{0_D}(s) = \sum_{m=1}^{\infty}\sum_{h=1}^{d}\left(\frac{2m\pi}{l_h}\right)^{-2s} = \sum_{m=1}^{\infty}(2m)^{-2s}\sum_{h=1}^{d}\left(\frac{\pi}{l_h}\right)^{-2s} . \tag{5.8}$$

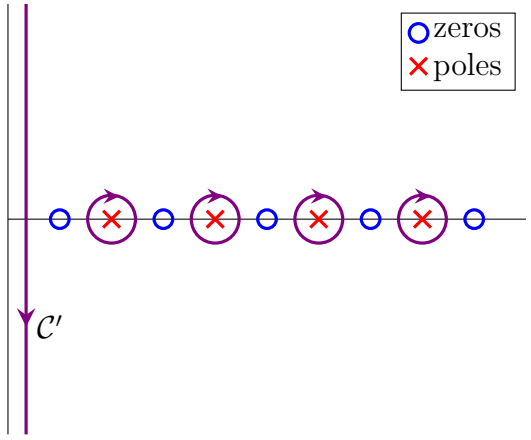

Figure 5.2. The contour $\mathcal{C}'$, which lies along the imaginary axis and loops around the poles of $f(z)$.

To find $\zeta_{0_P}(s)$, we sum the residues at the poles of $f_0(z)$. Since $f_0(z)$ is a sum of tan functions, the poles are located at $z = (2m-1)\pi/l_h$, and we have

$$\zeta_{0_P}(s) = \sum_{m=1}^{\infty}(2m-1)^{-2s}\sum_{h=1}^{d}\left(\frac{\pi}{l_h}\right)^{-2s} . \tag{5.9}$$

When combined with the Dirichlet eigenvalues (5.8), we obtain

$$\begin{aligned}\zeta_{0_D}(s) + \zeta_{0_P}(s) &= \sum_{m=1}^{\infty}(2m)^{-2s}\sum_{h=1}^{d}\left(\frac{\pi}{l_h}\right)^{-2s} + \sum_{m=1}^{\infty}(2m-1)^{-2s}\sum_{h=1}^{d}\left(\frac{\pi}{l_h}\right)^{-2s} \\ &= \left[\sum_{m=1}^{\infty}(2m)^{-2s} + \sum_{m=1}^{\infty}(2m-1)^{-2s}\right]\sum_{h=1}^{d}\left(\frac{\pi}{l_h}\right)^{-2s} \\ &= \zeta_R(2s)\sum_{h=1}^{d}\left(\frac{\pi}{l_h}\right)^{-2s} ,\end{aligned} \tag{5.10}$$

where $\zeta_R(s)$ is the Riemann zeta function.

We now turn to the integral along the imaginary axis,

$$\zeta_{0_I}(s) = \frac{1}{2\pi \mathrm{i}} \int_{\mathrm{Im}} z^{-2s} \frac{\mathrm{d}}{\mathrm{d}z} \log f_0(z)\, \mathrm{d}z = \frac{1}{2\pi \mathrm{i}} \int_{\infty}^{-\infty} (\mathrm{i}t)^{-2s} \frac{\mathrm{d}}{\mathrm{d}t} \log f_0(\mathrm{i}t)\, \mathrm{d}t \ . \tag{5.11}$$

As $\tan(\mathrm{i}t) = \mathrm{i}\tanh(t)$, we let $\hat{f}_0(t) = \sum_{h=1}^{d} \tanh\left(t l_h/2\right)$. Then write $\zeta_{0_I}(s)$ as

$$\begin{aligned}
\zeta_{0_I}(s) &= \frac{1}{2\pi \mathrm{i}} \int_{0}^{-\infty} (\mathrm{i}t)^{-2s} \frac{\mathrm{d}}{\mathrm{d}t} \log f_0(\mathrm{i}t)\, \mathrm{d}t \\
&\qquad\qquad + \frac{1}{2\pi \mathrm{i}} \int_{\infty}^{0} (\mathrm{i}t)^{-2s} \frac{\mathrm{d}}{\mathrm{d}t} \log f_0(\mathrm{i}t)\, \mathrm{d}t \\
&= \frac{(-\mathrm{i})^{-2s}}{2\pi \mathrm{i}} \int_{0}^{\infty} t^{-2s} \frac{\mathrm{d}}{\mathrm{d}t} \log\left(\frac{\hat{f}_0(t)}{t}\right) \mathrm{d}t \\
&\qquad\qquad - \frac{\mathrm{i}^{-2s}}{2\pi \mathrm{i}} \int_{0}^{\infty} t^{-2s} \frac{\mathrm{d}}{\mathrm{d}t} \log\left(\frac{\hat{f}_0(t)}{t}\right) \mathrm{d}t \\
&= \frac{\sin \pi s}{\pi} \int_{0}^{\infty} t^{-2s} \frac{\mathrm{d}}{\mathrm{d}t} \log\left(\frac{\hat{f}_0(t)}{t}\right) \mathrm{d}t \ .
\end{aligned} \tag{5.12}$$

To determine for what values of s this integral converges, we consider the asymptotic behavior of $\hat{f}_0(t)/t$,

$$\frac{\hat{f}_0(t)}{t} \sim \begin{cases} \displaystyle\sum_{h=1}^{d} \left(\frac{l_h}{2} - \frac{l_h^3 t^2}{24}\right) + \mathrm{O}(t^4) & \text{as } t \to 0 \ , \\ \displaystyle\sum_{h=1}^{d} \left(\frac{1}{t} + \mathrm{O}\left(\frac{\mathrm{e}^{-t l_h}}{t}\right)\right) & \text{as } t \to \infty \ . \end{cases} \tag{5.13}$$

Therefore $\frac{\mathrm{d}}{\mathrm{d}t} \log \hat{f}_0(t)/t$ is proportional to t near zero, and $\frac{\mathrm{d}}{\mathrm{d}t} \log \hat{f}_0(t)/t$ is asymptotic to $1/t$ as $t \to \infty$. Consequently, the integral representation (5.12) holds in the strip $0 < \Re(s) < 1$.

We are interested in using the spectral zeta function to compute the spectral determinant and vacuum energy of the graph, see sections 5.3 and 5.4. In order to do this, we need an analytic continuation of the spectral zeta function which is valid at

least for $-1/2 \leq \Re(s) \leq 0$. So, to extend the region where the integral representation of $\zeta_{0_I}(s)$ converges, we split the integral in (5.12) at $t = 1$ and expand the logarithm in the integral over $(1, \infty)$. We obtain

$$\zeta_{0_I}(s) = \frac{\sin \pi s}{\pi} \left[\int_0^1 t^{-2s} \frac{\mathrm{d}}{\mathrm{d}t} \log \frac{\hat{f}_0(t)}{t} \, \mathrm{d}t + \int_1^\infty t^{-2s} \frac{\mathrm{d}}{\mathrm{d}t} \log \hat{f}_0(t) \, \mathrm{d}t - \frac{1}{2s} \right] , \tag{5.14}$$

which converges for all s with $\Re(s) < 1$.

By combining (5.10) and (5.14), we obtain an analytic continuation convergent for $\Re(s) < 1$,

$$\begin{aligned} \zeta_0(s) = \zeta_R(2s) \sum_{h=1}^{d} \left(\frac{\pi}{l_h} \right)^{-2s} + \frac{\sin \pi s}{\pi} \Bigg[& \int_0^1 t^{-2s} \frac{\mathrm{d}}{\mathrm{d}t} \log \frac{\hat{f}_0(t)}{t} \, \mathrm{d}t \\ & + \int_1^\infty t^{-2s} \frac{\mathrm{d}}{\mathrm{d}t} \log \hat{f}_0(t) \, \mathrm{d}t - \frac{1}{2s} \Bigg] . \end{aligned} \tag{5.15}$$

This is an integral representation of the spectral zeta function for the subspectrum with eigenfunctions transforming according to the trivial representation, $\mathcal{R}_0$.

5.1.2 Integral Representation of $\zeta_j(s)$

For other values of j we follow the same procedure. Recall the definition of $p_j(k)$ for $1 \leq k \leq \lfloor (n-1)/2 \rfloor$ (3.31) and define for each j

$$f_j(z) = z \sum_{h=1}^{d} \left[\cos \left(\frac{2\pi j a_h}{n} \right) \csc(z l_h) - \cot(z l_h) \right] . \tag{5.16}$$

Observe that the zeros of f_j again correspond to the zeros of p_j, with now a pole removed at the origin by multiplication by z. We represent $\zeta_j(s)$ with the contour integral

$$\zeta_j(s) = \zeta_{j_D}(s) + \frac{1}{2\pi \mathrm{i}} \int_{\mathcal{C}} z^{-2s} \frac{\mathrm{d}}{\mathrm{d}z} \log f_j(z) \, \mathrm{d}z , \tag{5.17}$$

where $\mathcal{C}$ is the same contour as in figure 5.1 that encloses the zeros of $f_j(z)$ on the positive real axis and avoids its poles and $\zeta_{j_D}(s)$ is the sum over the Dirichlet eigenvalues corresponding to eigenfunctions transforming according to the irreducible representation $\mathcal{R}_j$. We again use the contour transformation from $\mathcal{C}$ to the contour $\mathcal{C}'$ shown in figure 5.2, and write

$$\zeta_j(s) = \zeta_{j_D}(s) + \zeta_{j_P}(s) + \zeta_{j_I}(s) \ . \tag{5.18}$$

To evaluate the integral along the imaginary axis, define

$$\hat{f}_j(t) = \sum_{h=1}^{d} \left[\coth\left(tl_h\right) - \cos\left(\frac{2\pi j a_h}{n}\right) \operatorname{csch}\left(tl_h\right) \right] \ . \tag{5.19}$$

Note that in this case, $f_j(\mathrm{i}t) = -t\hat{f}_j(t)$, so $\zeta_{j_I}(s)$ is

$$\zeta_{j_I}(s) = \frac{\sin \pi s}{\pi} \int_0^\infty t^{-2s} \frac{\mathrm{d}}{\mathrm{d}t} \log\left(t\hat{f}_j(t)\right) \, \mathrm{d}t \ . \tag{5.20}$$

Asymptotically as $t \to 0$, we see that

$$t\hat{f}_j(t) \sim \sum_{h=1}^{d} \left(\frac{1 - \cos(2\pi j a_h/n)}{l_h} + \frac{2 + \cos(2\pi j a_h/n)}{6} l_h t^2 \right) + \mathrm{O}(t^4) \ , \tag{5.21}$$

and as $t \to \infty$,

$$\begin{aligned} t\hat{f}_j(t) \sim \sum_{h=1}^{d} t \Bigg(& 1 - 2\cos\left(\frac{2\pi j a_h}{n}\right) \mathrm{e}^{-tl_h} + 2\mathrm{e}^{-2tl_h} \\ & - 2\cos\left(\frac{2\pi j a_h}{n}\right) \mathrm{e}^{-3tl_h} + \mathrm{O}\left(\mathrm{e}^{-4tl_h}\right) \Bigg) \ , \end{aligned} \tag{5.22}$$

so equation (5.20) is defined for $0 < \Re(s) < 1$. To extend the region of convergence, we can again split the integral at $t = 1$ and expand, so

$$\zeta_{j_I}(s) = \frac{\sin \pi s}{\pi} \left[\int_0^1 t^{-2s} \frac{\mathrm{d}}{\mathrm{d}t} \log t \hat{f}_j(t)\, \mathrm{d}t + \int_1^\infty t^{-2s} \frac{\mathrm{d}}{\mathrm{d}t} \log \hat{f}_j(t)\, \mathrm{d}t + \frac{1}{2s} \right] . \tag{5.23}$$

This integral representation of $\zeta_{j_I}(s)$ is valid for $\Re(s) < 1$.

To find $\zeta_{j_P}(s)$, we must determine the poles of $f_j(z)$. In general, these occur for $z = m\pi/l_h$, since these are roots of $\sin(zl_h) = 0$, but for those j and h which satisfy (3.51), a set of poles are removed. As mentioned in section 3.5, each missing pole corresponds to an added Dirichlet eigenvalue. We will see that the expression $\zeta_{j_P}(s) + \zeta_{j_D}(s)$ remains the same regardless of whether j is associated to Dirichlet eigenvalues or not.

To show this, first let n be even and fix a value $j \in \{1, \ldots, (n/2) - 1\}$. Define the sets

$$H_j^{(e)} := \{h \in \{1, \ldots, d\} : ja_h \equiv 0 \pmod{n}\} , \tag{5.24}$$

$$H_j^{(o)} := \{h \in \{1, \ldots, d\} : ja_h \equiv n/2 \pmod{n}\} . \tag{5.25}$$

These are the values of h for which there are Dirichlet eigenvalues $k^2 = (m\pi/l_h)^2$ replacing the poles of $f_j(z)$ for even and odd m, respectively. Notice that $H_j^{(e)}$ and $H_j^{(o)}$ are disjoint for a fixed j.

The contribution to $\zeta_j(s)$ from the Dirichlet eigenvalues is

$$\zeta_{j_D}(s) = \sum_{m=1}^{\infty} (2m)^{-2s} \sum_{h \in H_j^{(e)}} \left(\frac{\pi}{l_h} \right)^{-2s} + \sum_{m=1}^{\infty} (2m-1)^{-2s} \sum_{h \in H_j^{(o)}} \left(\frac{\pi}{l_h} \right)^{-2s} , \tag{5.26}$$

and consequently, the poles of $f_j(z)$ are

$$\zeta_{j_P}(s) = \sum_{m=1}^{\infty}(m)^{-2s}\sum_{h=1}^{d}\left(\frac{\pi}{l_h}\right)^{-2s} - \sum_{m=1}^{\infty}(2m)^{-2s}\sum_{h\in H_j^{(e)}}\left(\frac{\pi}{l_h}\right)^{-2s} - \sum_{m=1}^{\infty}(2m-1)^{-2s}\sum_{h\in H_j^{(o)}}\left(\frac{\pi}{l_h}\right)^{-2s} . \tag{5.27}$$

Combining (5.26) and (5.27)

$$\zeta_{j_D}(s) + \zeta_{j_P}(s) = \zeta_R(2s)\sum_{h=1}^{d}\left(\frac{\pi}{l_h}\right)^{-2s} , \tag{5.28}$$

where $\zeta_R(s)$ is the Riemann zeta function.

Now, let n be odd and observe that only those k^2 for which k is an even multiple of π/l_h will be present in the Dirichlet spectrum. Again, fix a value $j \in \{1,\ldots,(n-1)/2\}$ and define

$$H_j := \{h \in \{1,\ldots,d\} : ja_h \equiv 0 \pmod{n}\} , \tag{5.29}$$

which is the set of values of h for which the poles of $f_j(z)$ are replaced by Dirichlet eigenvalues. Then,

$$\zeta_{j_D}(s) = \sum_{m=1}^{\infty}(2m)^{-2s}\sum_{h\in H_j}\left(\frac{\pi}{l_h}\right)^{-2s} , \tag{5.30}$$

and

$$\zeta_{j_P}(s) = \sum_{m=1}^{\infty}(m)^{-2s}\sum_{h=1}^{d}\left(\frac{\pi}{l_h}\right)^{-2s} - \sum_{m=1}^{\infty}(2m)^{-2s}\sum_{h\in H_j}\left(\frac{\pi}{l_h}\right)^{-2s} , \tag{5.31}$$

which again yields (5.28) when combined.

The combined spectral zeta function for the subspectrum associated to $\mathcal{R}_j$, with $\Re(s) < 1$, is then

$$\zeta_j(s) = \zeta_R(2s) \sum_{h=1}^{d} \left(\frac{\pi}{l_h}\right)^{-2s} + \frac{\sin \pi s}{\pi} \left[\int_0^1 t^{-2s} \frac{\mathrm{d}}{\mathrm{d}t} \log t \hat{f}_j(t)\, \mathrm{d}t + \int_1^\infty t^{-2s} \frac{\mathrm{d}}{\mathrm{d}t} \log \hat{f}_j(t)\, \mathrm{d}t + \frac{1}{2s} \right] . \tag{5.32}$$

5.1.3 Integral Representation of $\zeta_{n/2}(s)$

For even n, we must also consider zeros of the function $p_{n/2}(k)$, which is defined slightly differently from the other $p_j(k)$ (3.33). Let,

$$f_{n/2}(z) = z \left(\sum_{\substack{h=1 \\ a_h \text{ is even}}}^{d} \tan\left(\frac{z l_h}{2}\right) - \sum_{\substack{h=1 \\ a_h \text{ is odd}}}^{d} \cot\left(\frac{z l_h}{2}\right) \right) , \tag{5.33}$$

so that $f_{n/2}(z)$ has the same zeros as $p_{n/2}(k)$ and the pole at the origin has been removed.

As before, we write $\zeta_{n/2}(s)$ as a contour integral and perform a contour transformation so that

$$\zeta_{n/2}(s) = \zeta_{n/2_D}(s) + \zeta_{n/2_P}(s) + \zeta_{n/2_I}(s) . \tag{5.34}$$

The derivation of $\zeta_{n/2_I}$ follows the previous cases, ultimately yielding

$$\zeta_{n/2_I}(s) = \frac{\sin \pi s}{\pi} \left[\int_0^1 t^{-2s} \frac{\mathrm{d}}{\mathrm{d}t} \log t \hat{f}_{n/2}(t)\, \mathrm{d}t + \int_1^\infty t^{-2s} \frac{\mathrm{d}}{\mathrm{d}t} \log \hat{f}_{n/2}(t)\, \mathrm{d}t + \frac{1}{2s} \right] , \tag{5.35}$$

valid for $\Re(s) < 1$, where

$$\hat{f}_{n/2}(t) = \sum_{\substack{h=1 \\ a_h \text{ is even}}}^{d} \tanh\left(\frac{t l_h}{2}\right) + \sum_{\substack{h=1 \\ a_h \text{ is odd}}}^{d} \coth\left(\frac{t l_h}{2}\right) . \tag{5.36}$$

When a_h is even, the poles of $f_j(z)$ are $z = (2m-1)\pi/l_h$. However, when a_h is even, $a_h n/2$ is a multiple of n, so the Dirichlet eigenvalues are $k^2 = (2m\pi/l_h)^2$. On

the other hand, when a_h is odd the poles are $z = 2m\pi/l_h$ and the Dirichlet eigenvalues are $k^2 = ((2m-1)\pi/l_h)^2$. In either case, summing over all h,

$$\zeta_{n/2_D}(s) + \zeta_{n/2_P}(s) = \zeta_R(2s) \sum_{h=1}^{d} \left(\frac{\pi}{l_h}\right)^{-2s} , \tag{5.37}$$

which is again the same as (5.28).

5.1.4 Full Symmetric Spectral Zeta Function

Summing the functions for each j according to equation (5.3), we obtain the spectral zeta function of a symmetric quantum circulant graph. This result appears in [62].

Theorem 5.1. *Let $C_n(\boldsymbol{l}; (a_1, \ldots, a_d))$ be a symmetric quantum circulant graph that is equipped with the Laplace operator and Neumann-like vertex conditions. The spectral zeta function for $C_n(\boldsymbol{l}; \boldsymbol{a})$, with $\Re(s) < 1$, is*

$$\begin{aligned}\zeta(s) = n\zeta_R(2s) \sum_{h=1}^{d} \left(\frac{\pi}{l_h}\right)^{-2s} + \frac{(n-2)\sin \pi s}{2\pi s} \\ + \frac{\sin \pi s}{\pi} \Bigg\{ \int_0^1 t^{-2s} \frac{\mathrm{d}}{\mathrm{d}t} \log \frac{\hat{f}_0(t)}{t} \, \mathrm{d}t + \int_1^\infty t^{-2s} \frac{\mathrm{d}}{\mathrm{d}t} \log \hat{f}_0(t) \, \mathrm{d}t \\ + 2 \sum_{j=1}^{(n-1)/2} \left[\int_0^1 t^{-2s} \frac{\mathrm{d}}{\mathrm{d}t} \log t\hat{f}_j(t) \, \mathrm{d}t + \int_1^\infty t^{-2s} \frac{\mathrm{d}}{\mathrm{d}t} \log \hat{f}_j(t) \, \mathrm{d}t \right] \Bigg\} ,\end{aligned} \tag{5.38}$$

when n is odd and

$$\begin{aligned}\zeta(s) = n\zeta_R(2s)\sum_{h=1}^{d}\left(\frac{\pi}{l_h}\right)^{-2s} + \frac{(n-2)\sin\pi s}{2\pi s} \\ + \frac{\sin\pi s}{\pi}\Bigg\{\int_0^1 t^{-2s}\frac{\mathrm{d}}{\mathrm{d}t}\log\frac{\hat{f}_0(t)}{t}\,\mathrm{d}t + \int_0^1 t^{-2s}\frac{\mathrm{d}}{\mathrm{d}t}\log t\hat{f}_{n/2}(t)\,\mathrm{d}t \\ + \int_1^\infty t^{-2s}\frac{\mathrm{d}}{\mathrm{d}t}\log\hat{f}_0(t)\,\mathrm{d}t + \int_1^\infty t^{-2s}\frac{\mathrm{d}}{\mathrm{d}t}\log\hat{f}_{n/2}(t)\,\mathrm{d}t \\ + 2\sum_{j=1}^{(n/2)-1}\left[\int_0^1 t^{-2s}\frac{\mathrm{d}}{\mathrm{d}t}\log t\hat{f}_j(t)\,\mathrm{d}t + \int_1^\infty t^{-2s}\frac{\mathrm{d}}{\mathrm{d}t}\log\hat{f}_j(t)\,\mathrm{d}t\right]\Bigg\}\,,\end{aligned} \tag{5.39}$$

when n is even.

5.2 Generic Circulant Graph Zeta Function

Although the structure of the secular equation is not quite as simple for a generic quantum circulant graph, we can still apply the contour integral technique to obtain its spectral zeta function. In this case, we assume that all the edge lengths of the quantum circulant graph are incommensurate in order to avoid any unaccounted for eigenvalues in the Dirichlet spectrum, which would superimpose eigenvalues and poles in the construction. Recall that the secular equation for such a graph is

$$\det M(k) = 0\,, \tag{5.40}$$

where the $n \times n$ matrix $M(k)$ (3.24)–(3.25) is defined by

$$[M(k)]_{ij} = \begin{cases} -\sum_{v\sim i}\cot kL_{i,v} & i = j\,, \\ \csc kL_{i,j} & i \sim j\,, \\ 0 & \text{otherwise}\,. \end{cases} \tag{5.41}$$

We define a complex-valued function whose zeros match those of $\det M(k)$ and use the argument principle to express the zeta function as a contour integral. Let

$$f(z) = z^{n-2} \det M(z) \ , \tag{5.42}$$

so that the zeros of f correspond to the roots of the secular equation. Multiplication by z^{n-2} removes the pole at the origin without introducing an additional zero. This is because the first nonzero coefficient in the expansion of $\det zM(z)$ about $z = 0$ belongs to the z^2 term, as we will see.

The zeta function for a generic quantum circulant graph is expressed as the contour integral,

$$\zeta(s) = \frac{1}{2\pi \mathrm{i}} \int_{\mathcal{C}} z^{-2s} \frac{\mathrm{d}}{\mathrm{d}z} \log f(z) \, \mathrm{d}z \ , \tag{5.43}$$

where $\mathcal{C}$ is a contour which encloses the zeros of f on the positive real axis and avoids its poles, as in figure 5.1. We deform the contour $\mathcal{C}$ to a contour $\mathcal{C}'$, as shown in figure 5.2, so that $\mathcal{C}'$ lies along the imaginary axis and loops around each pole of $f(z)$. This allows the zeta function to be written as the sum of residues at the poles of f, denoted $\zeta_P(s)$, and an integral along the imaginary axis, $\zeta_I(s)$, so

$$\zeta(s) = \zeta_P(s) + \zeta_I(s) \ . \tag{5.44}$$

The poles of f occur when $z = m\pi/L_e$, and so the sum of residues at the poles is

$$\zeta_P(s) = \sum_{m=1}^{\infty} \sum_{e \in \mathcal{E}} \left(\frac{m\pi}{L_e} \right)^{-2s} = \zeta_R(2s) \sum_{e \in \mathcal{E}} \left(\frac{\pi}{L_e} \right)^{-2s} \ . \tag{5.45}$$

If we define a function $\hat{f}(t) = \det \hat{M}(t)$ where $\hat{M}(t)$ is

$$\left[\hat{M}(t) \right]_{ij} = \begin{cases} -\sum_{v \sim i} \coth tL_{i,v} & i = j \ , \\ \operatorname{csch} tL_{i,j} & i \sim j \ , \\ 0 & \text{otherwise} \ , \end{cases} \tag{5.46}$$

then $t^{n-2}\hat{f}(t) = f(\mathrm{i}t)$. So the integral along the imaginary axis can be written,

$$\zeta_I(s) = \frac{\sin \pi s}{\pi} \int_0^\infty t^{-2s} \frac{\mathrm{d}}{\mathrm{d}t} \log t^{n-2} \hat{f}(t)\, \mathrm{d}t \ . \tag{5.47}$$

Expanding the elements of $t\hat{M}(t)$ near $t = 0$,

$$\left[t\hat{M}(t)\right]_{ij} \sim \begin{cases} -\sum_{v\sim i} \left(\dfrac{1}{L_{i,v}} + \dfrac{L_{i,v}}{3} t^2 + \mathrm{O}\left(t^4\right) \right) & i = j \ , \\ \dfrac{1}{L_{i,j}} - \dfrac{L_{i,j}}{6} t^2 + \mathrm{O}\left(t^4\right) & i \sim j \ , \\ 0 & \text{otherwise} \ . \end{cases} \tag{5.48}$$

From this, $t^n f(t) = \det[t\hat{M}(t)]$ tends to zero as t approaches zero, since the sum of the elements of each row of $t\hat{M}(t)$ is zero. So, we may write

$$t^n \hat{f}(t) = \det[t\hat{M}(t)] \sim ct^2 + \mathrm{O}(t^4) \tag{5.49}$$

near $t = 0$, since the expansions of $\coth(t)$ and $\mathrm{csch}(t)$ contain only odd powers of t. Without loss of generality we can assume $c \neq 0$. If c was zero for some choice of edge lengths it can be made non-zero by an arbitrarily small perturbation. Hence, the integral in equation (5.47) converges for $0 < \Re(s) < 1$.

To obtain an analytic continuation valid for all $\Re(s) < 1$ we can again split the integral at $t = 1$ and develop the integral over $(1, \infty)$,

$$\begin{aligned} \zeta_I(s) = \frac{\sin \pi s}{\pi} \Bigg[& \int_0^1 t^{-2s} \frac{\mathrm{d}}{\mathrm{d}t} \log t^{n-2} \hat{f}(t)\, \mathrm{d}t \\ & + \int_1^\infty t^{-2s} \frac{\mathrm{d}}{\mathrm{d}t} \log \hat{f}(t)\, \mathrm{d}t + \frac{(n-2)}{2s} \Bigg] \ . \end{aligned} \tag{5.50}$$

From this, we obtain the main result of this section.

Theorem 5.2. *Let $C_n(\boldsymbol{L};\boldsymbol{a})$ be a quantum circulant graph equipped with the Laplace operator and Neumann-like vertex conditions. If the edge lengths are incommensurate, the spectral zeta function for $\Re(s) < 1$ is*

$$\begin{aligned}\zeta(s) = \zeta_R(2s) \sum_{e\in\mathcal{E}} \left(\frac{\pi}{L_e}\right)^{-2s} + \frac{(n-2)\sin \pi s}{2\pi s} \\ + \frac{\sin \pi s}{\pi} \left\{ \int_0^1 t^{-2s} \frac{\mathrm{d}}{\mathrm{d}t} \log t^{n-2} \hat{f}(t)\, \mathrm{d}t + \int_1^\infty t^{-2s} \frac{\mathrm{d}}{\mathrm{d}t} \log \hat{f}(t)\, \mathrm{d}t \right\} .\end{aligned} \tag{5.51}$$

Although this theorem is only valid for quantum circulant graphs with incommensurate edge lengths, we notice that we can obtain the result for symmetric quantum circuant graphs, theorem 5.1, by letting $\hat{f}(t) = \det \hat{M}(t) = \prod_{j=0}^{n-1} \hat{f}_j(t)$.

5.3 Spectral Determinant

The spectral determinant is a generalization of the determinant of a matrix to infinite dimensional linear operators. Formally, the spectral determinant of a linear operator is the product of its eigenvalues. Since the spectral zeta function represents a sum over the spectrum of an operator, we may use it to define a regularized spectral determinant. For example, since formally

$$\zeta'(0) = -\log \prod_{i=1}^{\infty} k_i^2 , \tag{5.52}$$

the spectral determinant of the Laplace operator $\mathcal{H}$ can be defined as

$$\det \mathcal{H} = \mathrm{e}^{-\zeta'(0)} . \tag{5.53}$$

As we have obtained an analytic continuation of $\zeta(s)$ valid at $s = 0$, we are able to compute this quantity.

The spectral determinants of quantum graph Hamiltonians have been studied in [2, 33, 34, 111]. Here, we present a simplified version for quantum circulant graphs equipped with the Laplace operator with Neumann-like vertex conditions.

5.3.1 Spectral Determinant for Symmetric Circulant Graphs

From the zeta function for a quantum circulant graph with edge symmetry, theorem 5.1, one can compute the spectral determinant. Taking the derivative of $\zeta(s)$ for odd n,

$$\begin{aligned}\zeta'(0) = -dn\log 2\pi + n\sum_{h=1}^{d}\log\frac{\pi}{l_h} - \log\left(\frac{\hat{f}_0(t)}{t}\prod_{j=1}^{(n-1)/2}\left|t\hat{f}_j(t)\right|^2\right)\Bigg|_{t=0} \\ + \log\left(\hat{f}_0(t)\prod_{j=1}^{(n-1)/2}\left|\hat{f}_j(t)\right|^2\right)\Bigg|_{t\to\infty} \\ = -\log\left(\frac{2^{E-1}\mathcal{L}}{nd^n}\prod_{h=1}^{d}l_h^n\prod_{j=1}^{(n-1)/2}\left[\sum_{h=1}^{d}\frac{1}{l_h}\left(1-\cos\frac{2\pi j a_h}{n}\right)\right]^2\right)\ ,\end{aligned} \tag{5.54}$$

where $\mathcal{L} = n\sum_{h=1}^{d} l_h$ is the total length of the graph. Similarly, when n is even, we have,

$$\begin{aligned}\zeta'(0) = -dn\log 2\pi + n\sum_{h=1}^{d}\log\frac{\pi}{l_h} - \log\left(\hat{f}_0(t)\hat{f}_{n/2}(t)\prod_{j=1}^{(n/2)-1}\left|t\hat{f}_j(t)\right|^2\right)\Bigg|_{t=0} \\ + \log\left(\hat{f}_0(t)\hat{f}_{n/2}(t)\prod_{j=1}^{(n/2)-1}\left|\hat{f}_j(t)\right|^2\right)\Bigg|_{t\to\infty} \\ = -\log\left(\frac{2^{E-1}\mathcal{L}}{nd^n}\prod_{h=1}^{d}l_h^n\prod_{j=1}^{(n/2)-1}\left[\sum_{h=1}^{d}\frac{1}{l_h}\left(1-\cos\frac{2\pi j a_h}{n}\right)\right]^2\sum_{\substack{h=1\\ a_h\ \text{odd}}}^{d}\frac{2}{l_h}\right)\ .\end{aligned} \tag{5.55}$$

By exponentiating equations (5.54) and (5.55), we obtain the spectral determinant.

Theorem 5.3. *The spectral determinant of the Laplace operator of a quantum circulant graph $C_n(\boldsymbol{l}, \boldsymbol{a})$ with symmetric edge lengths and standard vertex conditions is*

$$\det \Delta = \frac{2^{E-1}\mathcal{L}}{nd^n} \prod_{h=1}^{d} l_h^n \prod_{j=1}^{(n-1)/2} \left[\sum_{h=1}^{d} \frac{1}{l_h} \left(1 - \cos \frac{2\pi j a_h}{n} \right) \right]^2 , \tag{5.56}$$

when n is odd and

$$\det \Delta = \frac{2^{E-1}\mathcal{L}}{nd^n} \prod_{h=1}^{d} l_h^n \prod_{j=1}^{(n/2)-1} \left[\sum_{h=1}^{d} \frac{1}{l_h} \left(1 - \cos \frac{2\pi j a_h}{n} \right) \right]^2 \sum_{\substack{h=1 \\ a_h \ odd}}^{d} \frac{2}{l_h} , \tag{5.57}$$

when n is even. In both cases, d is the number of elements in $\boldsymbol{a}$, $E = nd$ is the number of edges, and $\mathcal{L} = n \sum_{h=1}^{d} l_h$ is the total length of the graph.

5.3.2 Spectral Determinant for Generic Circulant Graphs

Similarly we can use theorem 5.2 to compute the spectral determinant of a generic quantum circulant graph.

Theorem 5.4. *The spectral determinant of the Laplace operator of a quantum circulant graph $C_n(\boldsymbol{L}; \boldsymbol{a})$ with standard vertex conditions is*

$$\det \Delta = (-1)^n c \left(\frac{2^{d-1}}{d} \right)^n \prod_{(i,j)\in\mathcal{E}} L_{i,j} , \tag{5.58}$$

where d is the number of elements in $\boldsymbol{a}$ and c is the first nonzero coefficient in the expansion of $\det[t\hat{M}(t)]$ about zero.

Proof. Note that

$$\zeta'(0) = -nd \log 2\pi + \sum_{(i,j)\in\mathcal{E}} \log \frac{\pi}{L_{i,j}} - \log \left(t^{n-2} \hat{f}(t) \right) \Big|_{t=0} + \log \hat{f}(t) \Big|_{t\to\infty} \tag{5.59}$$

where $\hat{f}(t) = \det \hat{M}(t)$ as defined in (5.46). As $t \to \infty$, $\hat{M}(t) \sim -2d\mathbb{I}_n$, and so $\hat{f}(t) \sim (-2d)^n$. To evaluate $t^{n-2}\hat{f}(t)$ as $t \to 0$, recall that $t^n \det \hat{M}(t) \sim ct^2 + \mathrm{O}(t^4)$, since the constant term in the expansion must be zero. For any given circulant graph, the elements of $t\hat{M}(t)$ can be expanded as in equation (5.48) and the first nonzero coefficient of its determinant, c, is straightforward to compute from (5.49). □

A form of the spectral determinant of a general quantum graph using the spectral zeta function was developed by Harrison, Kirsten, and Texier in [60, 61]. For the Laplace operator on a quantum graph, the zeta function can be written in terms of local vertex conditions given by the matrices $\mathbb{A}$ and $\mathbb{B}$. The spectral determinant is

$$\det \Delta = \frac{2^E}{c_N} \prod_{e=1}^{E} L_e \det \left(\mathbb{A} - \mathbb{B} \begin{pmatrix} \mathbf{L}^{-1} & -\mathbf{L}^{-1} \\ -\mathbf{L}^{-1} & \mathbf{L}^{-1} \end{pmatrix} \right) , \tag{5.60}$$

where c_N is the first non-zero coefficent belonging the highest power of t in $\det(\mathbb{A} - t\mathbb{B})$ and $\mathbf{L}$ is a diagonal matrix of the lengths of the edges.

In the case of the Laplacian with Neumann-like vertex conditions, Friedlander [41] explicitly computed the spectral determinant to be

$$\det \Delta = 2^E \frac{\mathcal{L}}{V} \frac{\prod_{e \in \mathcal{E}} L_e}{\prod_{v \in \mathcal{V}} d(v)} \det{}' R , \tag{5.61}$$

where E and V are the total edges and vertices, respectively, and $d(v)$ is the degree of the vertex v. The notation $\det' R$ refers the pseudo-determinant of R, the product of all its non-zero eigenvalues. The matrix R is the Dirichlet-Neumann operator evaluated at zero, which is given by

$$R_{ij} = \begin{cases} \sum_{v \sim i} L_{iv}^{-1} & i = j \\ \sum_{(i,j) \in \mathcal{E}} L_{ij}^{-1} & i \neq j \end{cases} . \tag{5.62}$$

For a quantum circulant graph, $V = n$, $E = nd$, and $d(v) = 2d$ for all v, where d is the length of the vector $\boldsymbol{a}$. The matrices $\hat{M}(t)$ and R are related, and in fact,

$$\lim_{t \to 0} -t\hat{M}(t) = R \ . \tag{5.63}$$

Equations (5.58) and (5.61) imply that $c = (-1)^n \mathcal{L} \det'(R)/n$.

5.4 Vacuum Energy

Another application of the spectral zeta function is to compute the regularized vacuum (Casimir) energy associated with the graph [60]. In quantum field theory, vacuum energy is the ground state energy of a quantum vacuum, that is the lowest possible energy a quantum system may have. To understand this, consider that the energy levels of a single quantum harmonic oscillator with potential $k^2x^2/2$ are given by

$$E_n = \left(\frac{1}{2} + n\right) k \ . \tag{5.64}$$

According to quantum field theory, the total energy of a system is given by the sum of the energies at all points in the space, so for a one-dimensional field, formally

$$E = \sum_{j=0}^{\infty} \left(\frac{1}{2} + n_j\right) k_j \ . \tag{5.65}$$

If we consider the vacuum state, where all the n_j are zero, this becomes

$$E_0 = \frac{1}{2} \sum_{j=0}^{\infty} k_j \ , \tag{5.66}$$

which is divergent. Experimental results show the existence of an attractive force between two uncharged parallel metallic plates in a vacuum, known at the Casimir effect. This force quickly drops off at large distances, but it demonstrates that the

change in energy in a vacuum with respect to the space between plates is a meaningful quantity.

To compute these differences in energy, a regularization is necessary to make the divergent sums of energies into finite quantities which can be compared. One common procedure for regularizing vacuum energy is to introduce a cutoff term e^{tk_j} and consider the limit $t \to 0$. Another regularized vacuum energy can be defined via analytic continuation of the spectral zeta function, which is the method we will employ here. Although vacuum energy in a one-dimensional graph does not have a clear physical meaning, the underlying ergodicity of a quantum graph can provide a simplified model for studying the vacuum energy in a chaotic system.

Since $k_j = \sqrt{\lambda_j}$, the vacuum energy is formally given as the sum of the square roots of the eigenvalues of the Laplacian,

$$\frac{1}{2}\sum_{j=0}^{\infty}\sqrt{\lambda_j} = \frac{1}{2}\sum_{j=0}^{\infty} k_j \ . \tag{5.67}$$

The zeta-regularized vacuum energy is then defined as,

$$E_c = \frac{1}{2}\zeta\left(-\frac{1}{2}\right) \ . \tag{5.68}$$

This quantity has been investigated for general quantum graphs in [13, 42, 44] using the trace formula and in [60] using the general spectral zeta function. Results on star graphs have also been obtained in [13, 60] using both methods. We develop explicit formulas for the vacuum energy of a quantum circulant graph using the spectral zeta function.

5.4.1 Results on Circulant Graphs

Using the zeta function in theorem 5.1, we evaluate $\zeta(-1/2)$ to compute the vacuum energy of a symmetric circulant graph.

Theorem 5.5. *The vacuum energy of the Laplace operator of a quantum circulant graph* $C_n(\boldsymbol{l}, \boldsymbol{a})$ *with symmetric edge lengths and standard vertex conditions is*

$$\begin{aligned} E_c = \frac{n-2}{2\pi} - \frac{1}{2\pi}\int_0^1 t\frac{\mathrm{d}}{\mathrm{d}t}\log\left(t^{n-2}\hat{f}_0(t)\prod_{j=1}^{(n-1)/2}\left[\hat{f}_j(t)\right]^2\right)\mathrm{d}t \\ - \frac{1}{2\pi}\int_1^\infty t\frac{\mathrm{d}}{\mathrm{d}t}\log\left(\hat{f}_0(t)\prod_{j=1}^{(n-1)/2}\left[\hat{f}_j(t)\right]^2\right)\mathrm{d}t - \frac{n\pi}{24}\sum_{h=1}^{d}(l_h)^{-1}\ , \end{aligned} \tag{5.69}$$

when n *is odd and*

$$\begin{aligned} E_c = \frac{n-2}{2\pi} - \frac{1}{2\pi}\int_0^1 t\frac{\mathrm{d}}{\mathrm{d}t}\log\left(t^{n-2}\hat{f}_0(t)\hat{f}_{n/2}(t)\prod_{j=1}^{(n-1)/2}\left[\hat{f}_j(t)\right]^2\right)\mathrm{d}t \\ - \frac{1}{2\pi}\int_1^\infty t\frac{\mathrm{d}}{\mathrm{d}t}\log\left(\hat{f}_0(t)\hat{f}_{n/2}(t)\prod_{j=1}^{(n-1)/2}\left[\hat{f}_j(t)\right]^2\right)\mathrm{d}t - \frac{n\pi}{24}\sum_{h=1}^{d}(l_h)^{-1}\ , \end{aligned} \tag{5.70}$$

when n *is even.*

Similarly the zeta function of a generic circulant graph, theorem 5.2, provides an integral formulation for its vacuum energy.

Theorem 5.6. *The vacuum energy of the Laplace operator of a quantum circulant graph* $C_n(\boldsymbol{L}, \boldsymbol{a})$ *with standard vertex conditions is*

$$\begin{aligned} E_c = \frac{n-2}{2\pi} - \frac{1}{2\pi}\int_0^1 t\frac{\mathrm{d}}{\mathrm{d}t}\log t^{n-2}\hat{f}(t)\,\mathrm{d}t \\ - \frac{1}{2\pi}\int_1^\infty t\frac{\mathrm{d}}{\mathrm{d}t}\log\hat{f}(t)\,\mathrm{d}t - \frac{\pi}{24}\sum_{(i,j)\in\mathcal{E}}(L_{i,j})^{-1}\ . \end{aligned} \tag{5.71}$$

For a symmetric quantum circulant graph, the spectral zeta function can be obtained from (5.51) where $\hat{f}(t) = \prod_{j=0}^{n-1}\hat{f}_j(t)$. Then, as expected, the vacuum energy for a symmetric quantum circulant graph in theorem 5.5 is a special case of theorem 5.6, when $\hat{f}(t)$ is defined in this way.

5.4.2 Comparison with Previous Results

The force between uncharged plates in a vacuum is the change in vacuum energy as the distance between the plates changes. This is known as the Casimir force and it can be computed by taking the derivative of the regularized vacuum energy with respect to an edge length. A formulation of this quantity using the spectral zeta function was studied in [60, 61].

For the Laplace operator on a quantum graph with local vertex matching conditions given by matrices $\mathbb{A}$ and $\mathbb{B}$, an analytic continuation of the zeta function can be written as

$$\begin{aligned}\zeta(s) = \frac{\zeta_R(2s)}{\pi^{2s}} \sum_{e\in\mathcal{E}} L_e^{2s} + \frac{\sin \pi s}{\pi} \Bigg[\int_0^1 t^{-2s} \frac{\mathrm{d}}{\mathrm{d}t} \log \hat{f}(t)\, \mathrm{d}t \\ + \int_1^\infty t^{-2s} \frac{\mathrm{d}}{\mathrm{d}t} \left(\log(t^{-N} \hat{f}(t)) - \frac{c_{N-j}}{c_N t^j} \right) \mathrm{d}t + \frac{N}{2s} - \frac{c_{N-j} j}{c_N (2s+j)} \Bigg] \,,\end{aligned} \tag{5.72}$$

where

$$\begin{aligned}\hat{f}(t) &= \det \left(\mathbb{A} - t\mathbb{B} \begin{pmatrix} \coth(t\mathbf{L}) & -\operatorname{csch}(t\mathbf{L}) \\ -\operatorname{csch}(t\mathbf{L}) & \coth(t\mathbf{L}) \end{pmatrix} \right) \\ &\sim \det(\mathbb{A} - t\mathbb{B}) = c_N t^N + c_{N-j} t^{N-j} + \mathrm{O}(t^{N-j-1})\end{aligned} \tag{5.73}$$

such that c_N and c_{N-j} are the highest non-zero coefficients in the expansion of the determinant. This analytic continuation converges for $\Re(s) > -(j+1)/2$, and in general, we expect that $j = 1$, so $\zeta(-1/2)$ diverges due to the last term in (5.72). Because of the divergence of the integral, E_c also diverges for a general quantum graph, but the Casimir force is well-defined and was found to be

$$F_c^\beta = \frac{\pi}{24 L_\beta^2} + \frac{1}{\pi} \int_0^\infty \frac{\partial}{\partial L_\beta} \log \hat{f}(t)\, \mathrm{d}t \,. \tag{5.74}$$

In our case, the vacuum energy for a quantum circulant graph was able to be computed because our formulation is not divergent at $s = -1/2$. Computing the Casimir force on a quantum circulant graph will give a similar result to (5.74).

Well-defined vacuum energies for star graphs in various cases were also found. In [13], the vacuum energy for a quantum star graph with Neumann conditions and equal edge lengths is

$$E_c = \frac{(E-3)\pi}{48L} \ , \tag{5.75}$$

where E is the number of edges and L is the length of an edge. This is consistent with the results found in [60] using the spectral zeta function. Vacuum energies were also found for quantum star graphs with both Neumann and Dirichlet vertex conditions, and also for quantum star graphs with incommensurate edge lengths [60].

CHAPTER SIX

Quantum Cayley Graphs of Finite Groups

Quotient graphs were first introduced by Band, Parzanchevski, and Ben-Shach [7, 96] and can be used to analyze the spectrum of a quantum graph with a symmetry group by decomposing its spectrum into subspectra transforming according to the irreducible representations of that symmetry group. The technique for constructing a quotient graph was introduced in section 2.5. The quotient graphs of quantum circulant graphs, the Cayley graphs of cyclic groups, were analyzed in section 3.3.2. This chapter considers a quotient graph model based on Cayley graphs of more general finite groups, which is joint work with Mark Sepanski.

6.1 Construction of the Model

We first encountered Cayley graphs in chapter three as one of the characterizations of circulant graphs. In general, a Cayley graph of a group G is determined by the choice of a set of generators, Ω. The vertices of the Cayley graph are the elements of the group, and two vertices are connected by an edge if one is obtained from the other by right multiplication with an element of Ω. The set Ω does not contain the identity and the inverse of every element in Ω is also in Ω. This ensures that the Cayley graph is not directed and that no vertex is connected to itself.

We consider a finite group G where Ω contains two elements of order at least three, α and β, and their inverses,

$$\Omega := \{\alpha, \alpha^{-1}, \beta, \beta^{-1}\} \, . \tag{6.1}$$

Then, Γ is the Cayley graph of the group G with generating set Ω, so that $\mathcal{V} = G$ and $\mathcal{E} = \{(\sigma, \sigma\tau) : \sigma \in G, \tau \in \Omega\}$. The set of edges in Γ can be partitioned into

two equivalence classes based on the group generators α and β. These are defined as $[\mathcal{E}]_\alpha = \{(\sigma, \sigma\tau) : \sigma \in G, \tau \in \{\alpha, \alpha^{-1}\}\}$ and $[\mathcal{E}]_\beta = \{(\sigma, \sigma\tau) : \sigma \in G, \tau \in \{\beta, \beta^{-1}\}\}$. To make Γ a metric graph $\mathcal{G}$, we assign edge lengths based on the equivalence classes of $\mathcal{E}$. For an edge $e \in [\mathcal{E}]_\alpha$, the length of e is $2l_\alpha$, and for $e \in [\mathcal{E}]_\beta$, the length of e is $2l_\beta$. Here, the factor of two is for convenience in future calculations.

The group G is a symmetry group for the metric graph $\mathcal{G}$ and acts on $\mathcal{G}$ by left multiplication. The graph $\mathcal{G}$ may be viewed as a quantum graph by considering the Laplace operator with Neumann-like vertex conditions at all the vertices. The group action of G on an eigenfunction f is defined by

$$(\sigma f)(x) = f(\sigma^{-1}x). \tag{6.2}$$

For a given D-dimensional irreducible representation $\mathcal{R}$ of G, we define the $D \times D$ matrix representation of the group elements by

$$\mathcal{M}_\sigma = \mathcal{R}(\sigma) \ . \tag{6.3}$$

Recall that the construction of a quotient graph relies on first choosing a fundamental domain for $\mathcal{G}$ (see section 2.5). For the quotient graph $\mathcal{G}/\mathcal{R}$, we want to construct a graph whose eigenfunctions transform according to the D-dimensional representation $\mathcal{R}$. In the case where $D \geq 2$, we have two equivalent ways of treating the group action of $\mathcal{R}$ on the eigenfunctions of $\mathcal{G}$. We can view f as a D-dimensional vector-valued function on each edge of the fundamental domain (see [68] for an example of this method), or we can take D copies of the fundamental domain where f is scalar-valued on each edge. The latter is the method used in [7, 96] and is the strategy we will employ here.

To construct $\mathcal{G}/\mathcal{R}$, we take D copies of a fundamental domain of $\mathcal{G}$ and determine vertex conditions on the quotient graph so that eigenfunctions transform

according to the D-dimensional irreducible representation $\mathcal{R}$. We do this by introducing dummy vertices at the midpoints of the edges of $\mathcal{G}$. As discussed in 3.3.2, this will not change the spectrum of the quantum graph. Using the same technique applied on circulant graphs, we will keep the coordinates of the edges unchanged by the introduction of the dummy vertices. The edge (ι, α) associated to the interval $[0, 2l_\alpha]$ splits into edges corresponding to the subintervals $[0, l_\alpha]$ and $[l_\alpha, 2l_\alpha]$. Similarly, the edge (ι, β) corresponding to $[0, 2l_\beta]$ splits into edges associated to $[0, l_\beta]$ and $[l_\beta, 2l_\beta]$. We will let α_0 denote the dummy vertex on the edge (ι, α) and similarly β_0 is the dummy vertex on (ι, β). The fundamental domain for $\mathcal{G}$ consists of the edges (ι, α_0), (α_0^{-1}, ι), (ι, β_0), and (β_0^{-1}, ι) and their endpoints, as depicted in figure 6.1. We assume the edges are oriented so that (ι, α_0) and (ι, β_0) are associated to $[0, l_\alpha]$ and $[0, l_\beta]$, respectively, and similarly, (α_0^{-1}, ι) and (β_0^{-1}, ι) correspond to $[l_\alpha, 2l_\alpha]$ and $[l_\beta, 2l_\beta]$.

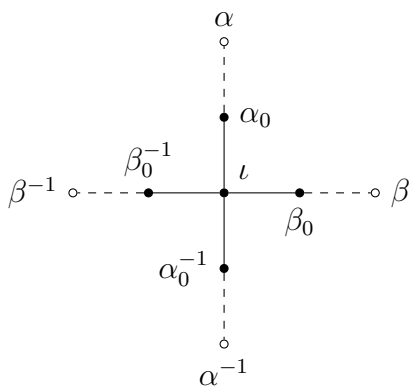

Figure 6.1. A subgraph of the quantum graph $\mathcal{G}$ with dummy vertices. The fundamental domain is shown with solid lines and vertices.

Since the fundamental domain contains four edges, taking D copies for the quotient graph implies that the quotient graph will have $4D$ edges. Let (ι_j, α_{0_j}), $(\alpha_{0_j}^{-1}, \iota_j)$, (ι_j, β_{0_j}), and $(\beta_{0_j}^{-1}, \iota_j)$ denote the edges on the jth copy of the fundamental domain. Then, define

$$\boldsymbol{f}_{(\boldsymbol{\iota},\boldsymbol{\alpha_0})} = \left(f_{(\iota_1,\alpha_{0_1})},\ldots,f_{(\iota_D,\alpha_{0_D})}\right)^T , \tag{6.4}$$

$$\boldsymbol{f}_{(\boldsymbol{\alpha_0^{-1}},\boldsymbol{\iota})} = \left(f_{(\alpha_{0_1}^{-1},\iota_1)},\ldots,f_{(\alpha_{0_D}^{-1},\iota_D)}\right)^T , \tag{6.5}$$

$$\boldsymbol{f}_{(\boldsymbol{\iota},\boldsymbol{\beta_0})} = \left(f_{(\iota_1,\beta_{0_1})},\ldots,f_{(\iota_D,\beta_{0_D})}\right)^T , \tag{6.6}$$

$$\boldsymbol{f}_{(\boldsymbol{\beta_0^{-1}},\boldsymbol{\iota})} = \left(f_{(\beta_{0_1}^{-1},\iota_1)},\ldots,f_{(\beta_{0_D}^{-1},\iota_D)}\right)^T , \tag{6.7}$$

as vectors of the function restricted to the D copies of an edge in the fundamental domain. The vectors of derivatives are defined similarly as

$$\boldsymbol{f}'_{(\boldsymbol{\iota},\boldsymbol{\alpha_0})} = \left(f'_{(\iota_1,\alpha_{0_1})},\ldots,f'_{(\iota_D,\alpha_{0_D})}\right)^T , \tag{6.8}$$

$$\boldsymbol{f}'_{(\boldsymbol{\alpha_0^{-1}},\boldsymbol{\iota})} = \left(f'_{(\alpha_{0_1}^{-1},\iota_1)},\ldots,f'_{(\alpha_{0_D}^{-1},\iota_D)}\right)^T , \tag{6.9}$$

$$\boldsymbol{f}'_{(\boldsymbol{\iota},\boldsymbol{\beta_0})} = \left(f'_{(\iota_1,\beta_{0_1})},\ldots,f'_{(\iota_D,\beta_{0_D})}\right)^T , \tag{6.10}$$

$$\boldsymbol{f}'_{(\boldsymbol{\beta_0^{-1}},\boldsymbol{\iota})} = \left(f'_{(\beta_{0_1}^{-1},\iota_1)},\ldots,f'_{(\beta_{0_D}^{-1},\iota_D)}\right)^T , \tag{6.11}$$

where the derivatives are taken with respect to the edge orientation previously defined.

The action of $\alpha \in G$ on $\mathcal{G}$ maps the edge (ι,α) to the edge (α^{-1},ι) and consequently maps (ι,α_0) to $(\alpha^{-1},\alpha_0^{-1})$. With the given edge orientation, Neumann-like conditions at the vertex α_0^{-1} require

$$\boldsymbol{f}_{(\boldsymbol{\alpha_0^{-1}},\boldsymbol{\iota})}(l_\alpha) = \mathcal{M}_\alpha \boldsymbol{f}_{(\boldsymbol{\iota},\boldsymbol{\alpha_0})}(l_\alpha) , \tag{6.12}$$

$$\boldsymbol{f}'_{(\boldsymbol{\alpha_0^{-1}},\boldsymbol{\iota})}(l_\alpha) = \mathcal{M}_\alpha \boldsymbol{f}'_{(\boldsymbol{\iota},\boldsymbol{\alpha_0})}(l_\alpha) . \tag{6.13}$$

Similarly, the action of $\beta \in G$ on $\mathcal{G}$ maps (ι,β) to (β^{-1},ι) and (ι,β_0) to $(\beta^{-1},\beta_0^{-1})$. So the Neumann-like conditions at β_0^{-1} require

$$\boldsymbol{f}_{(\boldsymbol{\beta_0^{-1}},\boldsymbol{\iota})}(l_\beta) = \mathcal{M}_\beta \boldsymbol{f}_{(\boldsymbol{\iota},\boldsymbol{\beta_0})}(l_\beta) , \tag{6.14}$$

$$\boldsymbol{f}'_{(\boldsymbol{\beta_0^{-1}},\boldsymbol{\iota})}(l_\beta) = \mathcal{M}_\beta \boldsymbol{f}'_{(\boldsymbol{\iota},\boldsymbol{\beta_0})}(l_\beta) \ . \tag{6.15}$$

Identification among the vertices is determined by the matrices $\mathcal{M}_\alpha$ and $\mathcal{M}_\beta$. Identify the vertices $\alpha_{0_j}^{-1}$ and α_{0_k} whenever $[\mathcal{M}_\alpha]_{jk} \neq 0$ and identify $\beta_{0_j}^{-1}$ and β_{0_k} whenever $[\mathcal{M}_\beta]_{jk} \neq 0$. For the purposes of visualizing the quotient graph under a generic representation $\mathcal{R}$, we may assume that all of the elements of $\mathcal{M}_\alpha$ and $\mathcal{M}_\beta$ are nonzero, so that the vertices α_{0_k} and $\alpha_{0_j}^{-1}$ are identified for all j and k, and similarly for β_{0_k} and $\beta_{0_j}^{-1}$, as shown in figure 6.2. When zero elements are present this can result in a decoupling phenomena, similar to Dirichlet boundary conditions, which would split the identified vertex. However, this information is encoded in the vertex conditions and need not affect the topology of the graph.

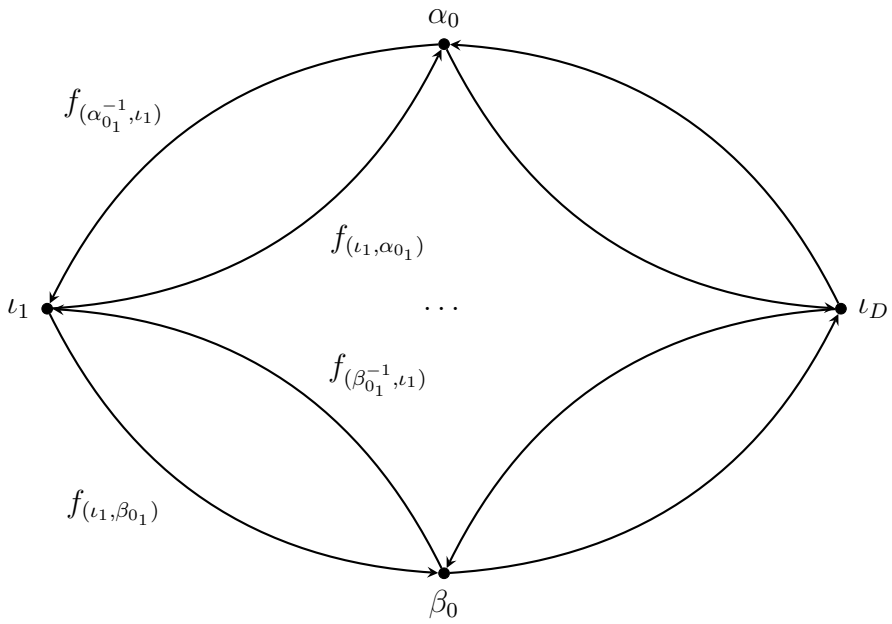

Figure 6.2. A general quotient graph $\mathcal{G}/\mathcal{R}$ with respect to a D-dimensional representation $\mathcal{R}$, where $\mathcal{G}$ is the Cayley graph of a finite group with two distinct generators, α and β, each with order at least three.

6.1.1 Secular Equation

A secular equation can be derived from the vertex conditions which produces a symmetric formula with similarities to the secular equations of star graphs and circulant graphs. Consider the Laplace equation on some edge e of the quotient graph

$$-\frac{\mathrm{d}^2}{\mathrm{d}x_e^2} f_e(x_e) = k^2 f_e(x_e) \ , \tag{6.16}$$

where f_e is the function f restricted to the edge e. For $k \neq 0$, we can write f_e as a linear combination of $\sin(kx)$ and $\cos(kx)$, where the e in x_e is suppressed for ease of notation. So,

$$\boldsymbol{f}_{(\iota,\boldsymbol{\alpha_0})}(x) = \boldsymbol{A_1}\sin(kx) + \boldsymbol{B_1}\cos(kx) \ , \tag{6.17}$$

$$\boldsymbol{f}_{(\boldsymbol{\alpha_0^{-1}},\iota)}(x) = \boldsymbol{A_2}\sin(kx) + \boldsymbol{B_2}\cos(kx) \ , \tag{6.18}$$

$$\boldsymbol{f}_{(\iota,\boldsymbol{\beta_0})}(x) = \boldsymbol{A_3}\sin(kx) + \boldsymbol{B_3}\cos(kx) \ , \tag{6.19}$$

$$\boldsymbol{f}_{(\boldsymbol{\beta_0^{-1}},\iota)}(x) = \boldsymbol{A_4}\sin(kx) + \boldsymbol{B_4}\cos(kx) \ , \tag{6.20}$$

where $\boldsymbol{A_i}$ and $\boldsymbol{B_i}$ are D-dimensional vectors of coefficients of the sine and cosine functions, for $i = 1, \ldots, 4$.

Since (ι_j, α_{0_j}) and (ι_j, β_{0_j}) are respectively identified with $[0, l_\alpha]$ and $[0, l_\beta]$ for $j = 1, \ldots, D$, continuity at the ι_j vertices implies that $\boldsymbol{B_1} = \boldsymbol{B_3} = \boldsymbol{\phi}$, where $\boldsymbol{\phi}$ is a vector with jth component $\phi_j = f(\iota_j)$. As we have chosen to identify the directed edge (α_0, ι_j) with $[l_\alpha, 2l_\alpha]$ and (β_0, ι_j) with $[l_\beta, 2l_\beta]$ for all j, the vertex conditions (6.12)–(6.13) at the identified α_0 vertex imply

$$\boldsymbol{A_2}\sin(kl_\alpha) + \boldsymbol{B_2}\cos(kl_\alpha) = \mathcal{M}_\alpha \boldsymbol{A_1}\sin(kl_\alpha) + \mathcal{M}_\alpha \boldsymbol{\phi}\cos(kl_\alpha) \ , \tag{6.21}$$

$$\boldsymbol{A_2}\cos(kl_\alpha) - \boldsymbol{B_2}\sin(kl_\alpha) = \mathcal{M}_\alpha \boldsymbol{A_1}\cos(kl_\alpha) - \mathcal{M}_\alpha \boldsymbol{\phi}\cos(kl_\alpha) \ . \tag{6.22}$$

Assuming $\sin(kl_\alpha) \neq 0$ and $\cos(kl_\alpha) \neq 0$, multiply (6.21) by $\sin(kl_\alpha)$ and (6.22) by $\cos(kl_\alpha)$ and add them together to obtain

$$\mathcal{M}_\alpha \boldsymbol{A_1} = \boldsymbol{A_2} \ . \tag{6.23}$$

Multiplying (6.21) by $\cos(kl_\alpha)$ and (6.22) by $\sin(kl_\alpha)$ gives

$$\mathcal{M}_\alpha \boldsymbol{\phi} = \boldsymbol{B_2} \ . \tag{6.24}$$

Similarly, substituting (6.19) and (6.20) in the vertex conditions (6.14)–(6.15) at the identified β_0 vertex and assuming $\sin(kl_\beta) \neq 0$ and $\cos(kl_\beta) \neq 0$, we obtain

$$\mathcal{M}_\beta \boldsymbol{A_3} = \boldsymbol{A_4} \ , \tag{6.25}$$

$$\mathcal{M}_\beta \boldsymbol{\phi} = \boldsymbol{B_4} \ . \tag{6.26}$$

By continuity at the ι_j vertices, $\boldsymbol{f}_{(\boldsymbol{\alpha_0^{-1}},\boldsymbol{\iota})}(2l_\alpha) = \boldsymbol{\phi} = \boldsymbol{f}_{(\boldsymbol{\beta_0^{-1}},\boldsymbol{\iota})}(2l_\beta)$. So, if $\sin(2kl_\alpha) \neq 0$ and $\sin(2kl_\beta) \neq 0$, we can solve for $\boldsymbol{A_1}$ and $\boldsymbol{A_3}$,

$$\boldsymbol{A_1} = \mathcal{M}_\alpha^{-1} \boldsymbol{\phi} \csc(2kl_\alpha) - \boldsymbol{\phi} \cot(2kl_\alpha) \ , \tag{6.27}$$

$$\boldsymbol{A_3} = \mathcal{M}_\beta^{-1} \boldsymbol{\phi} \csc(2kl_\beta) - \boldsymbol{\phi} \cot(2kl_\beta) \ . \tag{6.28}$$

This gives us a system of equations in terms of the vector $\boldsymbol{\phi}$ and the matrices $\mathcal{M}_\alpha$ and $\mathcal{M}_\beta$. Since the ι_j vertices are subject to Neumann-like conditions, taking the outgoing derivatives and summing to zero implies that

$$\boldsymbol{f}'_{(\boldsymbol{\iota},\boldsymbol{\alpha_0})}(0) + \boldsymbol{f}'_{(\boldsymbol{\iota},\boldsymbol{\beta_0})}(0) - \boldsymbol{f}'_{(\boldsymbol{\alpha_0^{-1}},\boldsymbol{\iota})}(2l_\alpha) - \boldsymbol{f}'_{(\boldsymbol{\beta_0^{-1}},\boldsymbol{\iota})}(2l_\beta) = 0 \ . \tag{6.29}$$

Substituting in (6.17)–(6.20), including the determined coefficients, gives

$$\csc(2kl_\alpha)\widehat{\mathcal{M}}_\alpha\boldsymbol{\phi} + \csc(2kl_\beta)\widehat{\mathcal{M}}_\beta\boldsymbol{\phi} - 2\left[\cot(2kl_\beta) + \cot(2kl_\alpha)\right]\boldsymbol{\phi} = 0 \ , \tag{6.30}$$

where

$$\widehat{\mathcal{M}}_\alpha = \left(\mathcal{M}_\alpha + \mathcal{M}_\alpha^{-1}\right) \ , \tag{6.31}$$

$$\widehat{\mathcal{M}}_\beta = \left(\mathcal{M}_\beta + \mathcal{M}_\beta^{-1}\right) \ . \tag{6.32}$$

This gives the following theorem.

Theorem 6.1. *Let $k \in \mathbb{C}$ be such that $k \neq m\pi/2l_\alpha$ and $k \neq m\pi/2l_\beta$ for $m \in \mathbb{Z}$. Then k^2 is an eigenvalue of the graph Laplacian whenever k is a root of*

$$\det\left[\csc(2kl_\alpha)\widehat{\mathcal{M}}_\alpha + \csc(2kl_\beta)\widehat{\mathcal{M}}_\beta - 2\left(\cot(2kl_\alpha) + \cot(2kl_\beta)\right)\mathbb{I}_D\right] = 0 \ . \tag{6.33}$$

6.2 Including Subgraphs

In order to see good spectral statistics, it is often desirable to have a large and well-connected quantum graph. One way of enlarging a graph without changing its underlying symmetry is to replace the vertices of the graph with identical subgraphs (see [5, 39] for the first known usages of this technique and [83] for an overview). This method was employed in [68] to find a quantum graph displaying GSE statistics.

6.2.1 The K_4 Subgraph

To increase the complexity of the quotient graph, we replace each of the ι_j vertices with a copy of K_4, the complete graph on four vertices. Each of these subgraphs must be identical in connectivity and length in order to preserve the symmetry of the quotient graph, and we assign Neumann-like conditions at all the new vertices. The new quotient graph, denoted $\hat{\mathcal{G}}/\mathcal{R}$, is shown in figure 6.3. We label the four vertices of the jth copy of K_4 as ι_j^m, for $m = 1, \ldots, 4$. Then, the subgraph is connected to

the α_0 and β_0 vertices as shown in figure 6.4. That is, we now have the edges (ι_j^1, α_0), $(\alpha_0^{-1}, \iota_j^2)$, (ι_j^3, β_0), and $(\beta_0^{-1}, \iota_j^4)$, which are associated to intervals of length l_α and l_β in the same manner as previously.

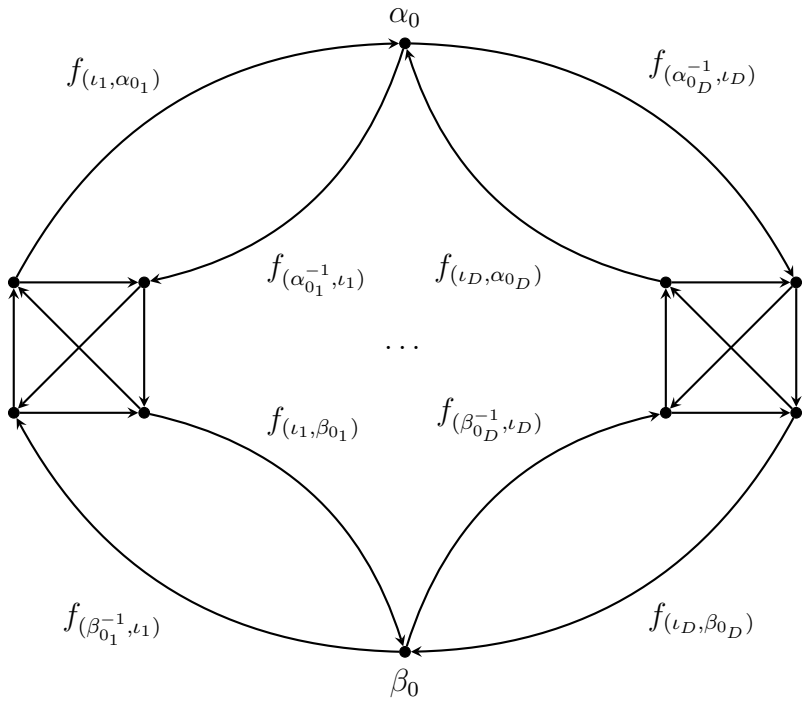

Figure 6.3. The quotient graph $\hat{\mathcal{G}}/\mathcal{R}$ where each vertex ι_j has been replaced with a copy of K_4.

Define $f_j^{(m_1,m_2)}$ as the function f restricted to some directed edge $(\iota_j^{m_1}, \iota_j^{m_2})$ in the jth copy of the subgraph K_4. The edge $(\iota_j^{m_1}, \iota_j^{m_2})$ is given the length l_{m_1,m_2} for all j and associated to the interval $[0, l_{m_1,m_2}]$ in such a way that $\iota_j^{m_1}$ corresponds to 0 and $\iota_j^{m_2}$ corresponds to l_{m_1,m_2}. Due to continuity at the ι_j^m vertices, we define four vectors $\boldsymbol{\phi^m}$ of length D, where $\phi_j^m = f(\iota_j^m)$ for $m = 1, \ldots, 4$, $j = 1, \ldots, D$. For ease of notation, write the vector form $\boldsymbol{f}^{(m_1,m_2)} = \{f_1^{(m_1,m_2)}, \ldots, f_D^{(m_1,m_2)}\}^T$. So then,

$$\boldsymbol{f}^{(m_1,m_2)}(x) = \boldsymbol{A}^{(m_1,m_2)} \sin(kx) + \boldsymbol{\phi}^{m_1} \cos(kx) \ . \tag{6.34}$$

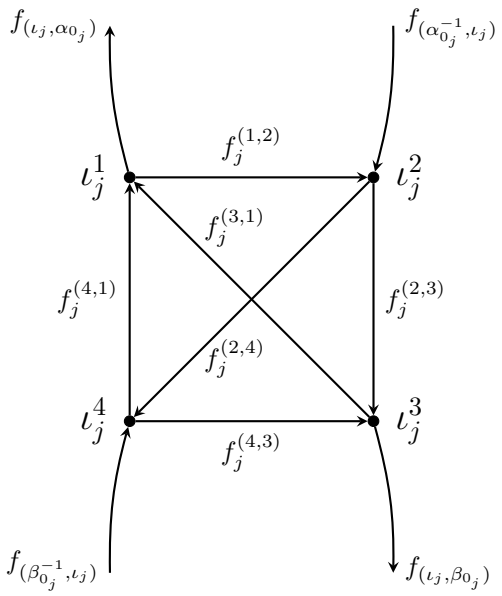

Figure 6.4. The jth copy of the subgraph K_4 in the quotient graph $\hat{\mathcal{G}}/\mathcal{R}$.

and by continuity at the ι_j^m vertices, if $\sin(kl_{m_1,m_2}) \neq 0$, then,

$$\boldsymbol{A}^{(m_1,m_2)} = \boldsymbol{\phi}^{m_2} \csc(kl_{m_1,m_2}) - \boldsymbol{\phi}^{m_1} \cot(kl_{m_1,m_2}) \ . \tag{6.35}$$

Proceeding as before, represent $\boldsymbol{f_{(\iota,\alpha_0)}}, \boldsymbol{f_{(\iota,\beta_0)}}, \boldsymbol{f_{(\alpha_0^{-1},\iota)}}, \boldsymbol{f_{(\beta_0^{-1},\iota)}}$ as in (6.17)–(6.20). By continuity, we now have $\boldsymbol{B_1} = \boldsymbol{\phi}^1$ and $\boldsymbol{B_3} = \boldsymbol{\phi}^3$. We may apply the vertex conditions (6.12)-(6.13) at the α_0 vertex in same manner as previously,

$$\boldsymbol{A_2} \sin(kl_\alpha) + \boldsymbol{B_2} \cos(kl_\alpha) = \mathcal{M}_\alpha \boldsymbol{A_1} \sin(kl_\alpha) + \mathcal{M}_\alpha \boldsymbol{\phi}^1 \cos(kl_\alpha) \ , \tag{6.36}$$

$$\boldsymbol{A_2} \cos(kl_\alpha) - \boldsymbol{B_2} \sin(kl_\alpha) = \mathcal{M}_\alpha \boldsymbol{A_1} \cos(kl_\alpha) - \mathcal{M}_\alpha \boldsymbol{\phi}^1 \cos(kl_\alpha) \ . \tag{6.37}$$

Assuming that $\sin(kl_\alpha) \neq 0$ and $\cos(kl_\alpha) \neq 0$, we again obtain

$$\mathcal{M}_\alpha \boldsymbol{A_1} = \boldsymbol{A_2} \ , \tag{6.38}$$

$$\mathcal{M}_\alpha \boldsymbol{\phi}^1 = \boldsymbol{B_2} \ , \tag{6.39}$$

and similarly at the β_0 vertex,

$$\mathcal{M}_\beta \boldsymbol{A_3} = \boldsymbol{A_4} \ , \tag{6.40}$$

$$\mathcal{M}_\beta \boldsymbol{\phi}^3 = \boldsymbol{B_4} \ . \tag{6.41}$$

Noting that $\boldsymbol{f}_{(\boldsymbol{\alpha_{0_1}^{-1}},\boldsymbol{\iota_1})}(2l_\alpha) = \boldsymbol{\phi}^2$ and $\boldsymbol{f}_{(\boldsymbol{\beta_{0_1}^{-1}},\boldsymbol{\iota_1})}(2l_\beta) = \boldsymbol{\phi}^4$, we have

$$\boldsymbol{A_1} = \mathcal{M}_\alpha^{-1}\boldsymbol{\phi}^2 \csc(2kl_\alpha) - \boldsymbol{\phi}^1 \cot(2kl_\alpha) \ , \tag{6.42}$$

$$\boldsymbol{A_3} = \mathcal{M}_\beta^{-1}\boldsymbol{\phi}^4 \csc(2kl_\beta) - \boldsymbol{\phi}^3 \cot(2kl_\beta) \ , \tag{6.43}$$

so that all the coefficients are written in terms of $\boldsymbol{\phi}^m$ for $m = 1, \ldots, 4$, and the $\mathcal{M}_\alpha$ and $\mathcal{M}_\beta$ matrices.

Taking the derivative along each and summing to zero at each of the ι_j vertices gives the four matrix equations,

$$\mathcal{M}_\alpha^{-1}\boldsymbol{\phi}^2 \csc(2kl_\alpha) - \boldsymbol{\phi}^1 \cot(2kl_\alpha) + \sum_{k=2}^{4} \left[\boldsymbol{\phi}^k \csc(kl_{1,k}) - \boldsymbol{\phi}^1 \cot(kl_{1,k})\right] = 0 \ , \tag{6.44}$$

$$\mathcal{M}_\alpha \boldsymbol{\phi}^1 \csc(2kl_\alpha) - \boldsymbol{\phi}^2 \cot(2kl_\alpha) + \sum_{\substack{k=1 \\ k\neq 2}}^{4} \left[\boldsymbol{\phi}^k \csc(kl_{2,k}) - \boldsymbol{\phi}^2 \cot(kl_{2,k})\right] = 0 \ . \tag{6.45}$$

$$\mathcal{M}_\beta^{-1}\boldsymbol{\phi}^4 \csc(2kl_\beta) - \boldsymbol{\phi}^3 \cot(2kl_\beta) + \sum_{\substack{k=1 \\ k\neq 3}}^{4} \left[\boldsymbol{\phi}^k \csc(kl_{3,k}) - \boldsymbol{\phi}^3 \cot(kl_{3,k})\right] = 0 \ , \tag{6.46}$$

$$\mathcal{M}_\beta \boldsymbol{\phi}^3 \csc(2kl_\beta) - \boldsymbol{\phi}^4 \cot(2kl_\beta) + \sum_{k=1}^{3} \left[\boldsymbol{\phi}^k \csc(kl_{4,k}) - \boldsymbol{\phi}^4 \cot(kl_{4,k})\right] = 0 \ . \tag{6.47}$$

If we let $\boldsymbol{\Phi}$ be the concatenated column vector of the $\boldsymbol{\phi}^m$, this system can be written in matrix form as

$$\hat{M}(k)\boldsymbol{\Phi} = \boldsymbol{0} \ , \tag{6.48}$$

where $\hat{M}(k)$ is a $4D \times 4D$ block matrix. Let $a = \csc(2kl_\alpha)$ and $b = \csc(2kl_\beta)$, so that $\hat{M}(k)$ is defined by

$$\hat{M}(k) = \left[\begin{array}{c|c|c|c} \mathbf{D}_1 & \mathbf{C}_{1,2} + a\,\mathcal{M}_\alpha^{-1} & \mathbf{C}_{1,3} & \mathbf{C}_{1,4} \\ \hline \mathbf{C}_{1,2} + a\,\mathcal{M}_\alpha & \mathbf{D}_2 & \mathbf{C}_{2,3} & \mathbf{C}_{2,4} \\ \hline \mathbf{C}_{1,3} & \mathbf{C}_{2,3} & \mathbf{D}_3 & \mathbf{C}_{3,4} + b\,\mathcal{M}_\beta^{-1} \\ \hline \mathbf{C}_{1,4} & \mathbf{C}_{2,4} & \mathbf{C}_{3,4} + b\,\mathcal{M}_\beta & \mathbf{D}_4 \end{array}\right] , \tag{6.49}$$

with $D \times D$ matrix subblocks,

$$\mathbf{D}_i = -\left(\sum_{\substack{k=1 \\ k\neq i}}^{4} \cot(kl_{i,k})\right) \mathbb{I}_D - \cot(2kl_\alpha)\mathbb{I}_D, \quad i = 1, 2 \tag{6.50}$$

$$\mathbf{D}_i = -\left(\sum_{\substack{k=1 \\ k\neq i}}^{4} \cot(kl_{i,k})\right) \mathbb{I}_D - \cot(2kl_\beta)\mathbb{I}_D, \quad i = 3, 4 \tag{6.51}$$

$$\mathbf{C}_{i,j} = \csc(kl_{i,j})\mathbb{I}_D \ . \tag{6.52}$$

A secular equation for $\hat{\mathcal{G}}/\mathcal{R}$ is then given by

$$\det\left[\hat{M}(k)\right] = 0 \ . \tag{6.53}$$

6.2.2 The K_5 Subgraph

The choice of K_4 for the subgraph replacing the ι_j vertices is arbitrary; in theory, any connected subgraph will do. As an example, we will provide part of the derivation of a secular equation where the ι_j vertices are replaced by K_5, the completely connected graph on five vertices. This quotient graph, which we will call

$\hat{\hat{\mathcal{G}}}/\mathcal{R}$, is shown in figure 6.5. The procedure follows nearly identical to the previous section.

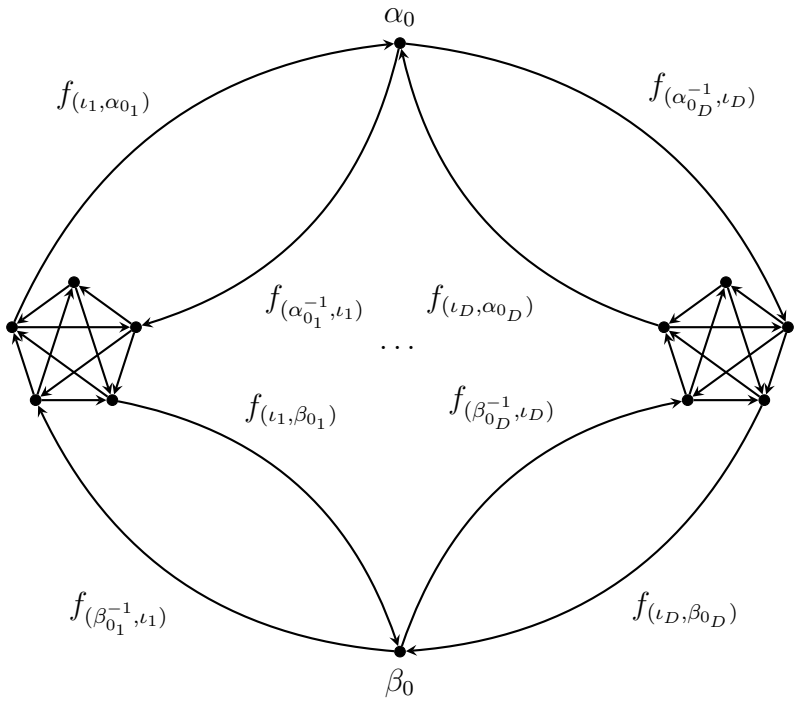

Figure 6.5. The quotient graph $\hat{\hat{\mathcal{G}}}/\mathcal{R}$ where each vertex ι_j has been replaced with a copy of K_5.

Label the five vertices of the jth copy of K_5 as ι_j^m for $m = 1, \ldots, 5$, so that we have the edges (ι_j^1, α_0), $(\alpha_0^{-1}, \iota_j^2)$, (ι_j^3, β_0), and $(\beta_0^{-1}, \iota_j^4)$, as shown in figure 6.6. Define $f_j^{(m_1,m_2)}$ as previously and assign the length l_{m_1,m_2} to the edge $(\iota_j^{m_1}, \iota_j^{m_2})$ for all j. By continuity, define the vectors $\boldsymbol{\phi^m}$ of length D for $m = 1, \ldots, 5$ analogously to the previous section. Using the vector form $\boldsymbol{f}^{(m_1,m_2)} = \{f_1^{(m_1,m_2)}, \ldots, f_D^{(m_1,m_2)}\}^T$, we may write

$$\boldsymbol{f}^{(m_1,m_2)}(x) = (\boldsymbol{\phi}^{m_2} \csc(kl_{m_1,m_2}) - \boldsymbol{\phi}^{m_1} \cot(kl_{m_1,m_2})) \sin(kx) + \boldsymbol{\phi}^{m_1} \cos(kx) \ , \quad (6.54)$$

for $\sin(kl_{m_1,m_2}) \neq 0$.

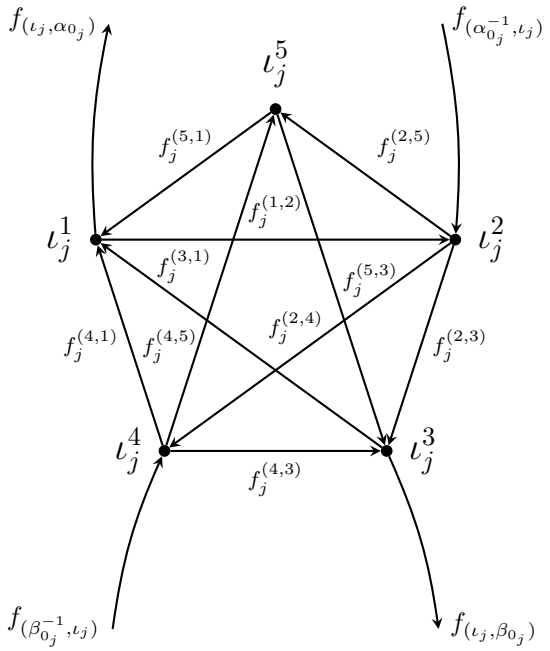

Figure 6.6. The jth copy of the subgraph K_5 in the quotient graph $\hat{\hat{\mathcal{G}}}/\mathcal{R}$.

The functions $\boldsymbol{f_{(\iota,\alpha_0)}}, \boldsymbol{f_{(\iota,\beta_0)}}, \boldsymbol{f_{(\alpha_0^{-1},\iota)}}, \boldsymbol{f_{(\beta_0^{-1},\iota)}}$ are given as in (6.17)–(6.20) and because of our choices for vertex labels, $\boldsymbol{A_i}$ and $\boldsymbol{B_i}$ for $i = 1, \ldots, 4$ are the same as in the K_4 case. Thus, the analogue to the system of equations given in (6.44)–(6.47) is given by

$$\mathcal{M}_\alpha^{-1}\boldsymbol{\phi}^2 \csc(2kl_\alpha) - \boldsymbol{\phi}^1 \cot(2kl_\alpha) + \sum_{k=2}^{5} \left[\boldsymbol{\phi}^k \csc(kl_{1,k}) - \boldsymbol{\phi}^1 \cot(kl_{1,k})\right] = 0 \ , \quad (6.55)$$

$$\mathcal{M}_\alpha \boldsymbol{\phi}^1 \csc(2kl_\alpha) - \boldsymbol{\phi}^2 \cot(2kl_\alpha) + \sum_{\substack{k=1 \\ k\neq 2}}^{5} \left[\boldsymbol{\phi}^k \csc(kl_{2,k}) - \boldsymbol{\phi}^2 \cot(kl_{2,k})\right] = 0 \ , \quad (6.56)$$

$$\mathcal{M}_\beta^{-1}\boldsymbol{\phi}^4 \csc(2kl_\beta) - \boldsymbol{\phi}^3 \cot(2kl_\beta) + \sum_{\substack{k=1 \\ k\neq 3}}^{5} \left[\boldsymbol{\phi}^k \csc(kl_{3,k}) - \boldsymbol{\phi}^3 \cot(kl_{3,k})\right] = 0 \ , \quad (6.57)$$

$$\mathcal{M}_\beta \boldsymbol{\phi}^3 \csc(2kl_\beta) - \boldsymbol{\phi}^4 \cot(2kl_\beta) + \sum_{\substack{k=1 \\ k\neq 4}}^{5} \left[\boldsymbol{\phi}^k \csc(kl_{4,k}) - \boldsymbol{\phi}^4 \cot(kl_{4,k})\right] = 0 \ , \quad (6.58)$$

$$\sum_{k=1}^{4} \left[\boldsymbol{\phi}^k \csc(kl_{5,k}) - \boldsymbol{\phi}^5 \cot(kl_{5,k})\right] = 0 \ , \quad (6.59)$$

where (6.59) is the equation for the ι_j^5 vertices. Letting $\mathbf{\Phi}$ be the concatenated column vector of $\boldsymbol{\phi}^1, \ldots, \boldsymbol{\phi}^5$, we may write

$$\hat{\hat{M}}(k)\mathbf{\Phi} = \mathbf{0} \ , \tag{6.60}$$

as in (6.48). In this case, $\hat{\hat{M}}(k)$ is the $5D \times 5D$ block matrix given by

$$\left[\begin{array}{c|c|c|c|c} \mathbf{D}_1 & \mathbf{C}_{1,2} + a\mathcal{M}_\alpha^{-1} & \mathbf{C}_{1,3} & \mathbf{C}_{1,4} & \mathbf{C}_{1,5} \\ \hline \mathbf{C}_{1,2} + a\mathcal{M}_\alpha & \mathbf{D}_2 & \mathbf{C}_{2,3} & \mathbf{C}_{2,4} & \mathbf{C}_{2,5} \\ \hline \mathbf{C}_{1,3} & \mathbf{C}_{2,3} & \mathbf{D}_3 & \mathbf{C}_{3,4} + b\mathcal{M}_\beta^{-1} & \mathbf{C}_{3,5} \\ \hline \mathbf{C}_{1,4} & \mathbf{C}_{2,4} & \mathbf{C}_{3,4} + b\mathcal{M}_\beta & \mathbf{D}_4 & \mathbf{C}_{4,5} \\ \hline \mathbf{C}_{1,5} & \mathbf{C}_{2,5} & \mathbf{C}_{3,5} & \mathbf{C}_{4,5} & \mathbf{D}_5 \end{array}\right] \ , \tag{6.61}$$

with subblocks

$$\mathbf{D}_i = -\left(\sum_{\substack{k=1 \\ k\neq i}}^{5} \cot(kl_{i,k})\right) \mathbb{I}_D - \cot(2kl_\alpha)\mathbb{I}_D, \quad i = 1, 2 \ , \tag{6.62}$$

$$\mathbf{D}_i = -\left(\sum_{\substack{k=1 \\ k\neq i}}^{5} \cot(kl_{i,k})\right) \mathbb{I}_D - \cot(2kl_\beta)\mathbb{I}_D, \quad i = 3, 4 \ , \tag{6.63}$$

$$\mathbf{D}_5 = -\left(\sum_{k=1}^{4} \cot(kl_{5,k})\right) \mathbb{I}_D \ , \tag{6.64}$$

$$\mathbf{C}_{i,j} = \csc(kl_{i,j})\mathbb{I}_D \ . \tag{6.65}$$

Here, a and b are defined as above and so we have the secular equation

$$\det\left[\hat{\hat{M}}(k)\right] = 0 \ , \tag{6.66}$$

for the quotient graph $\hat{\hat{\mathcal{G}}}/\mathcal{R}$.

6.3 Numerical Results

We took a slightly different approach from chapter four when searching for roots of these secular equations. Rather than searching for zeros of the matrix determinant directly, we considered the eigenvalues of the matrix as functions of k and searched for their roots. Although finding the eigenvalues of a large numerical matrix may be slightly more computationally expensive than finding the determinant, these eigenvalue functions are much more well-behaved in terms of the employed root-finding algorithm, which ultimately resulted in greater efficiency.

The justification for the procedure relies on the fact that eigenvalues of a matrix whose entries are continuous functions are themselves continuous. Clearly the elements of our matrix are not continuous on the whole real line since cosecant and cotangent have regularly spaced asymptotes. However, because we know the location of these poles, we can partition our interval into subintervals with the asymptotes serving as endpoints. Within any of these subintervals, the elements of the matrix will be continuous and therefore the eigenvalues will be also.

We evaluated $M(k)$ as defined in (6.49) at evenly spaced values of k on the subintervals determined by the asymptotes. We found the eigenvalues of each of these matrices and sorted them into a matrix so that each column was increasing smallest to largest. In this way, each row of the matrix corresponds to an eigenvalue viewed as a continuous function evaluated at evenly spaced values of k. We looked for sign changes on each row of the matrix and used a bracketing algorithm to find the roots. By checking against the Weyl law for quantum graphs (see 2.4), we were able to confirm that no roots were missed using this method.

6.3.1 Results for the Group $\mathrm{SL}(2,7)$

For the Cayley graph of the group $G = \mathrm{SL}(2,7)$ with generators

$$\alpha = \begin{pmatrix} 0 & 1 \\ -1 & 0 \end{pmatrix} \qquad \beta = \begin{pmatrix} 0 & -1 \\ 1 & -1 \end{pmatrix} , \tag{6.67}$$

let $\mathcal{G}$ denote the corresponding quantum graph. We looked at the spectral statistics of three quotient graphs of $\mathcal{G}$ with subgraphs included at the vertices. First, we looked at $\hat{\mathcal{G}}/\mathcal{R}_6$, which is the quotient graph with a copy of K_4 at each of the vertices with respect to the 6-dimensional representation $\mathcal{R}_6$. We also considered a quotient graph with respect to the same representation, $\hat{\hat{\mathcal{G}}}/\mathcal{R}_6$, where each of the vertices was replaced with a copy of K_5. Finally, we examined $\hat{\mathcal{G}}/\mathcal{R}_8$, the quotient graph with respect to the 8-dimensional representation $\mathcal{R}_8$ with a copy of K_4 included at each vertex.

The irreducible 6-dimensional representation $\mathcal{R}_6$ can be given as

$$\mathcal{M}_\alpha = \begin{pmatrix} 1 & 0 & 0 & 0 & 0 & 0 \\ 0 & 0 & 1 & 0 & 0 & 0 \\ 0 & 1 & 0 & 0 & 0 & 0 \\ 0 & 0 & 0 & 0 & 1 & 0 \\ 0 & 0 & 0 & 1 & 0 & 0 \\ 0 & 0 & 0 & 0 & 0 & 1 \end{pmatrix} , \tag{6.68}$$

for the generator α and

$$\mathcal{M}_\beta = \begin{pmatrix} 0 & 1 & 0 & 0 & 0 & 0 \\ 0 & 0 & 0 & 1 & 0 & 0 \\ 0 & 0 & 1 & 0 & 0 & 0 \\ 1 & 0 & 0 & 0 & 0 & 0 \\ 0 & 0 & 0 & 0 & 0 & 1 \\ -1 & -1 & -1 & -1 & -1 & -1 \end{pmatrix} , \tag{6.69}$$

for the generator β. Histograms of the nearest-neighbor spacing distribution for approximately 50,000 eigenvalues of $\hat{\mathcal{G}}/\mathcal{R}_6$ and $\hat{\mathcal{G}}/\mathcal{R}_6$ are shown in figures 6.7 and 6.9, respectively. The corresponding integrated distributions are in figures 6.8 and 6.10. We included the Poisson distribution in both sets of figures for comparison. Figures 6.11 and 6.12 show the two-point correlation function for $\hat{\mathcal{G}}/\mathcal{R}_6$ and $\hat{\hat{\mathcal{G}}}/\mathcal{R}_6$, respectively, which we computed using the method described in section 4.2.4.

The irreducible 8-dimensional representation $\mathcal{R}_8$ can be given as

$$\mathcal{M}_\alpha = \begin{pmatrix} 0 & 1 & 0 & 0 & 0 & 0 & 0 & 0 \\ -1 & 0 & 0 & 0 & 0 & 0 & 0 & 0 \\ 0 & 0 & 0 & 1 & 0 & 0 & 0 & 0 \\ 0 & 0 & -1 & 0 & 0 & 0 & 0 & 0 \\ 0 & 0 & 0 & 0 & 0 & 0 & 1 & 0 \\ 0 & 0 & 0 & 0 & 0 & 0 & 0 & 1 \\ 0 & 0 & 0 & 0 & -1 & 0 & 0 & 0 \\ 0 & 0 & 0 & 0 & 0 & -1 & 0 & 0 \end{pmatrix}, \tag{6.70}$$

for generator α and

$$\mathcal{M}_\beta = \begin{pmatrix} 1 & 0 & 0 & 0 & 0 & 0 & 0 & 0 \\ 0 & 0 & 1 & 0 & 0 & 0 & 0 & 0 \\ 0 & 0 & 0 & 0 & 1 & 0 & 0 & 0 \\ 0 & 0 & 0 & 0 & 0 & 1 & 0 & 0 \\ 0 & 1 & 0 & 0 & 0 & 0 & 0 & 0 \\ 0 & 0 & 0 & 0 & 0 & 0 & 0 & -1 \\ 0 & 0 & 0 & 0 & 0 & 0 & 1 & 0 \\ 0 & 0 & 0 & -1 & 0 & 0 & 0 & 0 \end{pmatrix}, \tag{6.71}$$

for generator β. The histogram of the nearest-neighbor spacing distribution for $\mathcal{G}/\mathcal{R}_8$ is shown in figure 6.13, the integrated nearest-neighbor distribution is in figure 6.14, and the two-point correlation function is in figure 6.15.

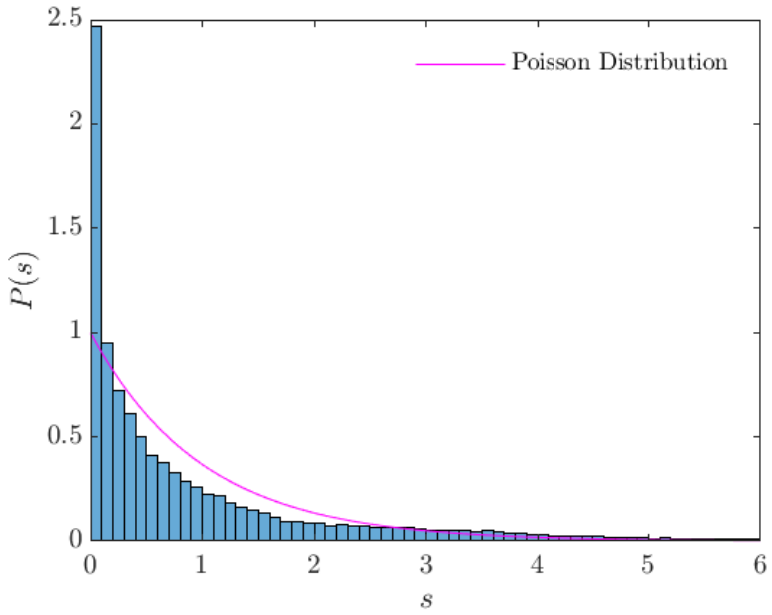

Figure 6.7. Histogram of the nearest-neighbor spacing distribution for the quantum graph $\hat{\mathcal{G}}/\mathcal{R}_6$ with respect to the irreducible 6-dimensional representation given in (6.68)–(6.69) for 49,927 eigenvalues plotted against the Poisson distribution.

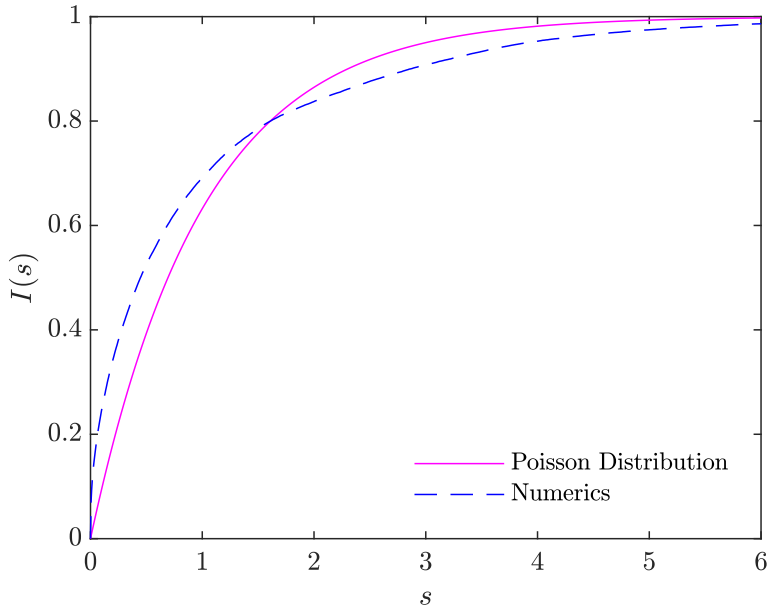

Figure 6.8. The integrated nearest-neighbor spacing distribution for the quantum graph $\hat{\mathcal{G}}/\mathcal{R}_6$ with respect to the irreducible 6-dimensional representation given in (6.68)–(6.69) plotted against the Poisson distribution.

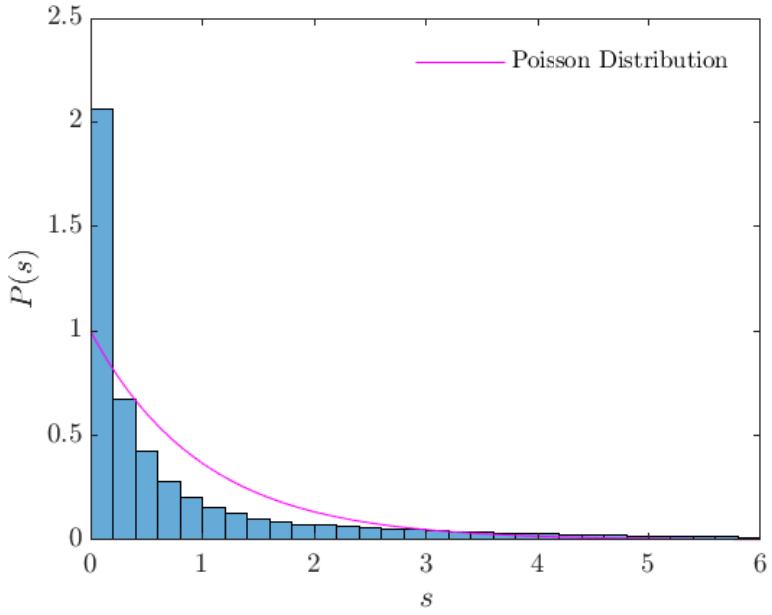

Figure 6.9. Histogram of the nearest-neighbor spacing distribution for the quantum graph $\hat{\hat{\mathcal{G}}}/\mathcal{R}_6$ with respect to the irreducible 6-dimensional representation given in (6.68)–(6.69) for 50,604 eigenvalues plotted against the Poisson distribution.

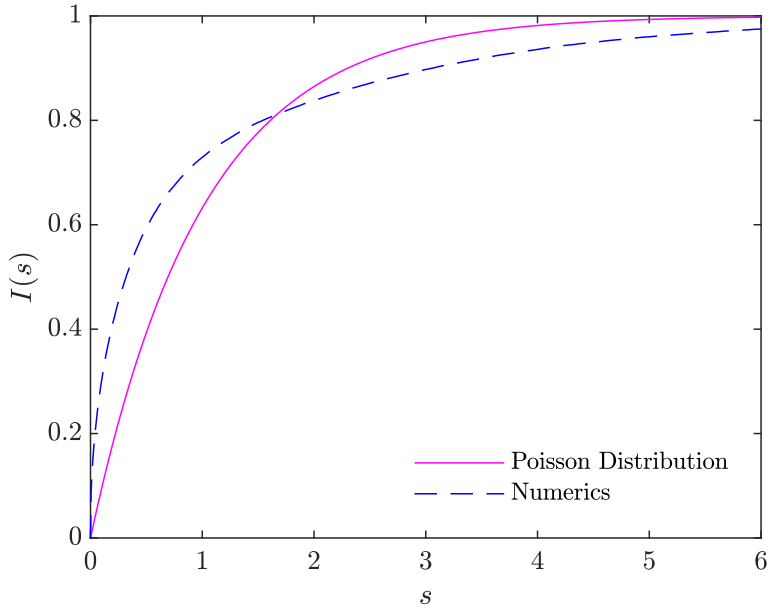

Figure 6.10. The integrated nearest-neighbor spacing distribution for the quantum graph $\hat{\hat{\mathcal{G}}}/\mathcal{R}_6$ with respect to the irreducible 6-dimensional representation given in (6.68)–(6.69) plotted against the Poisson distribution.

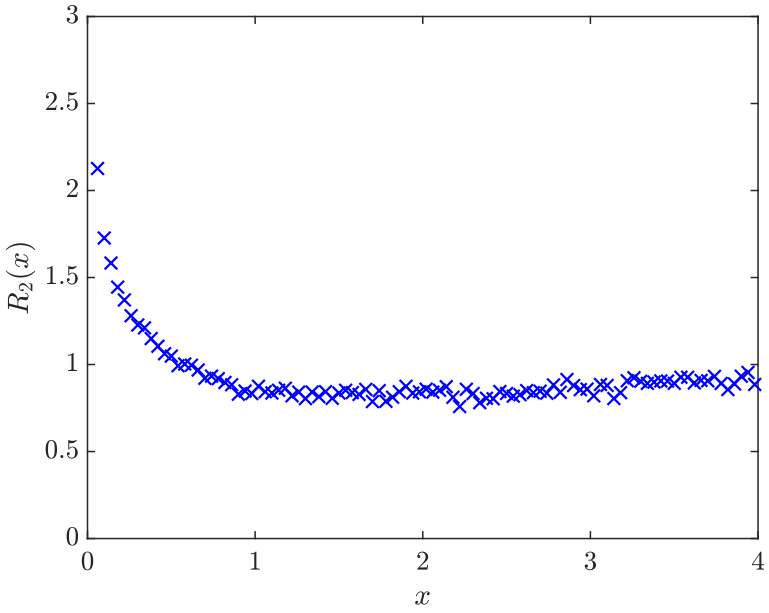

Figure 6.11. The two-point correlation function plotted for 49,927 eigenvalues for the quantum graph $\hat{\mathcal{G}}/\mathcal{R}_6$ with respect to the irreducible 6-dimensional representation given in (6.68)–(6.69).

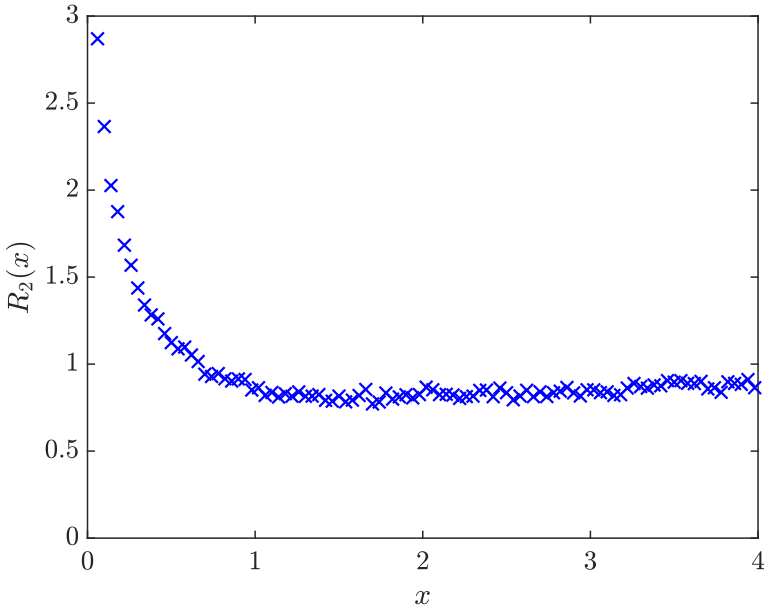

Figure 6.12. The two-point correlation function plotted for 50,604 eigenvalues for the quantum graph $\hat{\hat{\mathcal{G}}}/\mathcal{R}_6$ with respect to the irreducible 6-dimensional representation given in (6.68)–(6.69).

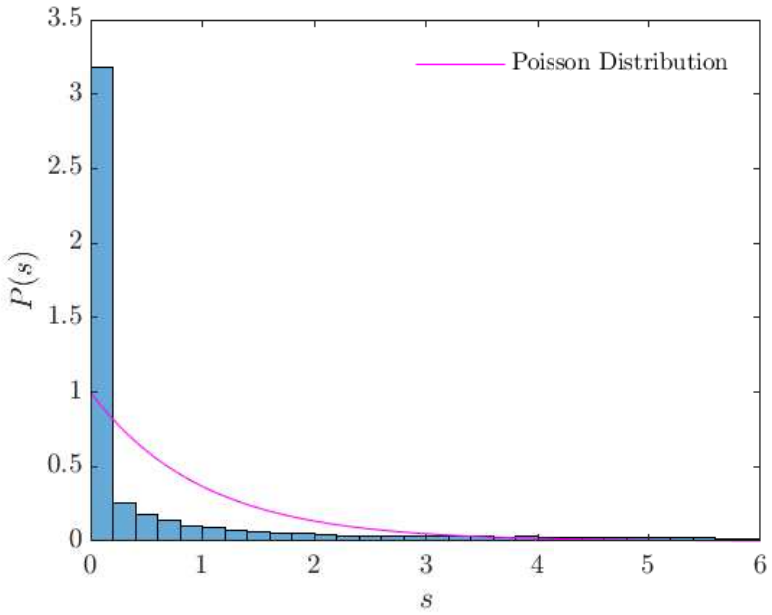

Figure 6.13. Histogram of the nearest-neighbor spacing distribution for the quantum graph $\hat{\mathcal{G}}/\mathcal{R}_8$ with respect to the irreducible 8-dimensional representation given in (6.70)–(6.71) for 50,212 eigenvalues plotted against the Poisson distribution.

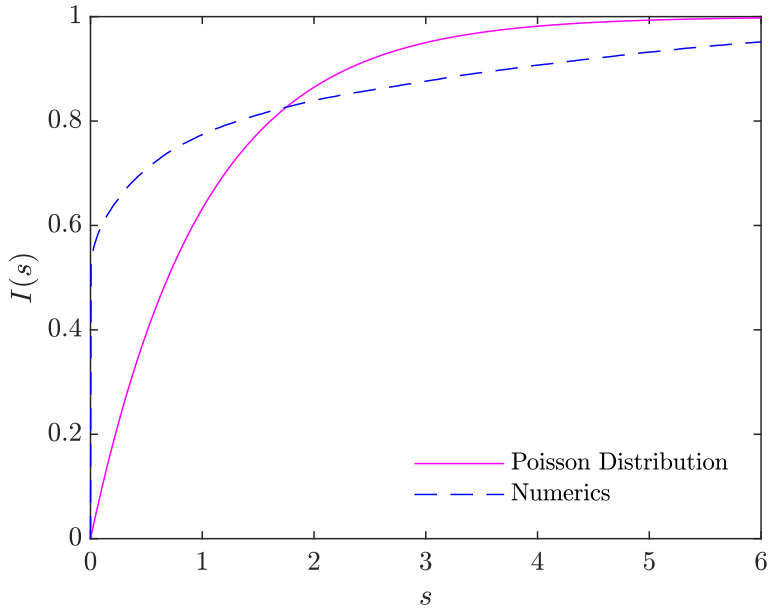

Figure 6.14. The integrated nearest-neighbor spacing distribution for the quantum graph $\hat{\mathcal{G}}/\mathcal{R}_8$ with respect to the irreducible 8-dimensional representation given in (6.70)–(6.71) plotted against the Poisson distribution.

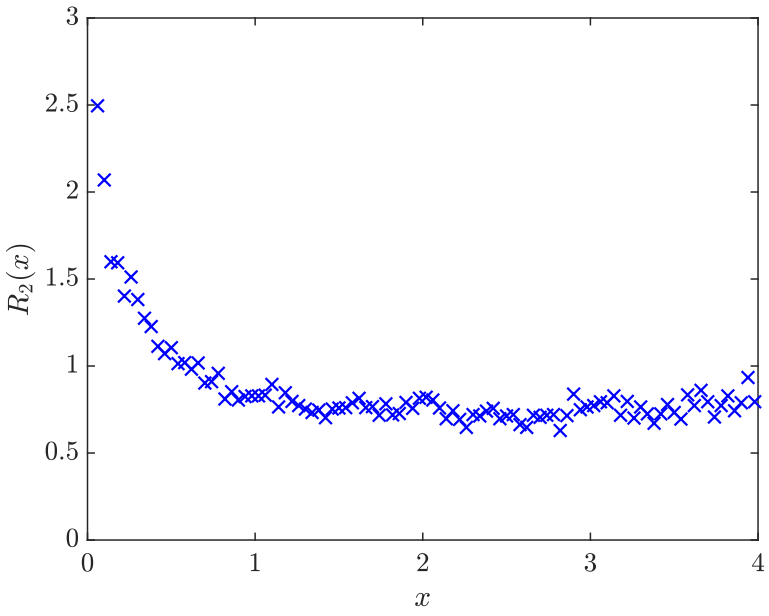

Figure 6.15. The two-point correlation function plotted for 50,212 eigenvalues for the quantum graph $\hat{\mathcal{G}}/\mathcal{R}_8$ with respect to the irreducible 8-dimensional representation given in (6.70)–(6.71).

APPENDIX

APPENDIX

List of Symbols and Notation

$(d)_j$	Pochhammer symbol (falling factorial), i.e. $d!/(d-j)!$
$\mathbb{A}, \mathbb{B}$	Matrices defining vertex conditions
A_p	Stability amplitude of periodic orbit p
b	Directed edge (bond)
$\bar{b}$	Reversal of the bond b
$\mathcal{C}$	A contour in the complex plane
$C(\mathcal{G})$	Space of continuous functions on the metric graph $\mathcal{G}$
$C_n(\boldsymbol{a})$	Circulant graph with n vertices generated by $\boldsymbol{a}$
$C_n(\boldsymbol{L}; \boldsymbol{a})$	Quantum circulant graph
$C_n(\boldsymbol{l}; \boldsymbol{a})$	Symmetric quantum circulant graph
d	Length of $\boldsymbol{a}$ in $C_n(\boldsymbol{a})$
d_v	Degree of the vertex v
D	Dimension of a representation
Δ	Laplace operator
$\mathrm{E}[x]$	Expectation value of x
$\mathcal{E}$	Set of edges
E	Number of edges (size of the set $\mathcal{E}$)
$\mathcal{E}_v$	Set of edges incident to the vertex v
$\mathbb{E}$	Matrix of ones
E_c	Regularized vacuum energy
$f_e(x_e)$	Function defined on the interval $[0, L_e]$ associated to the edge e
$\boldsymbol{F}(v)$	Vector of function values at v on each edge $e \in \mathcal{E}_v$
$\boldsymbol{F'}(v)$	Vector of outgoing derivative values at v on each edge $e \in \mathcal{E}_v$
G	A group
Γ	Combinatorial graph
$\mathcal{G}$	Metric graph (shorthand for quantum graph)
$(\mathcal{G}, \mathcal{H})$	Quantum graph
$\mathcal{G}/\mathcal{R}$	Quotient graph with respect to irreducible representation $\mathcal{R}$
$\mathcal{H}$	Differential operator (Hamiltonian)
$\widetilde{H^2}(\mathcal{G})$	Direct sum of the second Sobolev space on each edge of $\mathcal{G}$
$\mathbb{I}$	Identity matrix

ι	Identity element for the group G
$I(s)$	Integrated nearest-neighbor spacing distribution
J	Adjacency matrix
k	Root of secular equation, i.e. $\sqrt{\lambda}$
$\hat{k}_j$	Normalized root of secular equation, i.e. $k_j\pi/\mathcal{L}$
$K(\tau)$	Form factor (Fourier transform of $R_2(x)$)
λ	Eigenvalue
L_e	Length of the edge e
l_h	Length of an edge belonging to a set of edges with equal length
$\mathbf{L}$	Diagonal matrix of edge lengths
$\mathcal{L}$	Total metric length of a graph
$\mathfrak{L}$	Set of all possible lengths of periodic orbits
$L^2(\mathcal{G})$	Space of square-integrable functions on the metric graph $\mathcal{G}$
$\mathcal{M}_\sigma$	Matrix representation of σ by $\mathcal{R}$, i.e. $\mathcal{R}(\sigma)$
$N(a,b)$	Algebraic counting function
$o(b)$	Origin vertex of the bond b
Ω	Generating set for a Cayley graph
$\Phi(\lambda)$	Eigenspace of the graph with eigenvalue λ
$\Phi_j(\lambda)$	Subspace of $\Phi(\lambda)$ transforming according to $\mathcal{R}_j$
$p(z)$	Representer of a circulant matrix
$\mathcal{P}_m$	Set of periodic orbits of topological length m
$P(s)$	Nearest-neighbor spacing probability density function
$P_W(s)$	Wigner surmise for the Gaussian ensembles of random matrices
$\rho(x)$	Probability density function
r_p	Repetition number of periodic orbit p
$\mathcal{R}$	Irreducible representation
$R_2(x)$	Two-point correlation function
$\Re(s)$	Real part of s
$\sigma^{(v)}(k)$	Vertex scattering matrix at v
$S(k)$	Bond scattering matrix
$t(b)$	Terminal vertex of the bond b
$\mathcal{V}$	Set of vertices
V	Number of vertices (size of the set $\mathcal{V}$)
$\{u,v\}$	The (undirected) edge connecting u and v
$u \sim v$	The vertex u is adjacent to the vertex v
$\zeta(s)$	Spectral zeta function

BIBLIOGRAPHY

[1] Nobel Media AB 2019, *The Nobel Prize in Physics 2010 — NobelPrize.org*, 2019, (Online; accessed 25-May-2019).

[2] E. Akkermans, A. Comtet, J. Desbois, G. Montambaux, and C. Texier, *Spectral determinant on quantum graphs*, Ann. Physics **284** (2000), no. 1, 10–51. MR 1780489

[3] B. Alspach and T. D. Parsons, *Isomorphism of circulant graphs and digraphs*, Discrete Math. **25** (1979), no. 2, 97–108. MR 523083

[4] G. W. Anderson, A. Guionnet, and O. Zeitouni, *An introduction to random matrices*, Cambridge Studies in Advanced Mathematics, vol. 118, Cambridge University Press, Cambridge, 2010. MR 2760897

[5] J. E. Avron, P. Exner, and Y. Last, *Periodic schrödinger operators with large gaps and wannier-stark ladders*, Phys. Rev. Lett. **72** (1994), 896–899.

[6] R. Band and S. Gnutzmann, *Quantum graphs via exercises*, Spectral theory and applications, Contemp. Math., vol. 720, Amer. Math. Soc., Providence, RI, 2018, pp. 187–203. MR 3880377

[7] R. Band, O. Parzanchevski, and G. Ben-Shach, *The isospectral fruits of representation theory: quantum graphs and drums*, J. Phys. A **42** (2009), no. 17, 175202, 42. MR 2539297

[8] F. Barra and P. Gaspard, *On the level spacing distribution in quantum graphs*, J. Statist. Phys. **101** (2000), no. 1-2, 283–319. MR 1807548

[9] J. Behrndt and A. Luger, *On the number of negative eigenvalues of the Laplacian on a metric graph*, J. Phys. A **43** (2010), no. 47, 474006, 11. MR 2738101

[10] G. Berkolaiko, *Form factor for large quantum graphs: evaluating orbits with time reversal*, Waves Random Media **14** (2004), no. 1, S7–S27, Special section on quantum graphs. MR 2042542

[11] ———, *An elementary introduction to quantum graphs*, Geometric and computational spectral theory, Contemp. Math., vol. 700, Amer. Math. Soc., Providence, RI, 2017, pp. 41–72. MR 3748521

[12] G. Berkolaiko, E. B. Bogomolny, and J. P. Keating, *Star graphs and Šeba billiards*, J. Phys. A **34** (2001), no. 3, 335–350. MR 1822781

[13] G. Berkolaiko, J. M. Harrison, and J. H. Wilson, *Mathematical aspects of vacuum energy on quantum graphs*, J. Phys. A **42** (2009), no. 2, 025204, 20. MR 2525288

[14] G. Berkolaiko and J. P. Keating, *Two-point spectral correlations for star graphs*, J. Phys. A **32** (1999), no. 45, 7827–7841. MR 1732273

[15] G. Berkolaiko, J. P. Keating, and U. Smilansky, *Quantum ergodicity for graphs related to interval maps*, Comm. Math. Phys. **273** (2007), no. 1, 137–159. MR 2308752

[16] G. Berkolaiko, J. P. Keating, and B. Winn, *Intermediate wave function statistics*, Phys. Rev. Lett. **91** (2003), 134103.

[17] ———, *No quantum ergodicity for star graphs*, Comm. Math. Phys. **250** (2004), no. 2, 259–285. MR 2094517

[18] G. Berkolaiko and P. Kuchment, *Introduction to quantum graphs*, Mathematical Surveys and Monographs, vol. 186, American Mathematical Society, Providence, RI, 2013. MR 3013208

[19] G. Berkolaiko, H. Schanz, and R. S. Whitney, *Leading off-diagonal correction to the form factor of large graphs*, Phys. Rev. Lett. **88** (2002), 104101.

[20] ———, *Form factor for a family of quantum graphs: an expansion to third order*, J. Phys. A **36** (2003), no. 31, 8373–8392. MR 2007834

[21] J. C. Bermond, F. Comellas, and D. F. Hsu, *Distributed loop computer-networks: A survey*, Journal of Parallel and Distributed Computing **24** (1995), no. 1, 2 – 10.

[22] M. V. Berry and M. Tabor, *Level clustering in the regular spectrum*, Proceedings of the Royal Society of London. A. Mathematical and Physical Sciences **356** (1977), no. 1686, 375–394.

[23] F. Boesch and R. Tindell, *Circulants and their connectivities*, J. Graph Theory **8** (1984), no. 4, 487–499. MR 766498

[24] E. B. Bogomolny, B. Georgeot, M.-J. Giannoni, and C. Schmit, *Arithmetical chaos*, Phys. Rep. **291** (1997), no. 5-6, 219–324. MR 1480112

[25] E. B. Bogomolny, U. Gerland, and C. Schmit, *Models of intermediate spectral statistics*, Phys. Rev. E **59** (1999), R1315–R1318.

[26] ———, *Singular statistics*, Phys. Rev. E (3) **63** (2001), no. 3, part 2, 036206, 16. MR 1819755

[27] O. Bohigas, M.-J. Giannoni, and C. Schmit, *Characterization of chaotic quantum spectra and universality of level fluctuation laws*, Phys. Rev. Lett. **52** (1984), no. 1, 1–4. MR 730191

[28] J. Bolte and J. M. Harrison, *Spectral statistics for the Dirac operator on graphs*, J. Phys. A **36** (2003), no. 11, 2747–2769. MR 1965289

[29] ———, *Ths spin contribution to the form factor of quantum graphs*, J. Phys. A **36** (2003), no. 27, L433–L440. MR 2006502

[30] C. Cattaneo, *The spectrum of the continuous Laplacian on a graph*, Monatsh. Math. **124** (1997), no. 3, 215–235. MR 1476363

[31] F. R. K. Chung, *Spectral graph theory*, CBMS Regional Conference Series in Mathematics, vol. 92, Published for the Conference Board of the Mathematical Sciences, Washington, DC; by the American Mathematical Society, Providence, RI, 1997. MR 1421568

[32] P. J. Davis, *Circulant matrices*, John Wiley & Sons, New York-Chichester-Brisbane, 1979. MR 543191

[33] J. Desbois, *Spectral determinant of Schrödinger operators on graphs*, J. Phys. A **33** (2000), no. 7, L63–L67. MR 1746875

[34] ———, *Spectral determinant on graphs with generalized boundary conditions*, Eur. Phys. J. B Condens. Matter Phys. **24** (2001), no. 2, 261–266. MR 1875412

[35] R. Diestel, *Graph theory*, **173** (2017), xviii+428. MR 3644391

[36] B. Eckhardt, S. Fishman, J. P. Keating, O. Agam, J. Main, and K. Müller, *Approach to ergodicity in quantum wave functions*, Phys. Rev. E **52** (1995), 5893–5903.

[37] B. Elspas and J. Turner, *Graphs with circulant adjacency matrices*, J. Combinatorial Theory **9** (1970), 297–307. MR 0272659

[38] L. Euler, *Solutio problematis ad geometriam situs pertinentis. (Latin) [The solution of a problem relating to the geometry of position]*, Comment. Acad. Sci. Imp. Petropolitanae **8** (1741), no. 53, 128–140.

[39] P. Exner and R. Gawlista, *Band spectra of rectangular graph superlattices*, Phys. Rev. B **53** (1996), 7275–7286.

[40] P. Exner, M. Helm, and P. Stollmann, *Localization on a quantum graph with a random potential on the edges*, Rev. Math. Phys. **19** (2007), no. 9, 923–939. MR 2355567

[41] L. Friedlander, *Determinant of the Schrödinger operator on a metric graph*, Quantum graphs and their applications, Contemp. Math., vol. 415, Amer. Math. Soc., Providence, RI, 2006, pp. 151–160. MR 2277614

[42] S. A. Fulling, L. Kaplan, and J. H. Wilson, *Vacuum energy and repulsive Casimir forces in quantum star graphs*, Phys. Rev. A (3) **76** (2007), no. 1, 012118, 7. MR 2444998

[43] S. A. Fulling, P. Kuchment, and J. H. Wilson, *Index theorems for quantum graphs*, J. Phys. A **40** (2007), no. 47, 14165–14180. MR 2438118

[44] S. A. Fulling and J. H. Wilson, *Vacuum energy and closed orbits in quantum graphs*, Analysis on graphs and its applications, Proc. Sympos. Pure Math., vol. 77, Amer. Math. Soc., Providence, RI, 2008, pp. 673–679. MR 2459896

[45] S. Gnutzmann and A. Altland, *Universal spectral statistics in quantum graphs*, Phys. Rev. Lett. **93** (2004), 194101.

[46] ———, *Spectral correlations of individual quantum graphs*, Phys. Rev. E (3) **72** (2005), no. 5, 056215, 14. MR 2198317

[47] S. Gnutzmann, J. P. Keating, and F. Piotet, *Eigenfunction statistics on quantum graphs*, Ann. Physics **325** (2010), no. 12, 2595–2640. MR 2726648

[48] S. Gnutzmann and B. Seif, *Universal spectral statistics in Wigner-Dyson, chiral, and Andreev star graphs. I. Construction and numerical results*, Phys. Rev. E (3) **69** (2004), no. 5, 056219, 16. MR 2096549

[49] ———, *Universal spectral statistics in Wigner-Dyson, chiral, and Andreev star graphs. II. Semiclassical approach*, Phys. Rev. E (3) **69** (2004), no. 5, 056220, 16. MR 2096550

[50] S. Gnutzmann and U. Smilansky, *Quantum graphs: Applications to quantum chaos and universal spectral statistics*, Advances in Physics **55** (2006), no. 5-6, 527–625.

[51] S. Gnutzmann, U. Smilansky, and J. Weber, *Nodal counting on quantum graphs*, Waves Random Media **14** (2004), no. 1, S61–S73, Special section on quantum graphs. MR 2042545

[52] C. Godsil and G. Royle, *Algebraic graph theory*, Graduate Texts in Mathematics, vol. 207, Springer-Verlag, New York, 2001. MR 1829620

[53] C. Gordon, D. Webb, and S. Wolpert, *Isospectral plane domains and surfaces via Riemannian orbifolds*, Invent. Math. **110** (1992), no. 1, 1–22. MR 1181812

[54] ———, *One cannot hear the shape of a drum*, Bull. Amer. Math. Soc. (N.S.) **27** (1992), no. 1, 134–138. MR 1136137

[55] T. Gorin, M. Müller, and P. Seba, *Comment on "models of intermediate spectral statistics"*, Phys. Rev. E **63** (2001), 068201.

[56] D. Grieser, *Monotone unitary families*, Proc. Amer. Math. Soc. **141** (2013), no. 3, 997–1005. MR 3003691

[57] B. Gutkin and U. Smilansky, *Can one hear the shape of a graph?*, J. Phys. A **34** (2001), no. 31, 6061–6068. MR 1862642

[58] F. Haake, *Quantum signatures of chaos*, enlarged ed., Springer Series in Synergetics, Springer-Verlag, Berlin, 2010. MR 2604131

[59] M. Harmer, *Hermitian symplectic geometry and extension theory*, J. Phys. A **33** (2000), no. 50, 9193–9203. MR 1804888

[60] J. M. Harrison and K. Kirsten, *Zeta functions of quantum graphs*, J. Phys. A **44** (2011), no. 23, 235301, 29. MR 2800848

[61] J. M. Harrison, K. Kirsten, and C. Texier, *Spectral determinants and zeta functions of Schrödinger operators on metric graphs*, J. Phys. A **45** (2012), no. 12, 125206, 14. MR 2904390

[62] J. M. Harrison and E. Swindle, *Spectral properties of quantum circulant graphs*, J. Phys. A **52** (2019), no. 28, 285101.

[63] J. M. Harrison and B. Winn, *Intermediate statistics for a system with symplectic symmetry: the Dirac rose graph*, J. Phys. A **45** (2012), no. 43, 435101, 23. MR 2989218

[64] E. Hecke, *Lectures on the theory of algebraic numbers*, Graduate Texts in Mathematics, vol. 77, Springer-Verlag, New York-Berlin, 1981, Translated from the German by George U. Brauer, Jay R. Goldman and R. Kotzen. MR 638719

[65] N. E. Hurt, *Mathematical physics of quantum wires and devices*, Mathematics and its Applications, vol. 506, Kluwer Academic Publishers, Dordrecht, 2000. MR 1862155

[66] F. K. Hwang, *A survey on multi-loop networks*, Theoret. Comput. Sci. **299** (2003), no. 1-3, 107–121. MR 1973148

[67] Y. Ihara, *On discrete subgroups of the two by two projective linear group over* $\mathfrak{p}$*-adic fields*, J. Math. Soc. Japan **18** (1966), 219–235. MR 0223463

[68] C. H. Joyner, S. Müller, and M. Sieber, *GSE statistics without spin*, EPL (Europhysics Letters) **107** (2014), no. 5, 50004.

[69] M. Kac, *Can one hear the shape of a drum?*, Amer. Math. Monthly **73** (1966), no. 4, part II, 1–23. MR 0201237

[70] J. P. Keating, J. Marklof, and B. Winn, *Value distribution of the eigenfunctions and spectral determinants of quantum star graphs*, Comm. Math. Phys. **241** (2003), no. 2-3, 421–452. MR 2013805

[71] K. Kirsten and A. J. McKane, *Functional determinants by contour integration methods*, Ann. Physics **308** (2003), no. 2, 502–527. MR 2018683

[72] ———, *Functional determinants for general Sturm-Liouville problems*, J. Phys. A **37** (2004), no. 16, 4649–4670. MR 2065952

[73] V. Kostrykin and R. Schrader, *Kirchhoff's rule for quantum wires*, J. Phys. A **32** (1999), no. 4, 595–630. MR 1671833

[74] _____, *Quantum wires with magnetic fluxes*, Comm. Math. Phys. **237** (2003), no. 1-2, 161–179. MR 2007178

[75] _____, *Laplacians on metric graphs: eigenvalues, resolvents and semigroups*, Quantum graphs and their applications, Contemp. Math., vol. 415, Amer. Math. Soc., Providence, RI, 2006, pp. 201–225. MR 2277618

[76] T. Kottos and U. Smilansky, *Quantum chaos on graphs*, Phys. Rev. Lett. **79** (1997), 4794–4797.

[77] _____, *Periodic orbit theory and spectral statistics for quantum graphs*, Ann. Physics **274** (1999), no. 1, 76–124. MR 1694731

[78] _____, *Chaotic scattering on graphs*, Phys. Rev. Lett. **85** (2000), 968–971.

[79] _____, *Quantum graphs: a simple model for chaotic scattering*, J. Phys. A **36** (2003), no. 12, 3501–3524. MR 1986432

[80] P. Kuchment, *The mathematics of photonic crystals*, Mathematical modeling in optical science, Frontiers Appl. Math., vol. 22, SIAM, Philadelphia, PA, 2001, pp. 207–272. MR 1831334

[81] _____, *Differential and pseudo-differential operators on graphs as models of mesoscopic systems*, Analysis and applications—ISAAC 2001 (Berlin), Int. Soc. Anal. Appl. Comput., vol. 10, Kluwer Acad. Publ., Dordrecht, 2003, pp. 7–30. MR 2022737

[82] _____, *Quantum graphs. I. Some basic structures*, Waves Random Media **14** (2004), no. 1, S107–S128, Special section on quantum graphs. MR 2042548

[83] _____, *Quantum graphs. II. Some spectral properties of quantum and combinatorial graphs*, J. Phys. A **38** (2005), no. 22, 4887–4900. MR 2148631

[84] _____, *Quantum graphs: an introduction and a brief survey*, Analysis on graphs and its applications, Proc. Sympos. Pure Math., vol. 77, Amer. Math. Soc., Providence, RI, 2008, pp. 291–312. MR 2459876

[85] P. Kuchment and L. Kunyansky, *Differential operators on graphs and photonic crystals*, Adv. Comput. Math. **16** (2002), no. 2-3, 263–290. MR 1892252

[86] P. Kuchment and O. Post, *On the spectra of carbon nano-structures*, Comm. Math. Phys. **275** (2007), no. 3, 805–826. MR 2336365

[87] J. Marklof, *Arithmetic quantum chaos*, Encyclopedia of Mathematical Physics (Jean-Pierre Françoise, Gregory L. Naber, and Tsou Sheung Tsun, eds.), Academic Press, Oxford, 2006, pp. 212 – 221.

[88] J. Marklof and Z. Rudnick, *Quantum unique ergodicity for parabolic maps*, Geom. Funct. Anal. **10** (2000), no. 6, 1554–1578. MR 1810753

[89] J. Marklof and A. Strömbergsson, *Diameters of random circulant graphs*, Combinatorica **33** (2013), no. 4, 429–466. MR 3133777

[90] M. L. Mehta, *On the statistical properties of the level-spacings in nuclear spectra*, Nuclear Phys. **18** (1960), 395–419. MR 0112645

[91] ———, *Random matrices*, second ed., Academic Press, Inc., Boston, MA, 1991. MR 1083764

[92] E. A. Monakhova, *A survey on undirected circulant graphs*, Discrete Math. Algorithms Appl. **4** (2012), no. 1, 1250002, 30. MR 2913088

[93] A. M. Ozorio de Almeida, *Hamiltonian systems: chaos and quantization*, Cambridge Monographs on Mathematical Physics, Cambridge University Press, Cambridge, 1990, Translated and revised from the Portuguese. MR 1161623

[94] P. Pakoński, G. Tanner, and K. Życzkowski, *Families of line-graphs and their quantization*, J. Statist. Phys. **111** (2003), no. 5-6, 1331–1352. MR 1975931

[95] K. Pankrashkin, *Spectra of Schrödinger operators on equilateral quantum graphs*, Lett. Math. Phys. **77** (2006), no. 2, 139–154. MR 2251302

[96] O. Parzanchevski and R. Band, *Linear representations and isospectrality with boundary conditions*, J. Geom. Anal. **20** (2010), no. 2, 439–471. MR 2579517

[97] L. Pauling, *The diamagnetic anisotropy of aromatic molecules*, The Journal of Chemical Physics **4** (1936), no. 10, 673–677.

[98] H. Poincaré, *Sur le problème des trois corps et les équations de la dynamique. (French) [The three-body problem and the equations of dynamics]*, Acta Math. **13** (1890), no. 1-2, 1–270.

[99] ———, *New methods of celestial mechanics. Vol. 1*, History of Modern Physics and Astronomy, vol. 13, American Institute of Physics, New York, 1993. MR 1194622

[100] ———, *New methods of celestial mechanics. Vol. 2*, History of Modern Physics and Astronomy, vol. 13, American Institute of Physics, New York, 1993. MR 1194623

[101] ———, *New methods of celestial mechanics. Vol. 3*, History of Modern Physics and Astronomy, vol. 13, American Institute of Physics, New York, 1993. MR 1194624

[102] J.-P. Roth, *Le spectre du laplacien sur un graphe*, Théorie du potentiel (Orsay, 1983), Lecture Notes in Math., vol. 1096, Springer, Berlin, 1984, pp. 521–539. MR 890375

[103] K. Ruedenberg and C. W. Scherr, *Free-electron network model for conjugated systems. I. Theory*, The Journal of Chemical Physics **21** (1953), no. 9, 1565–1581.

[104] P. Sarnak, *Recent progress on the quantum unique ergodicity conjecture*, Bull. Amer. Math. Soc. (N.S.) **48** (2011), no. 2, 211–228. MR 2774090

[105] H. Schanz and U. Smilansky, *Periodic-orbit theory of Anderson localization on graphs*, Phys. Rev. Lett. **84** (2000), 1427–1430.

[106] S. Severini and G. Tanner, *Regular quantum graphs*, J. Phys. A **37** (2004), no. 26, 6675–6686. MR 2076460

[107] C. G. Smith, *Low-dimensional quantum devices*, Rep. Prog. Phys. **59** (1996), no. 2, 235–282.

[108] H.-J. Stöckmann, *Quantum chaos*, Cambridge University Press, Cambridge, 1999. MR 1724809

[109] T. Sunada, *Riemannian coverings and isospectral manifolds*, Ann. of Math. (2) **121** (1985), no. 1, 169–186. MR 782558

[110] G. Tanner, *Unitary-stochastic matrix ensembles and spectral statistics*, J. Phys. A **34** (2001), no. 41, 8485–8500. MR 1876609

[111] C. Texier, *ζ-regularized spectral determinants on metric graphs*, J. Phys. A **43** (2010), no. 42, 425203, 20. MR 2726712

[112] C. Texier and G. Montambaux, *Scattering theory on graphs*, J. Phys. A **34** (2001), no. 47, 10307–10326. MR 1872417

[113] T. J. Thornton, *Mesoscopic devices*, Rep. Prog. Phys. **58** (1995), no. 3, 311–364.

[114] V. Vilfred, *On circulant graphs*, Graph Theory and Its Applications (Proc. of the Conf. on Graph Theory and Its Applications March 14-16, 2001 Chennai) (2001), 34–36.

[115] H. Weyl, *Über die asymptotische verteilung der eigenwerte*, Nachrichten von der Gesellschaft der Wissenschaften zu Göttingen, Mathematisch-Physikalische Klasse **1911** (1911), 110–117.

[116] E. P. Wigner, *Results and theory of resonance absorption*, Conference on neutron physics by time-of-flight, 1956, pp. 1–2.

[117] S. Zelditch, *Uniform distribution of eigenfunctions on compact hyperbolic surfaces*, Duke Math. J. **55** (1987), no. 4, 919–941. MR 916129

[118] ———, *Recent developments in mathematical quantum chaos*, Current developments in mathematics, 2009, Int. Press, Somerville, MA, 2010, pp. 115–204. MR 2757360